ENGINEERING RESEARCH INSTITUTE
UNIVERSITY OF MICHIGAN
ANN ARBOR

EMP-16

# Interim Report

# Intermittent Supersonic Wind Tunnel

June 1948

Project MX - 794

(AAF Contract W33-038 ac-14222)

Prepared by Raymond I. Schneyer
Raymond I. Schneyer

1 June 1948

INDEX

# INDEX

## APPENDIX

## List of Figures

Figure V (9) - Range III (down) Scale Reading $V_g$. Load

Figure VII(1) - Typical Manometer Photograph

Figure VII(2) - Test Section Mach Number from Pressure Measurements Horizontal Traverses

Figure VII(3) - Mach Number from Wall Pressure Measurements Test Section, (Empty), Left Hand Wall (Looking Upstream)

Figure VII(4) - Mach Number and Flow Inclination from Pressure Measurements in the Interior of M = 1.9 Wind Tunnel

Figure VII(5) - Total Head Pressure Measruements in the Interior of M = 1.9 Wind Tunnel

## ACKNOWLEDGMENT

This report has been prepared with the collaboration of the present wind tunnel operational group, in particular Mr. Louis Garby and Mr. W. S. Bradfield.

General coordination has also been accomplished through the Wind Tunnel Advisory Committee (Dr. A. M. Kuethe, Dr. M. V. Morkovin, Dr. F. W. Ross, and Professor W. C. Nelson, Chairman).

## I. Introduction

In June 1946, the Army Air Forces approved a proposal that the University of Michigan, under the sponsorship of the Air Forces, construct and operate an intermittent supersonic wind tunnel. The tunnel was to operate at Mach Numbers from 1.5 to approximately 5, with run durations of about 20 seconds throughout this range.

In that same month the design was begun and the subsequent construction, operation and modification of the tunnel during the past two years has revealed many of the problems and possibilities of this type of design. No other wind tunnel in this country used so brief a run duration; the problem of a closed return circuit was unique, and for many of the problems there was little or no background. The first supersonic flow, at a Mach Number of about 1.9, was obtained in April 1947, but a survey of the first tunnel results indicated that a rather extensive modification and development program was necessary. The accomplishment of this program is still underway and this report is an interim report in that the results of some of the modifications still remain to be determined. However, it is believed that much of what has been learned thus far is of general interest in the field of supersonic testing and there is little reason to delay this report until all problems have been successfully solved.

## II. Purpose

It is the purpose of this report to furnish as complete a summary of the information concerning the construction and operation of the supersonic wind tunnel at the University of Michigan as is practicable at this time. It is intended that this report shall be as detailed as possible where the discussion is concerned with the problems, solutions, and subsequent modifications found by experience to be necessary.

III-A Method of Operation

The wind tunnel is a closed-return, intermittent-operation tunnel utilizing the pressure difference between atmospheric pressure and the low pressure of an evacuated system as the basic motivating force. Figure 1, which is a semi-schematic drawing of the wind tunnel installation in the housing hangar, illustrates the operating cycle. The tanks (T) are evacuated by the pump (P), the air removed being stored in the bag (B). When the tanks are at a pressure sufficiently low for operation, the valve (V) is quickly opened. The air from the bag flows through the test channel into the tanks. As the run progresses, the bag partially collapses, the outside air maintaining a steady upstream pressure equal to the barometric pressure. At the end of the run the valve (V) is again closed, the recharging cycle begun.

In order to avoid condensation in the test section the air must be dried prior to the first operation, and maintained at extremely low humidity throughout the successive runs. A drier (W) was included in the system for this purpose. Then, to minimize pitting of the model by dust particles in the airstream, a filter (F) was placed in the return circuit so that the air could be cleaned during the charging cycle.

The test channel is made up of four main parts: (1) The subsonic converging channel (E), which is the entrance ducting system; (2) the nozzle section (N), in which the supersonic flow is produced; (3) the test section (M), in which the model is mounted and the resulting phenomena observed; and (4) the diffusor system (D), in which pressure recovery occurs.

Computations were carried out (see Appendix I) to estimate the performance which might be expected of the tunnel. The calculated times of runs for various initial pressures in the vacuum tanks and for various Mach numbers are shown in Figure 2. Figure 3 indicates the temperature, pressure and den-

sity in the test section for Mach numbers up to 5.0, and the Reynold's number for a one-foot model tested at these Mach numbers.

III-B Vacuum Tanks

The vacuum tanks represent the energy storage of the system. As they are evacuated the potential energy of the system is gradually built up, and this energy is very quickly converted to kinetic energy when the operating valve is opened. An analysis of the mass flow requirements of the tunnel with a cross-sectional area of 100 sq. in. showed that 10,000 cubic ft. of tank space would be sufficient for runs of at least 15 seconds at all Mach numbers considered. However, the vacuum tank system utilized war surplus equipment, and the actual total volume which resulted was 13,000 cubic ft.

The vacuum volume is made up of a set of nine tanks manifolded together by a four-foot diameter piping. The dimensions of a typical tank are given in Figure 4. The tanks are set in three vertical rows of three tanks each, as shown in Figure 5, and the manifolding pipe connects each of the eight external tanks directly to the center tank. These manifold pipes were kept close to the forward end of the center tank. This insures that the air coming through the tunnel disperses through the nine tanks with as little time lag as possible, as the downstream section of the wind tunnel channel also opens directly into the forward end of this center tank.

The original purpose of the tanks established their design for 60 psi internal pressure. Analysis showed these tanks to be critical under 14.7 psi external pressure. Evacuation tests of a spare full-scale tank resulted in collapse at 14.5 psi external pressure. Experimental work with scaled models was then carried out and the results indicated that each tank would require four reinforcing rings for satisfactory strength. The tanks were therefore reinforced by 4 in. x 4 in. x 1/2 in. angles, formed to the surface contour

and welded to the tanks as shown in Figure 6.

The heat of the cutting and welding work caused separations in the seams of the tanks and serious leakage problems developed. Air leaking into the system from the outer atmosphere carries with it high water vapor content, complicating the problem of drying the air to be used in successive runs. At the same time, such leakage, by increasing the absolute pressure in the tanks, decreases the length of each test run.

Several sealing methods were tried, but with very little success until standard auto "body deadener" was tried. This tar-like material was sprayed on all seams and joints, with highly satisfactory results. A small vacuum was kept in the tanks while the spraying was carried out, and the deadener was thus drawn into the cracks. Since the material hardens after a period of exposure to air, it could then withstand the pressure differential when a high vacuum was drawn in the tanks. Large cracks were first stuffed with thick "deadener" mixed with heavy fiber and this combination was allowed to dry before the thin "deadener" was applied. Leaks were located by drawing a high vacuum and then locating the whistle which resulted from air seeping through a small hole. After several coats of sealing compound the tanks were able to maintain an absolute pressure of 0.15 psi with a leak rate of 0.8 in. of mercury per hour. This is considered satisfactory.

Even though the sealing described above has proved satisfactory, there is still some air leakage into the system. It is therefore necessary that the drying capacity be sufficient to remove the moisture which this air adds to the system. It is also necessary that precautions be taken that this extra air does not so increase the storage bag pressure (when the tanks are evacuated) that the bag splits open. To limit this leakage as much as possible, the tunnel is "run down"; i.e., the tanks are filled to atmospheric

pressure, whenever the day's runs have been completed.

III-C Vacuum Pump

The vacuum pump represents the power input point of the tunnel. It is a Chicago Pneumatic TVB-2 piston-type pump, displacing 1700 cubic ft. of air per minute, and capable of producing vacuums of 14.6 psi. At peak load, the pump uses 67 horsepower, but the average horsepower used over a complete charging cycle is not much over 40. The pump is shown in Figure 7.

This pump is water-cooled, and some difficulty with water seepage was experienced when it was first put into operation. A careful check of the pump, tightening of the head bolts and good general maintenance cleared up this problem. Two precautionary measures were taken. A screen was placed over the inlet duct leading from the tanks to the pump to keep any foreign bodies out of the pump. An oil filter, consisting of a screen cartridge filled with machinist waste and clean metal turnings, Figure 8, was placed in the exit duct leading from the pump to the bag. The pump introduces very little oil (10 drops per minute) into the air, and no trouble has been experienced with the existing arrangement. However, if it proves necessary, oil consumption may be reduced by the use of oilite-type bearings.

III-D Air Storage Bag

The bag has the specific purpose of supplying clean dry air for the run, maintaining constant pressure and temperature conditions throughout the run. Thus it is basically a flexible segregating device to keep the dry wind tunnel air from becoming contaminated by the high moisture content external air. It must have sufficient capacity so that the bag does not completely collapse by the end of the run. With 13,000 cubic feet of evacuated tank space, the 24,000 cubit ft. bag has proved adequate.

The bag itself was obtained as war surplus material, formerly being

a model ZKA barrage balloon. It was stripped of all extraneous equipment, such as stabilizing surfaces, and then modified for use with the tunnel. Originally manufactured by the Goodyear Rubber Company, the basic balloon material is made of two layers of fabric with a neoprene coating between them and a coat of neoprene on the inside and outside surface. The balloon shown in Figure 9 is about 60 ft. long with a 24-ft. maximum diameter.

For use in the tunnel several openings had to be cut in the bag: the main duct inlet and outlet, and inlet and outlet openings for connections to the drying equipment. The main duct outlet required considerable care. The nose of the bag was split open, a round opening cut in the most forward section, and a metal frame nose section inserted. This frame section, shown in Figure 10, is made of tube steel with wire mesh stretched over the outside of the tubing. The frame matches the nose contour of the bag. The metal frame is fastened to a metal duct which converges to a 4 ft. x 4 ft. square section, as shown in Figure 10. With the frame inside the nose of the bag, the split in the bag was closed by cementing sealing strips of neoprene-coated fabric on both inner and outer surfaces. The bag was then cemented to the metal duct, and an external clamping ring added for safety. This is shown in Figure 11.

The nose section keeps the nose portion of the balloon from being sucked into the tunnel duct, and permits smooth transition for the air from its position at rest in the bag to the subsonic flow through the initial converging section.

The other bag openings were handled in a slightly different manner. Holes were cut to match the entering pipes, and then reinforced with a layer of fabric inside and out. A flange angle was welded to the duct pipe, and a matching flange bolted directly to it, with the bag fabric clamped between the two flanges, as shown in Figure 12. Rubber gaskets were used. No leakage has

been detected at any of these openings.

For supporting the bag in the proper position in the tunnel arrangement, the original hold-down metal cables were utilized. The bag was actually inverted from its normal position and the cables fastened to the rafters of the hangar in which the tunnel is housed. Additional tie-downs to the floor were added to keep lateral motion at a minimum, since the hangar is open to wind currents along one side.

One safety feature of the original bag, a safety hatch which opens when the bag pressure builds up to 2-1/2 in. $H_2O$ gage, was retained and an extra safety device added. A mercury switch automatically shuts off the evacuating pump when the internal bag pressure reaches 1/2 in. $H_2O$ gage.

The bag material, although waterproof, is not impervious to water vapor. The neoprened fabric proved to be as good as any of several flexible materials tested for segregating the dry air for the tunnel run, but some vapor leakage exists. This vapor must be continuously removed by the drying equipment. A complete discussion of this is given in section III-F below.

III-E Butterfly Valve

The butterfly valve represents the master control of the tunnel operation. The unit used was furnished by the Henry Pratt Company of Chicago, Ill. It contains a 24-in. diameter valve which is forced into a rubber valve seat when closed. The unit is shown in Figure 13. The closed valve can maintain pressure as low as 0.1 psia without leakage. With the valve in the open position during a run, no tendency to "flutter" has been noticed. However, the rubber seat has deteriorated under use, and one replacement seat has been installed. Since the seat can be replaced in a few days, this is not considered a serious problem, but the valve seat must be periodically checked.

The valve is opened and closed by a valve operator manufactured by the Philadelphia Gear Company. The complete opening (or closing) cycle takes about 1-1/2 seconds, but only during half this time does any air flow take place. The first 3/4 seconds is used in "cracking" the valve from the rubber seat, and the air flow is negligible during this part of the cycle. Thus only about 3/4 seconds of the maximum usable run time is lost in valve operation. The operation is controlled from the main control panel. The control unit, shown in Figure 14, utilizes a 2.5 h.p. motor.

III-F Drying Equipment

The drying unit originally installed was a Lectrodryer No. AWC-200, manufactured by the Pittsburgh Lectrodryer Company. This model, with a limit flow rate of 200 cfm, can remove 22 lbs. of water before reactivation is required. The dessicant used is an activated alumina with an output dewpoint of about -50°F, and this unit was steam reactivated. It requires about 5 hours to reactivate the unit. The unit is shown in Figure 15.

Under ordinary conditions, on a typical humid summer day, there is about 20 lbs. of water in the 24,000 cu.. ft. of air contained in the bag. This means that there is little margin left, once the bag air is dried, to handle any leakage without reactivating. It was planned that the air would first be dried completely, i.e., to a dewpoint of -45°F, the drier would be reactivated and then after each run some of the air would be shunted through the drier on the charging cycle. Thus originally the drier was set in a line shunted off the main return duct, and by partially closing a valve in the main duct some of the air being pumped through could be forced through the drier. A schematic of this circuit is shown in Figure 16a. Since the vacuum pump could handle the circulation, no additional pumping equipment was required. A flow-meter in the drier shunt insured that the capacity of the drier would not be surpassed.

This original layout proved to be inadequate. The heat of compression increased the temperature of the air to about 120° or 130°F through the pump, and it was found that the adsorptive ability of the dessicant decreases sharply if the air used is over 100°F. This meant that air could not be fed directly from the pump to the drier. One solution to this problem would be to add an aftercooler to the system, just downstream of the pump. It was believed, however, that better results would be obtained if the drier was established in a separate circuit, so a blower unit and the duct work of Figure 16b were installed. The blower was capable of circulating 110 cfm through the drier, but now the air circulated had a maximum temperature of only 5° above room temperature.

The separate drying circuit improved operation of the drier, but satisfactory results still could not be obtained. An investigation showed that the permeability (i.e., the inability to resist passage of moisture due to differences in vapor pressure) of the neoprene-coated fabric used in the air storage bag was high enough to cancel much of the drying capacity. In effect, what was happening was that after a certain dewpoint (around 20°F) was obtained inside of the bag, as much moisture was leaking in through the walls of the bag as was being removed by the drier and a condition of equilibrium was established. As soon as the drier became loaded and needed reactivation (a five-hour process) the bag dewpoint would increase as more moisture seeped in and none was removed. Thus the system had a lower limit of 20°F dewpoint. A more thorough study was made of the bag permeability, methods of decreasing it, the possibility of materials more impervious to vapor pressure differentials, etc. This study is presented in Appendix IIA. In brief, it was found that the neoprene-coated fabric was as good as any available flexible material although its permeability may increase with age. However, the possibility exists of decreasing its permeability by coating it with a plastic.

Assuming that it is not possible to decrease the bag permeability to the point that it is impermeable, one must establish an adequate drier circulation system. The air is taken from the bag, passed through a drier and returned to the bag. The size of the drier necessary to give the desired bag dewpoints then becomes a function of the fabric permeability. The analysis of this problem is given in detail in Appendix IIB.

Using the present balloon size and fabric permeability a drier flow rate was selected which would give bag dewpoints of the order of -25°F (currently considered usable but not excessive) on a humid summer day. A second consideration was the fact that at some time in the future it might be desirable to make combustion model tests and these products of combustion would be discharged to the atmosphere. Thus it is necessary that the driers be also of such air capacity as to recharge the balloon bag well within the allotted time for pumping out the vacuum tanks. Oil vapor problems might also necessitate breaking the flow return circuit. With these considerations a drier flow rate of 1200 cfm with an outlet dewpoint of -40°F was selected as desirable. In order to produce these conditions two Lectrodryer Model BWC-1500 driers have been ordered.

These units, having a combined flow rate of 1200 cfm with an outlet dewpoint of -40°F or lower, will insure a dew point of -25°F in the bag at all times. These units are electrically reactivated and are dual operating; i.e., the reactivation cycle is carried on simultaneously with the drying cycle, so that no stoppage of the drying circuit for reactivation is necessary.

As a stop gap measure, until these units are delivered, a surplus air conditioning unit (a Lectrodryer CHK dehumidifer) has been installed as

the drying unit in the circuit. This unit has been consistently supplying dewpoints of 0°F in the storage bag, but when it was first installed, checks of the dewpoint in the bag gave values much higher. Investigation showed that "zoning" was occurring; i.e., the dry air was not thoroughly mixing with the moist air in the bag. Installing a fan in the bag, to help mix the air, solved this problem satisfactorily.

III-G Precipitron

The dust collector used to remove dirt and other foreign particles from the air, is an electronic precipitator manufactured by the American Air Filter Company. Particles passing through the unit are given a charge as they enter, while at the downstream end of the precipitron there is a set of oppositely charged plates, covered with a sticky oil. The dirt particles are attracted to the plates, where they are held by the oil. The unit used has an efficiency rating, based on a chemical test for dirt-free air, of 90 per cent at an air flow rate of 1850 cfm. The collector is shown in Figure 17.

The precipitron must be cleaned and serviced regularly, so it is housed in a plenum chamber which has access doors to both the upstream and downstream sides of the collector. The original chamber, shown in Figure 17, was made of No. 16 gage sheet metal. It was all welded construction, except for the access doors and the fastening to the collector which was done with bolts. The doors slid off after retaining nuts were removed from stud bolts. The doors were made air-tight by using a strip 1/2 in. soft rubber gasketing around the perimeter.

This original plenum chamber proved almost immediately to be inadequate. The reciprocating operation of the vacuum pump caused pressure waves of high amplitudes, even at high vacuums when the air flow was negligible. These waves started oil-canning of the flat sheet-metal surfaces, and cracks

and leaks began to develop. In an attempt to damp out the pressure waves near their origin, a settling tank was installed between the pump and the plenum chamber. This tank is shown schematically in Figure 18, and actually in Figure 19. The holes in the first baffle wall could be completely closed by plates if more resistance to flow was required. This tank did damp out some of the effects of the pressure waves, but only at low air flow rates.

A new plenum was then installed. This chamber was made of two surplus waterheater tanks of about 3/16-in. steel. Doors were cut out, the cut-away forming the basic structure of the door itself. Each door was bolted onto two hinges and locked in place by hand-operated locking nuts. This afforded much easier access than existed with the original chamber. The 1/2-in. rubber gasketing was again used around the cut-out. The collector itself was completely welded into place between the two tanks, and the inlet and outlet ducts were also welded into place. The final arrangement, shown in Figure 20, has proved to be satisfactory.

III-H Entrance Duct

The air entering the tunnel from the storage bag first passes through a subsonic duct which gradually decreases area until it meets the entrance to the nozzle section. This entrance duct is made of four component parts shown schematically in Figure 21. The first component is the converging portion of the nose section inserted in the bag, as described in section III-D and Figure 10. The second section has a constant cross-section, a square duct 4 ft. on a side. Housed in this section are three No. 30 brass screens, set transverse to the flow and 8 in. apart. These screens reduced any large amplitude-turbulance which may form in the air stream. The screen section is shown in Figure 22. The screens are removable for cleaning and checking. The screen section is built up of aluminum channel and plate.

From the screen section the air enters a converging section made of 1/8-in. steel plate. The dimensions of this converging section are shown in Figure 23, the cross-sectional duct area being reduced from 4 ft. x 4 ft. to 8 in. x 15 in. The section is all welded, and the inner walls are ground smooth. The section fastens to the preceding screen section and to the slide valve section which follows by bolts through attachment angles. Gasketing at all joining angles keeps the moist external air out of the air duct. The converging section is shown in Figure 22.

The last segment of the entrance duct is a constant area section containing a sliding plate which acts as a valve. The plate is made of 1/4-in. steel, with a strip of extruded rubber along the edges. When the main butterfly valve is closed and the slide valve is closed, access can be made to the nozzle testing and diffusor section without any loss of dry air. With the plate out, a fitted filler seals off the opening in the top of this section so that a smooth duct is presented to the air. The section is made of 1/4-in. steel plate, with bolting angles to fasten it to the adjacent sections. It is shown in Figure 24.

The entrance duct has remained substantially as originally designed. The slide valve section has been replaced, but only to match a redesigned nozzle section. All of the joints must be carefully gasketed, for even though the pressure differential between the air inside the duct and the outside atmosphere is small, the vapor pressure differential is large and vapor leakage can occur.

III-I Nozzle Section

The nozzle section houses the contoured blocks which form the converging-diverging channel in which the supersonic flow is obtained. This channel is basically two-dimensional, all changes in contour being made by

varying the vertical dimension of the duct while the side walls of the housing section form the channel sides. Accordingly, the inner surfaces of these walls must be kept very smooth. Furthermore, the walls must be removable so that the contoured blocks may be replaced for each of the various Mach numbers.

The original nozzle section is shown in Figure 25 with one side wall removed, and assembled and in position in Figure 26. A sketch showing the basic components is given in Figure 27. The top and bottom channels were built up of steel angles and 1/4-in. brass plate. These channels fastened directly to the slide valve section upstream and the test section pressure box downstream, with .020 in. vellumoid gasketing to seal the joints. The side plates bolted to these channels and to the valve section and pressure box, with vellumoid gasket seals. These plates were 1/4-in. brass. Two windows were mounted in each plate, for purposes of optical observations of the flow. The window mountings were studs set on the side plates onto which the window frame bolted. All studs, and all rivets used for setting attachment angles onto the side plates, were ground flush on the inner surface of the plate.

The windows used in the section were made identical in shape to those windows used in the test section. This permitted interchangeability in case of damage to a window, and also facilitated wall pressure measurements as only one pressure plate was required. At first 2-in. thick Plexiglas windows were tried, but their optical quality proved too poor for good Schlieren photographs, so 1-in. commercial plate glass windows were used. The glass was picked for freedom from striations and for reasonably parallel faces, and proved to be quite satisfactory for the initial phases of the tunnel work. The glass was set in the frames, which were aluminum castings, with a cement called Xpandtite. The cement tended to chip a little when the tunnel was in operation, so the windows were reset using Wood's metal. The inside wall was

kept flush. Details of the window mounting are shown in Figure 28, while a window set in its frame is shown in Figure 29.

The nozzle contour blocks were held in place by bolts (four per nozzle) which fastened to the top and bottom channels and were threaded into the contour blocks. These can be seen in Figure 25. Adjustment of the nozzle blocks could be made by raising or lowering through these bolts. Thus it was hoped that any disturbance caused by the juncture of the nozzle block and the test section could be eliminated by differential movement of the block through these bolts.

The initial operations of the tunnel with this nozzle section showed up several imperfections. The section was not rigid enough. As soon as the test run began, the high external pressure (relative to the very low pressure in the supersonic region) pushed the nozzle blocks inward so that the vertical dimension of the duct changed as much as 1/16 in. This caused an unavoidable discontinuity at the nozzle-test section junction and a shock wave originated. The side walls deflected slightly under load, but not as seriously as the blocks. However, their deflection caused leakage around the gasketing and the inflow of air into the nozzle affected the boundary layer build-up along the nozzle. It was also found that once removed, the side walls were extremely difficult to replace so that changing nozzle blocks was time consuming and a good seal along the side wall was questionable.

With these facts in mind the nozzle section was redesigned. To provide easy access for changing the nozzle blocks, the nozzle doors are clamped shut by quick-opening clamps along the upper and lower edges. The blocks are held in place by a tongue and groove arrangement at each end, and several locking cams, as shown in Figure 30. The side walls were first reinforced to reduce the side deflections, but permanent set existed due to local stress concentrations. They were then replaced by solid 1-in. steel plates reinforced

with welded T-sections. (See Figure 31).

The nozzle channel is sealed by inflatable rubber tubing gasketing, kept under pressure, which rings the side walls and the nozzle inserts. The seals were found satisfactory under static tests. Views of the new nozzle section are shown in Figures 31 to 33.

III-J Nozzle Blocks

The nozzle blocks are the contoured blocks which shape the channel in which supersonic flow is established. The blocks are fixed contour, so that each set of blocks produce only one Mach number and they must be changed to vary the Mach number. The original blocks were made of a gypsum plaster commercially known as Hydromite. This material, when cast against a smooth surface like Plexiglas or polished steel, assumes a smooth hard surface. Experiment showed that by making a mold of two contour plates with thin Plexiglas fitted over the top, the cast Hydromite had good surface appearance. However, the Plexiglas deformed under the weight of the plaster and the heat given off by the plaster in hardening, and the surface was not true to the contour desired. Metal cross bars were added to relieve the Plexiglas of the weight, and a set of nozzle blocks cast. The mold and one block are shown in Figure 34. Inserts were set in the plaster for fastening it into the nozzle section.

A check of the set of blocks cast showed that some "dishing" of the Plexiglas had occurred across the throat section. The nozzle blocks were filed down to contour by hand at this section, but the results of the first runs indicated some shock waves which were credited to the deviations from the computed contour.

Some experimental work has been carried on with small scale nozzle blocks in plaster. A new material, Hydrocal B-11, was tried and in initial work has shown promise. Instead of requiring casting, this plaster can be

screeded. The surface obtained depends upon the fluidity of the mix, the amount of screeding required, and the solidity of the material at the final screeding, but some excellent surfaces have been obtained. After taking its initial set, in which its form becomes slightly harder than dried putty, the Hydrocal B-11 can be screeded, with a sharp screeding tool, to its finished dimensions. Its dimensional change in the final set is almost negligible. After the final set, the plaster surface is very hard, but it may not withstand the rigors of supersonic flow. As yet no nozzles of this type have been tried in the wind tunnel.

A set of standard type aluminum blocks was machined for use in the tunnel while further experimental work was carried out on the plaster nozzles. The aluminum blocks were supposedly held to ±.001 in. in contour but when checked, they proved to be as much as .004 in. to .005 in. off contour. They were installed and used, however, and the results showed at least one wave that may have originated on the nozzle. Figure 31 shows these blocks.

A wood nozzle has been constructed for Mach 4 operation. The purpose of this unit is to develop a satisfactory contour on the inexpensive wood nozzle and then to construct a metal nozzle, which would maintain tolerances unobtainable with wood, to these dimensions. The nozzles were made of laminated pine with 1/2-in. steel plates along each side and with numerous drift bolts pushed through the metal and wood. The nozzle blocks have steel end plates.

The contour of these blocks was worked to within 0.01 in. of the computed value. A final rub-down is being left until just prior to installation. A photograph of these nozzles is shown in Figure 35.

The nozzle contours are designed according to the method of Foelsch, considering source flow with radial streamlines in the region downstream of the throat and patching to this flow a field which turns the radial streamlines into uniform and parallel flow. A complete discussion of the method is given in Appendix III.

III-K Test Section

The main channel of the test section is 8 in. wide, 13 in. deep and 48 in. long. Within this channel, a model is fixed in the airstream and the observational, force, and pressure measurement means are employed.

The basic design of the test section is determined to a large extent by the type of force measurement system used. In this tunnel, a mechanical force balance (described in detail in section IV-B) occupies the volume about the test channel and has a vertical strut which passes through the channel and to which the model sting is attached. Since any airflow about this vertical strut would adversely affect the balance measurements, the force balance volume must operate at zero pressure differential with the test channel, and therefore, the whole mechanism is enclosed within a pressure box. Figure 36 shows the main channel with the balance system, model and pressure box in place.

Visual observations and optical measurements are made by means of two windows placed in the vertical side walls of the test channel and in line with the model center position. These windows were cut from one-inch thick plate glass. By means of the Foucault test, areas were selected that were relatively free from striations. These windows have not been finished to an optical flatness and are, therefore, unsatisfactory for Schlieren work requiring great sensitivity. While results at Mach numbers of about two have been

good, work at Mach numbers of four will require greater Schlieren sensitivity due to low test channel air density. For this work, new windows have been ordered that were selected in the same manner as before. These windows will be 1-1/4 in. thick and stress relieved to less than 10 millimicrons per centimeter. After annealing, they will be ground and polished to the following limits:

1. Wedge defect not greater than .002 in. at one edge.
2. Surface to be optically flat: i.e., a spherical radius greater than two thousand feet.
3. Surface accuracy - less than five wave lengths of yellow sodium light. It is believed that these windows will be sufficiently accurate to handle the entire Mach number range of the tunnel.

The original test section was made from 1/4 in. brass plate, and while care was taken in construction to ensure that the inside surfaces were smooth and free from discontinuities, some operations carried on with the pressure box open caused excessive deflections of the material, and permanent deformations were experienced. For this reason, modification was undertaken as soon as enough calibration runs were completed to indicate the magnitude of the effects.

The four surfaces were strengthened by cycle welding 9/16 in. brass plate to the originals. The top and bottom surfaces were further reinforced with two 3/4 by 2 in. steel stringers bolted along the length of the plates. The window fasteners were changed from 1/4 in. SAE to 5/16 in. AN bolts. The revised section is shown in Figure 37. Static test of this unit showed a maximum deflection of .007 in. under one atmosphere of pressure differential.

While the modification of the old test channel enabled it to be used for pressure and model test work, it no longer was able to accommodate the

force balance system; also, modifications in the development of the balance system resulted in structural interferences with the pressure box; consequently, a new design for a test channel and pressure box resolving these difficulties was begun.

The new test section has been designed for a maximum deflection of .0005 in. under a pressure difference of one atmosphere. The four surfaces are cast from manganese bronze. This material was chosen because of its density and free machining characteristics.

The principal access to the model remains through the window; however, the method of window installations has been changed. The frame of the window is of bucket shape; the window glass forms the bottom of the bucket. The sides of the buckets form the walls of the recess into the pressure box and are bolted directly to the pressure box walls. An air seal is effected between the top of the bucket and the pressure box wall. A sketch of this revised arrangement is given in Figure 38.

A new method of venting the pressure box to the downstream end of the test section was devised and inserts to accommodate this vent were incorporated in the design of the side walls of the test channel. A study of the influence of the orifice effect of this vent was made and is presented in Appendix IV.

As stated earlier, the volume of the first pressure box was inadequate to accommodate the later developments in the force balance system. Also, deflections of the box walls produced the problem of finding adequate air seals. A new pressure box has been designed which overcomes these difficulties. The new pressure box is made from 3/8-in. dural plate set in a heavy steel framework. Numerous handholes are located about the pressure box to provide access to all parts of the balance system.

In general, the entire test section has been redesigned with the primary objective of keeping deflections under loads to a minimum, accommodating adequate air seals, and providing for easy access to the model and all parts of the force balance system. It is anticipated that both pressure and force tests will be made in the new section. Pressure leads will be carried through the sting and out of the balance support windshield. The balance system will be locked in a stationary position during pressure runs.

III-L Diffusor Section

The diffusor section represents that portion of the tunnel in which pressure recovery is accomplished. In the original design, the diffusor section was in two parts. A rectangular box section fastened directly to the downstream end of the testing channel. This section was 8 in. x 13 in. inside cross-section and was 48 in. long. Inside the section was mounted a sharp-edged airfoil section, made of thin steel plate. This airfoil spanned the duct vertically. A cam set inside the airfoil could be rotated to increase the airfoil thickness. The intention was to permit the initial normal shock wave, which passes along the channel when the run begins, to pass downstream of the airfoil, after which the thickness of the airfoil was increased by means of the cam forming a converging-diverging type of supersonic diffusor. An increased efficiency of the diffusor would result. A sketch of the arrangement is shown in Figure 39, and pictures of the airfoil used with the cam in different positions shown in Figures 40 and 41,

In the intial runs of the tunnel, it was found that the airfoil section was choking the flow, even when the cam was in its "closed" position, and no supersonic flow occurred over the airfoil. The cross-section of this airfoil was well below the theoretical blocking area given by simplified analyses,

but the effects of air leaks, boundary layer and shock losses were apparently enough to decrease the area required for blocking. The airfoil was removed, and the tunnel performance improved.

The second part of the diffusor section was a steel section forming a divergence from the 8-in. x 13-in. section at the end of the box section to 24-in. diameter at the valve. This section is seen in Figure 26, which shows a complete installation of the original diffusor.

While the removal of the airfoil helped the tunnel performance, it was decided that as long as no converging-diverging channel was being utilized, the long constant-area box section was actually detrimental. It permitted build-up of the boundary layer, with no "relief" at the walls. A new diffusor, a diverging section going directly from the test section to the valve, was built and installed. It is shown in Figure 42.

III-M Miscellaneous

1. Ducting. All of the return duct work was made of 12-in. steel pipe. All joints were welded with triple beads to insure no vapor leakage. Hand-operated valves were set at the exit from the vacuum tanks and at the entrance to the air storage bag. Thus these two valves could be closed and maintenance of the units in the return duct carried on without contaminating any of the air stored in the tunnel proper. A diverging section four ft. long, changing from 24-in. diameter at the butterfly valve to 48-in. diameter is fastened into a 48-in. diameter pipe which connects directly to the center tank of the vacuum system. All joints downstream from the valve are welded. All pipe is 1/4-in. thick steel.

2. Heater. A small steam heating unit was installed in the return duct, to heat the air on particularly cold days. However, the heat of compression of the pump has proved to be sufficient, so that this unit is not used.

3. Operating Panel. All of the major tunnel controls have been concentrated on one panel. A picture of this unit is shown in Figure 43, with the individual controls indicated.

4. Crew necessary for operation. Experience thus far has indicated that a normal operating staff at the wind tunnel will probably be comprised of the following:

| | |
|---|---|
| 1 | supervisor |
| 1 | control panel operator |
| 1 | mechanic |
| 5 | data analysis, Schlieren, report writing |
| 1 | miscellaneous, development work |
| 1 | photographic laboratory technician |
| 2 | secretary and typist |
| 12 | total |

In addition to this operating crew there will be a variable staff in the design group concerned with problems of model design, test equipment design, and wind tunnel modifications.

## IV-A Pressure Measuring Equipment

Pressures are measured in the tunnel by means of a 50-tube manometer board, using mercury as a manometer liquid. The board itself is shown in Figure 44. Its tubes are heavy-walled glass, with an inside diameter of 4 mm. They have been picked for constancy of diameter so that there is little meniscus effect. With approximately 15 seconds to record pressures it is important that the time required to reach equilibrium be as short as possible. The tube diameter was chosen after a set of tests in which the reaction time; i.e., the time it takes the mercury to reach its level, was studied. Larger diameter tubing proved to be poorer because of the increased inertia of the mercury and the resulting longer period of time to damp the mercury oscillations, and smaller diameter tubing introduced too many maintenance difficulties.

The 50 tubes are connected to a common mercury reservoir. This can be raised or lowered to set the "zero" of the mercury at any desired level. The tubes themselves are set in a Plexiglas board which is calibrated in tenths of an inch from zero to 60 in. The board is lighted from the back for fluorescent tubes mounted in a case which fastens directly to the framework holding the manometer board. This gives an even distribution of light over the entire board and results in excellent photographs.

At first it was planned to "trap" the mercury at the various levels in the tubes by clamping a bar across small rubber tubes leading from the bottoms of the glass tubes to the common mercury source. This was tried, but the effects of the clamping were not consistent and could not be read out. Mercury driven out of one tube would climb in another, raising its level. Hence, this method had to be abandoned. Instead, the rubber tubes leading from the various pressure orifices to the manometer board were first passed through a clamping device. The amount of air displaced by the clamp in any tube had a

negligible effect on the pressure in the tube, and the mercury level was trapped by sealing off the tubes. This clamp is shown in Figure 45. Even this method was subject to some slight errors, and finally photographs of each run were taken and the pressures read from the photographs. This proved to be the most reliable method.

It was found that in obtaining pressures, about 25 seconds were required to completely damp out the oscillations of the mercury. A procedure was devised that appreciably reduced the running time required, however. A brief five-second run is made, and the vacuum clamping device closed. During this run the mercury columns rise to approximately the correct levels. The oscillations are then permitted to die out before the test is resumed. A run of about 12 seconds is then made and the clamp is opened about two seconds after the valve has opened and closed one second before the valve is closed. With this procedure, the photograph is taken just before the clamp closes, and the mercury has no noticeable oscillatory movement. Test results can be repeated to within .04 in. of mercury. An example of a typical manometer photograph is shown in Figure 46.

IV-B Force Measuring Equipment

The balance system is designed to measure three of the six force and moment components, i.e., lift, drag and pitching moment. Three main considerations affected the design: the force range, the accuracy required, and the time available to establish complete equilibrium in the measuring system. The force range was chosen to be 0-100 lbs., but this was divided into three separate ranges of 0-1, 0-10 and 0-100 lbs., with a desired accuracy of the measuring apparatus of 1 per cent of the full-scale value in each range. With about 12 to 14 seconds available for measurements, it was considered necessary to bring the balance to equilibrium within 5 to 7 seconds after the start of the

run, leaving about the same period of time for obtaining the data.

To meet the specifications, a floating model-support structure was designed, as this permitted the strucutral members of the support system and the sensitive elements of the balance to be mounted outside the testing section. The sensitivity requirement over the wide range of loading implied that the system move as free of friction as possible, and also required the development of a sensitive element which could be changed in some way to accommodate the three force ranges. The short time available for reaching equilibrium imposed the need for a damping system, and the short time available for obtaining data dictated some method of automatically recording the forces. The unit designed transmits the aerodynamic loads from the model into units sensitive, through wire strain gages, to displacements. The resulting strains are electrically recorded and converted to load values through calibration charts.

The balance system is made up of three essentially separable units. The aerodynamic forces are transmitted by the model to a mechanical linkage which comprises the first of these units. As shown in Figure 36, the model is mounted by a sting, or support strut, to a vertical semi-circular strut. This strut fastens to tubes that are part of a box-like arrangement which is essentially buoyant. This "floating box", which surrounds the test section, is made buoyant by suspending it from four flexible steel tapes and then counterbalancing its weight. It floats freely in position relative to the test section, and has no resistance to motion when a force is applied to the model. This freedom of motion is illustrated in Figure 47, which shows that motions along the axis of the tunnel or up and down normal to this axis are almost friction-free. A windhsield around the vertical strut reduces the tare forces on the system, and a gear and rack arrangement permits the changing of the angle of attack of the model.

In order to provide for evaluation of the aerodynamic tares arising from forces on the exposed model support strut, the strut is to be split vertically lengthwise. The forces on the structure supporting the model may then be separated from the forces on the model itself. To avoid mechanical interference between the two halves of the support strut, a system of yaw restraint for the floating section must be employed. The use of taut wires in this application is contemplated.

The motion of the "floating box" is resisted by the second unit of the balance system, the strain sensitive elements, shown in Figure 48, which are mounted in the positions indicated by $G_I$, $G_{II}$ and $G_{III}$ in Figure 47. It will be noted that there are actually five separate cantilever beams in the assembly. The load is applied to the central beam through thin metal straps attached to the cross T-bar. By shifting the double roller assembly shown, one, three, or all five of the beams are bent by the load. When only the centerbeam carries the load, the operating range is 0-1 lb. (1 per cent of the full-scale load. See Appendix V). When the three middle beams are connected through the roller assembly, the range is 0-10 lbs., and when all five beams are bent as a single cantilever, the load range is 0-100. Wire strain gages are mounted on the upper and lower surfaces of the middle beam only. These gages are so arranged electrically that only bending strains in the beam are recorded, axial strains giving no electrical response. Deflections of the cantilever beams are limited to 1/8 in. in either direction.

A summary of the physical characteristics of the strain element for ranges 1 and 2 is given in Appendix V. Calibrations indicate that the desired accuracies cannot be obtained with the present roller clutch assembly because of unavoidable "looseness" in the assembly. To obviate this difficulty, the

beams are being redesigned to completely eliminate the clutch. The calibration work in Appendix V indicates that if the clutch is eliminated, the accuracy of ±1 per cent of full-scale reading will be obtained.

The strains obtained from the strain sensitive elements are transmitted electrically to the third unit of the balance system, the recording equipment. The equipment in use, all manufactured by the Consolidated Engineering Corporation of Pasadena, is shown in Figure 49. The main recording unit is a 12-channel carrier type recording oscillograph, fed by a power supply and a set of 12 amplifying units, one for each channel. The circuit of operation, indicating the function of these components, is given in Figure 50. The equipment can record both static and dynamic (up to about 125 cps) data. A maximum of six channels will be used at any one time for the operation of the balance system, so it is anticipated that the remaining channels may be used to record transient pressures or dynamic forces. With pressure tests, when no forces are being recorded, all 12 channels may be utilized.

A great deal of work has been done on the problem of damping the "floating box" oscillation. The work is discussed in Appendix VI. The problem appears to be solved, but actual dynamic tests of the damped system under air load have not yet been conducted. At the present time the balance system is being subjected to bench tests to determine its characteristics, and modifications are being made as they are proved necessary. Upon completion of this program the system will be mounted in the tunnel and final calibration work carried out.

IV-C Optical Equipment

The optical equipment consists of a conventional type of Schlieren system for air flow visualization. This Schlieren system was designed to give

a picture of the air flow in the wind tunnel at the test section windows or at either of two sets of windows in the nozzle section. Therefore, two sets of mounts were built. One set of mounts was permanently fastened to the concrete floor in line with the test section windows. The second set of mounts are tripod stands which can be moved about and used for Schlieren through either of the two sets of windows in the nozzle and for some special secondary uses. The optical units, such as the mirrors and light source, can fit on either the permanent mounts or on the moveable tripod mounts. Traversing heads on the permanent mounts allow for a six-inch movement either way parallel to the wind tunnel.

The optical diagram of the system is shown in Figure 51. The source of light is a General Electric B-H6 lamp, an air-cooled high intensity mercury arc lamp. An image of the lamp is formed on an adjustable aperture by means of a condensing lens. This image then serves as a rectangular light source for the system. The light formed by this source is bent by a small plane mirror toward the first parabolic mirror, the source being effectively placed the focal distance from the first parabolic mirror. This mirror then sends a beam of parallel light through the test section. Both parabolic mirrorsare 16 in. in diameter and have a focal length of 10 ft. The second parabolic mirror forms an image of the light source at its focal distance after reflection by another small plane mirror. The Schlieren stop is then adjusted so that it lies in the same plane as this image. A camera with a 40-in. focal length lens is located just behind the Schlieren stop and adjusted so that the test section of the wind tunnel is in sharp focus. The optical combination of the second parabolic mirror and the camera lens form the image of the test section on the viewing screen.

The Schlieren system is free from most aberrations in the imaging of the Schlieren light source. Spherical aberration is eliminated by the use of parabolic reflectors. Both the light source and the Schlieren stop are 2.3 degrees off the optical axis of the parabolic mirrors. Since these angles are equal, there is no coma, but astigmatism remains. This, however, does not affect the Schlieren as long as a vertical or horizontal knife edge is used.

As stated, the source of light is a General Electric B-H6 high intensity mercury arc lamp. The lamp can be either operated steadily or flashed. Under normal operating conditions the lamp draws 1.2 amperes at 900 volts. Its flash duration is 4 microseconds when flashed from a 2 microfarad condenser charged to 2000 volts. When operating steadily the lamp gives 60,000 lumens at a brightness almost 20 times that of filament sources. The lamp is cooled by two jets of compressed air directed at the ends of the tungsten electrodes. The compressed air and lamp voltage can be controlled from a remote control panel through the Schlieren control unit shown in Figure 52. A schematic of the control unit is shown in Figure 53. The three control switches, the steady switch, the flash switch, and the selector switch are located on the remote control panel. The steady switch closes a magnetic contactor and starts the cooling air. When the air pressure reaches 20 psi, the pressure switch closes, putting voltage into the lamp transformer primary. The selector switch must be in the steady position, or the lamp transformer output voltage will not carry to the lamp. If the air pressure drops below 20 psi, the pressure switch opens, shutting off the lamp voltage. When the steady switch is opened, the cooling air continues for about 30 seconds longer. This is done with a time delay unit.

The flash switch puts 115 volts A.C. into the flash unit which is shown schematically in Figure 54. The selector switch operates a high voltage

relay located in the flash unit. When the flash unit is on and the selector switch is in the flash position, the mercury lamp flashes when the camera shutter is tripped. A microswitch on the shutter closes just before the shutter opens; this puts a positive voltage on the grid of the 2050 thyratron, through a delay circuit consisting of a 1.5-meg. resistor and a 0.1-microfarad condenser. The tube conducts when the shutter is fully open, letting the one-microfarad condenser on the plate of the thyratron discharge through the tube through the ignition coil primary. The secondary puts out a high voltage pulse which triggers the capacitron tube. This in turn discharges the two-microfarad condenser, which is charged to 2000 volts, through the mercury lamp causing it to flash. This flash circuit was modified slightly from the circuit of the flash unit used with the Schlieren system at the Army Ordnance supersonic wind tunnel at Aberdeen, Md.

The B-H6 mercury lamp is mounted in a holder and air nozzle assembly which can be rotated through 90° in a horizontal plane. The lamp is held at the ends by two brass electrodes. Above the lamp is a condensing lens which can be raised and lowered by means of a rack and gear arrangement. These parts can be seen in Figure 55. The condenser lens has a focal length of about three inches and an "F" number of 2. It was made up of two war surplus lenses. Above the lens is a surface-silvered mirror which turns the optic axis from vertical to horizontal. The image of the lamp formed by the condenser lens is focused on the adjustable aperture shown in Figure 56. This image then serves as the rectangular slit source for the Schlieren system. The light source can be changed from a horizontal to a vertical slit by turning the lamp holder and air nozzle assembly through 90° and by turning the aperture from horizontal to vertical. The image of the lamp is changed from horizontal to vertical by

rotating the lamp holder and air nozzle assembly. In order to adjust the condenser lens, the lamp is operated from a spark coil. This gives enough lamp brightness for purposes of adjustment, but not too much for the eyes. The light box can be traversed by a screw to adjust the distance from the light source to the first parabolic mirror.

Three parabolic mirrors were ground and polished from 16-in. diameter Pyrex glass blanks. The specifications called for a surface accuracy of 1/10 the wavelength of the yellow line of sodium. The surfaces were chrome aluminized. One of the parabolic mirror mounts is shown in Figure 57. The mirrors are mounted in aluminum frames which can be rotated about both the horizontal and vertical axes by opposed screw adjustments. The opposed screws located under the aluminum frame rotate the mirror about a horizontal axis. The opposed screws on the side of the mount rotate the base of the mirror mount about a vertical axis. With these adjustments the parallel beam can be easily centered through the windows by adjusting the first parabolic mirror, and the image of the light source can be placed on the Schlieren stop by adjusting the second parabolic mirror. The mirrors and the wind tunnel windows were made by the Wm. Buchele Optical Company of Toledo, Ohio.

The Schlieren stop, camera and a small plane mirror are mounted on one frame. This combination is shown in Figure 58. The small plane mirror reflects the light from the second parabolic mirror to the Schlieren stop. This small mirror has the same type of adjustments as the large parabolic mirrors. A close-up view of the Schlieren stop assembly is shown in Figure 59. This assembly has five independent adjustments to control the position of the knife edge. The first adjustment is a traversing screw which moves the Schlieren stop assembly along the optic axis. A second adjustment is a screw which moves

the knife edge up or down to intercept more or less of the image of the light source. The knife edge can also be rotated through 360° about the optic axis with 90° stops to give either a horizontal or a vertical knife edge. In addition to these stops, a fine rotational adjustment is provided to correct slight angular differences between the slit image and the knife edge. The fifth adjustment is a small rotation of the knife edge to accommodate slight lateral variations in the focal length.

The camera uses a 40-in. focal length telephoto lens of the type used in the K-22 Army Air Corps serial camera. The shutter is an Ilex Universal No. 5 with an externally mounted microswitch for synchronization. The micro switch is set to make contact just before the shutter opens, the delay circuit in the flash unit causing the lamp to flash when the shutter is open. The shutter is operated by a solenoid so that the length of time between the closing of the microswitch and the opening of the shutter is the same whenever the shutter is tripped. A 4-x-5-in. graphic type back with a viewing screen is used with the camera. This back takes standard 4-x-5-in. cut film holders or film pack adaptors. The camera is built in two sections separated by a flexible bellows. The rear section of the camera can be moved back and forth for focusing by a gear and rack arrangement.

The Schlieren system was found to operate equally well using either the combination of a horizontal light source and horizontal knife edge or a vertical light source and vertical knife edge. The image of the vertical source, however, focuses at a different distance from the second parabolic mirror than the image of the horizontal source. This is due to astigmatism in the Schlieren system which is caused by having the light source and the image located off the optic axis of the parabolic mirrors.

For wind tunnel work at a Mach number of 2, the light source is adjusted to about 2 mm. width. The knife edge is then adjusted to intercept 1 mm. of the image and to pass 1 mm. This gives an even background with good contrast of both lighter and darker areas. The length of the light source is adjusted until the illumination on the viewing screen is 10-ft. candles as measured with a photographic light meter. Then when the lamp is flashed, the density of the resulting photographic negative will be about right to give the best prints. The illumination of 10-ft. candles on the screen was found to be best in a series of tests using Super Panchro Press film with a daylight speed of 125.

In addition to the Schlieren system shown in Figure 51, several other variations are possible with the equipment. A Schlieren view of the test section almost two-thirds actual size may be thrown on a screen using the third parabolic mirror as shown in Figure 60. A shadowgraph setup may be made by using the light source and one parabolic mirror. The viewing screen is placed about three ft. beyond the wind tunnel windows. This arrangement is shown in Figure 61.

## V Experimental Work

Some work was carried on in the wind tunnel when all of the components were in their first stages of development. Pressure surveys, which included wall pressure measurements, flow inclination measurements and total head data, were carried out. These data are presented in Appendix VII, which also includes information on the accuracy of the pressure measurements.

Information on the permissible model size, based on blocking effects, is also given in Appendix VII. At a Mach number of 1.9, a projected area of 8.5 sq. in. from a 40° cone resulted in satisfactory flow, but any area greater than this will probably choke the tunnel. A Schlieren photograph of a 2-1/2-in. diameter cone, with a 40° nose angle, mounted in the tunnel is shown in Figure 62. It is believed that larger models may be used in the tunnel with the revised test chamber because of the reduction in leakage in the nozzle and test sections.

## VI Conclusion

A. Development work on this type of wind tunnel circuit indicated the following:

(1) The air storage bag permeability to water vapor is critical with respect to drier capacity, and must be minimized. This may possibly be accomplished by the application of a suitable plastic coating to the bag material.

(2) A drier circuit which constantly circulates and dries the air in the storage bag is essential. This circuit must be such as to overcome storage bag permeability and system leakage and provide a sufficiently low dewpoint to air entering the test section.

(3) A settling tank is needed downstream from the position displacement-vacuum pump in order to reduce pressure surges in the return circuit. Oil vapor discharge from the vacuum pump has not as yet been noticeable in the circuit.

B. Development work on instrumentation has indicated the following:

(1) Pressure measurements can be satisfactorily obtained over the short time interval of operation by means of a five-second cutoff run followed by a 15-second stabilization run.

(2) Force measurements appear feasible with the present three component, strain gage balance system although dynamic runs in the air stream have yet to be made. Some difficulties in estimating tares are anticipated.

(3) The present Schlieren system appears adequate although runs above Mach number two have yet to be made.

C. Experimental work in the original nozzle and test sections has indicated the following:

(1) Excessive leakage combined with wall and nozzle block deflection resulted in strong shocks from the nozzle lip junction upstream from the test section combined with excessive boundary layer thickness.

(2) Mach number variations from 1.98 to 1.85 were measured horizontally along the test section centerline.

(3) Blocking occurred in the test section with a three-inch diameter, 40° cone. A 2-1/2-in. diameter, 40° cone was satisfactory.

# APPENDIX I

## THEORETICAL OPERATION OF THE TUNNEL

A. Determination of length of run versus Mach number for various initial vacuum tank pressures.

Nomenclature:

$\rho$ = density (lb $sec^2/ft^4$)

a = velocity of sound (ft/sec)

A = area of nozzle throat ($ft^2$)

t = time (sec.)

E = internal energy

W = work

Q = ~~heat energy~~ mass flow slugs/sec

$C_V$ = specific heat (const. vol.)

T = temperature

V = volume

$\lambda_t$ = minimum pressure ratio required to maintain desired Mach number.

Subscripts: o refers to state in storage air bag

1 refers to state in test section

f refers to final state at end of run

Superscripts: o refers to initial conditions in vacuum tank

* refers to conditions at nozzle throat

With no subscripts or superscripts, condition refers to state in vacuum tank at time t.

The mass flow per second at the nozzle throat is equal to the mass increase in the vacuum tank per second:

$$\rho^* A^* a^* = +V \frac{d\rho}{dt} \tag{1}$$

Upon integration this yields

$$t = \frac{V}{\rho^* a^* A^*} (\rho - \rho^o) \tag{2}$$

Since

$$\rho^* = \rho_o \left(\frac{2}{\gamma + 1}\right)^{\frac{1}{\gamma - 1}} \tag{3}$$

$$a^* = a_o \left(\frac{2}{\gamma + 1}\right)^{1/2} \tag{4}$$

$$A^* = A_1 M_1 \left(\frac{2}{\gamma' + 1}\right)^{\frac{\gamma'+1}{2(\gamma'-1)}} \left(1 + \frac{\gamma'-1}{2} M_1^2\right)^{\frac{\gamma'+1}{2(\gamma'-1)}} \tag{5}$$

equation (2) reduces to

$$t = \frac{V}{a_o A_1 M_1} \left(1 + \frac{\gamma'-1}{2} M_1^2\right)^{\frac{\gamma'+1}{2(\gamma'-1)}} (\rho/\rho_o - \rho^o/\rho_o) \tag{6}$$

Consider now the simplfication of the expression $(\rho/\rho_o - \rho^o/\rho_o)$. The energy equation may be written $0 = dE + dW$ or, change in internal energy = work done on gas:

$$QtC_V T_o + \rho^o V C_V T^o = \rho V C_V T - P_o \frac{Qt}{\rho_o} \tag{7}$$

Since

$$\frac{P_o}{\rho_o} = RT_o = (C_P - C_V) T_o \tag{8}$$

equation (7) reduces to

$$\rho = \frac{\rho^o V C_V T^o + C_P Q t T_o}{V C_V T} \tag{9}$$

From continuity

$$Qt = \rho V - \rho^{o} V \tag{10}$$

Substituting (10) into equation (9) and simplifying yields the following:

$$\frac{\rho - \rho^{o}}{\rho_o} = \frac{\rho T - \rho^{o} T^{o}}{\gamma \rho_o T_o} \tag{11}$$

where

$$\gamma = \frac{C_P}{C_V}$$

By substituting P/R for $\rho T$, etc. in equation (11), then

$$\frac{\rho}{\rho_o} - \frac{\rho^{o}}{\rho_o} = \frac{1}{\gamma} \left(\frac{P}{P_o} - \frac{P^{o}}{P_o}\right) \tag{12}$$

or

$$\frac{\rho}{\rho_o} - \frac{\rho^{o}}{\rho_o} = \frac{1}{\gamma} \left(\frac{1}{\lambda_T} - \frac{P^{o}}{P_o}\right) \tag{13}$$

where

$$\lambda_T = \frac{P_o}{P}$$

The expression for time (equation 6) finally reduces, therefore, to

$$t = \frac{V}{\gamma a_o A_1 M_1} \left(1 + \frac{\gamma - 1}{2} M_1^2\right)^{\frac{\gamma+1}{2(\gamma-1)}} \left(\frac{1}{\lambda_T} - \frac{P^{o}}{P_o}\right) \tag{14}$$

For

$V$ = 13000 cu. ft.

$\gamma$ = 1.4

$a_o$ = 1120 ft/sec

$A_1$ = 0.772 sq. ft.

$P_o$ = 2116 lb/sq.ft. = 14.7 lbs/sq.in.

$\lambda_T$ = estimate according to L. Grocco (see Figure I(1)).

$$t = \frac{11.48}{M_1}(1 + 0.2M_1^2)^3 \left(\frac{1}{\lambda_T} - \frac{P^o}{P_o}\right) \qquad (15)$$

This equation is shown graphically in Figure 2, where length of run, t, is plotted against Mach number, $M_1$, for various amounts of initial tank pressure, $P^o$.

B. Determination of test section pressure versus Mach number

$$P = P_o\left[1 + \frac{\gamma-1}{2} M_1^2\right]^{\frac{\gamma}{1-\gamma}} \qquad (16)$$

This equation is plotted in Figure 3 for $\gamma = 1.4$ and $P_o = 2116$ lbs/sq.ft.

C. Determination of test section density versus Mach number

$$\rho = \rho_o\left[1 + \frac{\gamma-1}{2} M_1^2\right]^{\frac{1}{1-\gamma}} \qquad (17)$$

This equation is plotted in Figure 3 for $\gamma = 1.4$ and $\rho_o = 0.002378$ slugs/cu.ft.

D. Determination of test section temperature versus Mach number

$$T = T_o\left[1 + \frac{\gamma-1}{2} M_1^2\right]^{-1} \qquad (18)$$

This equation is plotted in Figure 3 for $\gamma = 1.4$ and $T_o = 518.6$ °R = 59.0 °F.

E. Determination of Reynolds number versus Mach number

$$R = \frac{\rho V l}{\mu} \qquad (19)$$

where

$\rho$ = density

$v = Ma$ = velocity

$l$ = characteristic dimension

$\mu$ = viscosity

Knowing the test section temperature T, $\mu$ is determined from the relationship

$$\mu = \mu_o' \frac{T_o' + C}{T + C} \left(\frac{T}{T_o'}\right)^{3/2} \tag{20}$$

where

$\mu_o' = 3.725 \times 10^{-7}$ lb-sec/ft$^2$

$T_o' = 518.4$ °R

$C$ = constant = 216

Reynolds number versus Mach number is shown graphically in Figure 3 for a one-foot model.

# APPENDIX II

## DRYING STUDIES

### A. Influence of Various Coatings upon Balloon Fabric Permeability

A study has been made of the permeability of the balloon fabric and influence of coatings upon its permeability. The results so far obtained show that coatings based on a Saran* type resin give excellent resistance to moisture penetration. The ordinary type of varnishes using resins have relatively poor resistance, while waxes and paraffin materials have an intermediate resistance.

Tests were also conducted on metal foils to determine their permeability to water vapor. As would have been expected, their permeability is very low and the data so obtained will serve as a means of evaluating the coatings for the balloon cloth.

A coating has been prepared based on Saran resin with aluminum bronze powder as a pigment. In this way, it was hoped that the excellent qualities of Saran and metal foil could be combined. On the basis of uncompleted tests, this coating promises to be far superior to anything yet tried and to compare favorably with a metal foil on a basis of permeability. It has good wear and corrosion resistant properties.

#### Technical Considerations

The search for an impermeable coating has been carried on using techniques that are more or less standardized in the paint industry.

The general technique of testing paint films has involved the preparation and testing of the permeability of films independent of their

---

* Dow trademark (Modified Vinyl Type Resin).

application to a surface. The case of a cloth coating is somewhat different. Here the properties of the cloth and coating are closely intermingled and it would be unrealistic to try to distinguish the properties of the coating separately from those of the cloth. Therefore, the tests have been performed on the balloon cloth as coated and not on the coating material alone.

The usual method of preparing films of paints, varnishes, laquers, etc., is to dip amalgamated tin plates into the paint and to let them dry, the excess paint running off. A variation on this technique is to spin a disc of amalgamated tin in a horizontal position and to introduce the paint at the center of the plate. A more uniform film is secured in this way, Figure (a).

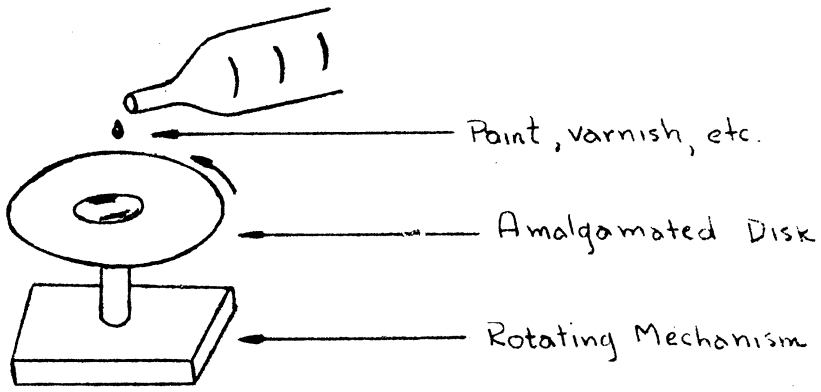


Figure (a). Apparatus for preparing paint films

The testing of the film for permeability involves creating a pressure differential across the film with respect to water vapor. This is conveniently accomplished by sealing the film across the top of a flat dish such as a petri dish, and creating a humidity differential across the film. Humidities ranging from 100 per cent to practically 0 per cent can be obtained by placing certain chemical salts inside the dish.

A sketch of the permeability measuring set-up is shown in Figure (b). A salt solution is placed in a petri dish and the top of the dish is

then sealed with the coated balloon fabric. The salt solution used is selected for the water vapor pressure which is to be established inside the dish. The petri dish is carefully weighed, and the unit is then placed in a desiccator which has water in its base. Because of the water, the relative humidity of the atmosphere of the desiccator is 100 per cent. Over a period of time, the weight of the petri dish is noted. This weight will constantly increase, and from the time rate of increase, the permeability factor can be obtained. This factor is the direct indication of the ability of the fabric to pass moisture vapor. The majority of these tests were made at 70°F. However, some were made at 100°F in order to check the influence of temperature.

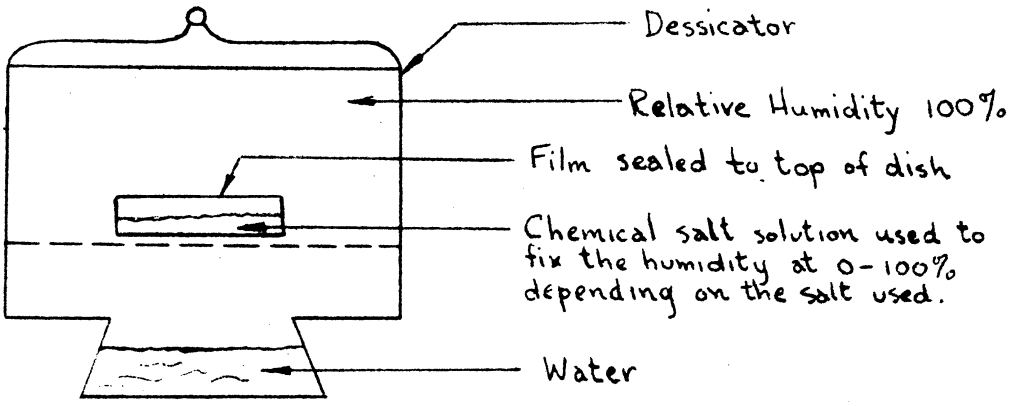


Figure (b). Apparatus used for determining permeability of films by water vapor

In Table II-1 are listed the relative humidities of the salt solutions existing inside the petri dish. Included also are the vapor pressure differentials in terms of millimeters of mercury. The fabrics tested are tabulated in Table II-2, and in Table II-3 are listed the chemical compositions of these coatings.

In Figure II (1) the permeability factor is plotted as a function of the vapor pressure differential for the various fabrics tested. From this plot it may be seen that coating 7 is desirable.

The plot of the permeability work done at 100°F is shown in Figure II (2). The data indicate that the relative influence of the various coatings remains approximately the same.

Theory

Grahams law of diffusion may be summarized in the following formula:

$$ds/dt = \frac{K(P_2 - P_1)\, T^{1/2}}{D\sqrt{M}}$$

$ds/dt$ = linear velocity of gas

$P_2 - P_1$ = pressure differential across film

$T$ = absolute temperature

$D$ = thickness of film

$M$ = molecular weight of diffuser gas

$K$ = proportionality factor depending on characteristics of the material.

This formula is based on the statistical chance that a molecule will follow a certain path. It assumes no affinity between the film and the gas. It is probable that no physical system actually follows Grahams law, but the diffusion of hydrogen or helium probably approaches it. If all systems followed Grahams law, the calculation of permeability would be a simple matter. In the case of water vapor penetrating organic materials, there is a profound effect of the water vapor on the material and its properties. The transmission of water vapor seems to be a combination of Grahams law diffusion and a chemical absorption whereby the water is "wicked" through the material and evaporated on the other side. The factors that affect Grahams law diffusion in a general way affect the transmission of water vapor through a film. However, the effect is not quantitative. For example, rubber passes

water vapor about 50 times as readily as hydrogen, and yet water is more dense than hydrogen.

The amount of water vapor that passes a film is related to the amount of "bound" water in the film. As a rule, the more "bound" water present, the faster the water passes the film. In the same manner of thought, a film will usually pass more water at a given pressure differential when the total humidity is high than it will when the total humidity is low.

In the same way, materials which have low affinity for water are, in general, less permeable to water vapor transmission than materials which have high water affinity.

Edwards and Wray* have shown how the rate of moisture penetration varies with humidity for a homogeneous film of paint, Figure (c). At the high levels of humidity the total "bound" moisture increases sharply and at

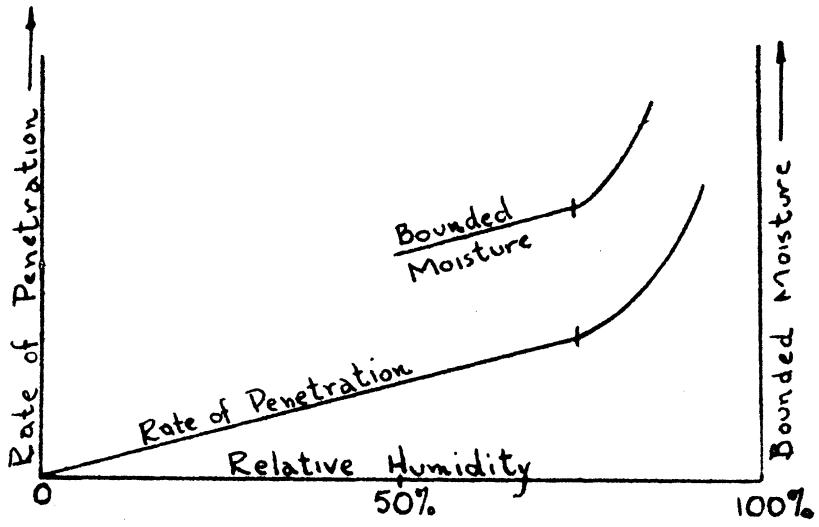


Figure (c). Relationship of "bound" moisture and rate of penetration with humidity on one side of a film. On the opposite sides, humidity was constant.

* Ind. Eng. Chem. 28, 549-53 (1936).

the same time the rate of penetration increases sharply. Where the film under consideration is made up of several layers of different materials, it is unlikely that the breaks in the curves for all the materials would occur simultaneously. The result would be a more gradual curvation over the entire humidity range. This presumption would fit cloth which is a multilayer fabric.

The rate of penetration, transmission, or diffusion is commonly called permeability and is expressed as a permeability factor

$$K = \frac{\text{Wt. of water passed}}{(\text{Unit Pressure Differential})(\text{Unit Area})(\text{Unit Time})}$$

and common units are

$$\text{Dimensions (K)} = \frac{\text{Milligrams } H_2O}{(\text{mm hg})(\text{cm}^2)(\text{Hr})}$$

Sometimes the thickness of the film is considered in the permeability factor and then the dimensions are

$$\text{Dimensions (K)} = \frac{\text{Milligrams}}{(\text{mm Hg})(\text{cm}^2)} \times \frac{H_2O}{(\text{hr})} \times \frac{1}{\text{mm}}$$

TABLE II-1

RELATING HUMIDITIES OF SALT SOLUTIONS USED

| Chem. Salt | Temp. | Rel. Hum. % | Vap. Press. mm Hg | Temp. | Rel. Hum. % | Vap. Press. mm hg |
|---|---|---|---|---|---|---|
| $H_2O$ | 70°F | 100 | 18.8 | 100°F | 100 | 49.2 |
| $KNO_3$ | 70°F | 94 | 17.6 | 100°F | 90 | 44.2 |
| $NH_4H_2PO_4$ | 70°F | 93 | 17.5 | 100°F | 93 | 45.7 |
| NaCl | 70°F | 76 | 14.3 | 100°F | 75 | 30.4 |
| MgCl | 70°F | 33 | 6.2 | 100°F | 31 | 15.2 |
| $P_2O_5$ | 70°F | 0 | 0.0 | 100°F | 0 | 0.0 |

TABLE II-2

FABRICS TESTED

| Cloth | |
|---|---|
| I | Balloon cloth treated with coating A. Saran, Amt. 0.0014 gm/cm$^2$ |
| II | Balloon cloth treated with coating B. Saran, Amt. 0.0013 gm/cm$^2$ |
| III | Balloon cloth treated with coating C. Paraffin, Amt. 0.0031 gm/mm$^2$ |
| IV | Balloon cloth treated with coating D. Glyptal varnish Amt. 0.0021 gm/cm$^2$ |
| V | Untreated balloon cloth |
| VI | Aluminum foil cemented to a fabric backing |
| VII | Balloon cloth treated with coating E. Saran and aluminum flakes |

TABLE II-3

COATINGS USED

A. Saran F-120 - 200 CPS

In a solution of 3 Vol. acetone and 1 Vol. cyclohexanone

17% F-120 - 200 CPS by wt.

B. Saran F-120 - 1000 CPS

3 Vol. acetone and 1 Vol. cyclohexanone

8.5% Saran F-120 - 1000 CPS by wt.

C. Paraffin Dissolved in Chloroform

30% by wt.

D. G. E. Glyptal with mineral spirit thinner and Manganese naphthanate dryer.

E. Vehicle - Methyl Ethyl Ketone

90% by wt., Saran F-120 - 2000 CPS, 10% by wt.

to this add:

Alcoa albron powder standard varnish

7.6% of wt. of vehicle

B. Computations on Dryer Size

Recognizing that the bag is permeable, a study was made of the influence of the various parameters involved in the flow circuit. The circuit consists of air taken from the bag, passed through the drier and then returned to the bag as shown in Figure (d).

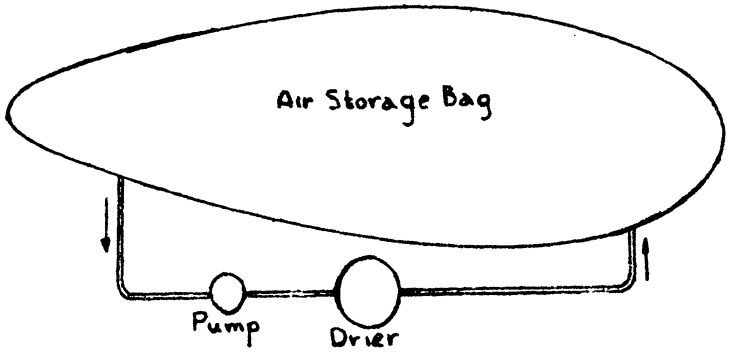


Figure (d). Drier Circuit

A fundamental assumption made is that the moisture conditions at the outlet of the drier are independent of the inlet moisture condition as long as the desiccant has not fully absorbed all the moisture it is capable of.

The following equations may be written:

$$dM/dt = dM_1/dt + dM_2/dt$$

where:

$t$ = time in seconds

$M$ = total mass of water per unit surface of fabric area

$M_1$ = mass of water vapor associated with bag permeability

$M_2$ = mass of water vapor associated with drier action

$$dM_1/dt = KRT\ (\rho_1 - \rho_2)$$

$$dM_2/dt = -\zeta\ (\rho_2 - \rho_o)$$

$$dM/dt = KRT\ (\rho_1 - \rho_2) - \zeta(\rho_2 - \rho_o)$$

$$M = \rho_2 V_2$$

with

$P$ = vapor pressure in pounds per square foot

$\rho$ = density of water vapor in slugs

$K$ = permeability constant in slugs per second per square foot per pounds per square foot

$R$ = gas constant for water vapor

$T$ = temperature in degrees Rankine; it is assumed $T_1 = T_2$

$V_2$ = volume inside balloon per unit surface area of fabric

$\zeta$ = flow rate through drier in C.P.S. per unit surface area of balloon fabric.

Subscripts:

1 = atmosphere conditions

2 = conditions inside the bag

0 = conditions at drier outlet

The following constants are required for calculation purposes:

Bag Surface Area = 4,400 $ft^2$

Bag Volume = 24,000 cu. ft.

Temperature = 550°R

Then

$$\frac{d\rho_2}{\frac{KRT\rho_1 + \zeta\rho_0}{KRT + \zeta} - \rho_2} = \frac{KRT + \zeta}{V_2}\, dt$$

$$\log\left\{\frac{KRT\rho_1 + \zeta\rho_0}{KRT + \zeta} - \rho_2\right\} = -\left\{\frac{KRT + \zeta}{V_2}\right\} t + C$$

Using the above equation, computations were made as to the influence of $\zeta$ and K upon the bag dew point.

In Figure II (3), bag dew point is plotted versus time. The calculations are made assuming a value of $K = 0.0214 \times 10^{-9}$ and a drier outlet dew

point of -40°F. The influence of $\zeta$ is shown in this figure.

Using this circulation technique, the bag dew point approaches a limit value as time approaches infinity. The equation used to compute this limit dew point is:

$$\frac{KRT\rho_1 + \zeta\rho_o}{KRT + \zeta} - \rho_2 = 0$$

By the above equation, the influence of K, $\zeta$ and $\rho_o$ upon the limit bag dew point for atmospheric conditions of temperature 90°F, and dew point of 70°F, are shown in Figure II (4).

Figure II (5) shows the influence of the atmospheric dew point upon the limit bag dew point for values of $\zeta$ of $0.5 \times 10^{-3}$ and $4 \times 10^{-3}$. From this curve it can be seen that by using a large drier flow rate, the effect of change in atmospheric dew point can be minimized.

The following conclusions may be drawn:

1. The influence of K upon the limit bag dew point decreases as $\zeta$ increases.

2. The limit bag dew point will approach the drier outlet dew point as $\zeta$ approaches infinity.

3. For a permeability constant of $K = 3 \times 0.0214 \times 10^{-9}$, a value of $\zeta$ of $4 \times 10^{-3}$ or larger is desired.

4. For values of $\zeta$ of $4 \times 10^{-3}$ or larger, operation of the tunnel could be started within two hours.

5. A drier should be selected which will consistently give dew points of -40°F or lower.

6. The fabric surface area should be kept as small as possible for a given drier size.

# APPENDIX III

## NOZZLE DESIGN

### A. Contour Design

The nozzles in question are designed after the method of Foelsch.* The salient features of the flow field of such a nozzle are:

(1) Source flow with radial streamlines in a region downstream of the throat.

(2) Patched to the source flow a field in which one family of characteristics is a family of straight lines. In this field the flow is turned from the radial streamlines into uniform and parallel flow.

### Discussion of the Method:

A property of the solution which is of importance is the fact that there is one degree of freedom, the angle between the walls in region (1). This makes it possible to specify any divergence angle up to a certain maximum value, retaining the same Mach number at the exit of the nozzle.

The chief merit of this method as compared with other methods is that the streamlines in region (2) are given by closed expressions. The streamline which is taken from the wall contour may therefore be calculated to any accuracy at as many points desired. This work may be done by anyone who is capable of using tables of mathematical functions and can use a computing machine. The graphical method requires a person with some theoretical background and skilled in drafting techniques.

*North American Report NA-46-235-2, "A New Method of Designing Two-Dimensional Laval Nozzles for a Parallel and Uniform Jet." by Kuno Foelsch. (1946)

The principle weakness of the method is that it is not possible to establish theoretically the source field which is the crux of the entire development. It is in fact necessary for the walls of the nozzle to be parallel at the throat. Consider the region (0) which extends from the throat to the downstream surface at which the flow has been turned into source flow with radial streamlines. It is necessary to design the walls of region (0) with no theoretical aid whatever. It should be pointed out, however, that this is a difficulty which is also suffered by the well known graphical methods for the design of nozzles. As a matter of fact source flow is often postulated in connection with the graphical methods exactly as in the present method.* If, on the other hand, a uniform and parallel flow at the throat is postulated the weakness is still present, since a method of designing a subsonic contraction which will ensure such a flow is not known. In view of the fact that all supersonic nozzle design methods may be criticized in this respect it is felt that the source flow assumption is not unreasonable.

It is not unlikely that a more careful treatment of the problem is possible since there is in existence some information concerning the flow at the throat which has not as yet been applied to the problem. For instance, by a linearization of the equation of motion near the sonic speed, Sauer has developed an appropriate approximation to the flow in the neighborhood of the throat.** This flow is incidentally not uniform and parallel. If the

*A Bailey and S.A. Wood, "The Conversion of the Stanton 3-in. High Speed Wind Tunnel to the Open-Jet Type." Proc. Inst. Mech. Eng. (London), 135, pp. 445-466. (1937)

**R. Sauer, "General Characteristics of the Flow Through Nozzle at Near Critical Speeds." NACA TM 1147 (1947)

method of characteristics were to be applied in a region bounded on the upstream side by this flow with the object of creating a source flow pattern farther downstream, one might find it possible to establish throat contours in a more theoretically satisfactory fashion.

Two functions, $r$ and $\psi$, are used continually in the nozzle calculations. As shown in Figure III-1, these quantities are the polar coordinates of the characteristic in source flow which originates at the intersection of the M = 1 circle with the x-axis.* All the other characteristics of this family are obtained by the addition of a constant to $\psi$, that is, by rotation. The characteristics of the second family are obtained by replacing $\psi$ by $-\psi$, that is, by reflection in a radial line. These quantities are related to M, the Mach number at each point of the source flow field by the equations:

$$\frac{r}{r_*} = \tau = \frac{(M^2 + 5)^3}{216M} \tag{1}$$

$$\psi = \sqrt{6}\tan^{-1}\sqrt{\frac{M^2 - 1}{6}} - \tan^{-1}\sqrt{M^2 - 1} \tag{2}$$

The value of the gas constant $\gamma$ has been taken as 1.4, $r_*$ is the value of $r$ when M = 1 and is therefore the radius of the M = 1 circle.

This source flow field continues on the nozzle axis to the point Q where the final desired Mach number is reached, Figure III-2. The pair of characteristics which pass through Q are the patching lines which patch the source flow region (1) onto the region (2) where the radial streamlines are turned into uniform and parallel flow. The same pair of characteristics when extended downstream of Q are the patching lines which patch region (2) onto

*For an exiomatic treatment of the theory of characteristics see Edmonson, Murnaghan and Snow, "The Theory and Practice of Two-Dimensional Supersonic Pressure Calculations," Bumblebee Report No. 26. (1945)

the region of uniform and parallel flow. The point Q is therefore common to regions(1) and (2) and also the region of uniform and parallel flow. Region (2) is given by AQB in Figure III-2 where A and B lie on a streamline which has been arbitrarily selected.

In the original report by Foelsch it is stated that one family of characteristics in region (2) is a family of straight lines and a geometrical argument (the same one used in the approximate graphical construction method) is offered to support the statement. In the Bumblebee Report No. 26, however, the following theorem is quoted and proved:

> The patching curve which patches a uniform flow to a second flow (uniform or non-uniform) is not only a straight line but is a family of straight lines each of which is a patching curve; furthermore the velocity vector is constant along each member of this family of straight lines.

This theorem is applicable to the flow of region (2) and justifies the use of the family of straight line characteristics. Moreover, it determines the flow conditions at every point of region (2) since at the points where the straight line characteristics intersect the source flow characteristic QA the slope must coincide with the slope of the corresponding source flow characteristics which are known. Since the flow in region (2) is completely defined it is possible to calculate the streamlines in region (2). Foelsch presents this result.

Consider the streamline passing through point A, Figure III-3. In the source flow field its inclination is given by $\nu = \psi_E - \psi_A$, since $\psi$ is different from the polar coordinate angle $\theta$ by a constant and the equations of the source flow streamlines are $\theta$ = constant. In region (2) the equations of the source flow streamlines are in parametric form with the Mach number of

patchine line A as the parameter. The equations are:

$$\frac{x}{h} = \frac{\cos(\psi_E - \psi)}{2\nu} \frac{\tau}{\tau_E} \left\{ 1 + (\psi - \psi_A)\left[\sqrt{M^2 - 1} - \tan(\psi_E - \psi)\right]\right\} \quad (3)$$

$$\frac{y}{h} = \frac{\sin(\psi_E - \psi)}{2\nu} \frac{\tau}{\tau_E} \left\{ 1 + (\psi - \psi_A)\left[\sqrt{M^2 - 1} + \cot(\psi_E - \psi)\right]\right\} \quad (4)$$

$$M_A = M = M_E$$

where h is the nozzle depth, x is measured from the source point and y is measured from the nozzle axis.

Nozzle Calculations:

When a nozzle is to be designed one knows h, the height of the test section and $M_E$ the desired test section Mach number. The maximum included angle between the nozzle walls, $2\nu$ is usually specified also. $\psi_E$ is found by using $M = M_E$ in formula (2). $\psi_A = \psi_E - \nu$ may then be found. One then finds $M_A$ from equation (2). When these constants have been evaluated the design formulas (3) and (4) yield the nozzle contour between A and B. For the calculation there are presented in Foelsch's report plots of $\psi$ and $\tau$. These plots are inadequate, however, if it is necessary to calculate contours to an accuracy of $\pm$ 0.0005 inch on nozzles of the size used by the University of Michigan. It has been found practical to calculate these functions as needed making use of tables such as those put out by the WPA Mathematical Tables Project. Upstream of point A the contour is the source streamline $x = r\cos\nu$, $y = r\sin\nu$. When h, $M_E$, and $\nu$ are given they are sufficient to determine the length of the supersonic portion of the nozzle. Strictly speaking the throat contour must also be given but the length of the nozzle is approximately $x_E - x_o$. This quantity is plotted in Figure III-4.

The throat sections of the present nozzles have been generated by an arc of a circle subject to the condition to tangency to the straight-line portion of the nozzle and giving the appropriate throat depth which is found from the one-dimensional flow equations. If the circular arc is to be tangent to the straight line portion of the contour an upper limit to the radius exists which makes the curvatuve at the throat quite great for large $\mathcal{V}$. Apart from this consideration, the radius is arbitrary.

There is no satisfactory theory which gives the boundary layer thickness on the nozzle walls. If it is necessary to make some correction the method described in part B below will be used. This method is probably no worse than any other and gives reasonable values when applied to nozzles.

## B. Calculation of Boundary Layer Thickness

The property of boundary layers which affects nozzle design is the displacement thickness. If the dimensions of the cross-section of a channel are reduced by the value of the displacement thickness, the effective area is found. This effective area is the quantity which determines the Mach number of the flow. Experimental evidence indicates that the effect is small for the nozzle which operates at low Mach numbers, but that the effect increases with Mach number. The displacement thickness is small at the throat and usually is considered to be zero there but it increases downstream of the throat. The effective area ratio is thereby diminished resulting in a Mach number smaller than the value computed for a frictionless gas. If the displacement thickness can be accurately estimated the nozzle designed for a frictionless gas can be altered so that the design Mach number may be obtained. Also the nozzle contours may be altered so that uniform parallel flow is obtained.

The results of the calculations indicated herein have been applied to nozzles of Mach numbers 2 and 4. The calcuations confirm the general trends noted above. For 33.5" nozzles discharging from an atmospheric reservoir to a Mach number $M_E$ at an 8" x 13" cross-section, the following data has been computed. Subscripts T and E indicate nozzle throat and nozzle exit respectively. $\Delta A_E$ is the amount $A_E$ is diminished by the presence of the boundary layer. $\Delta M_E$ is the change in Mach number obtained in a nozzle due to the presence of a boundary layer.

| $M_E$ | $E^*$ | $(\Delta A_E/A_T)$ | $\Delta M_E$ |
|---|---|---|---|
| 2 | 0.131" | 0.178 | -0.127 |
| 4 | 0.479" | 2.013 | -0.210 |

1. Nomenclature

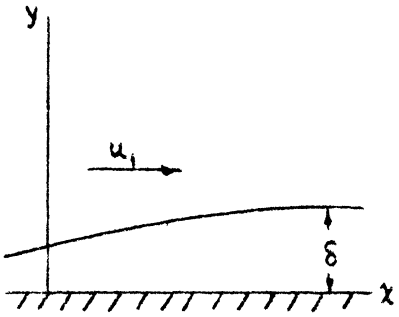


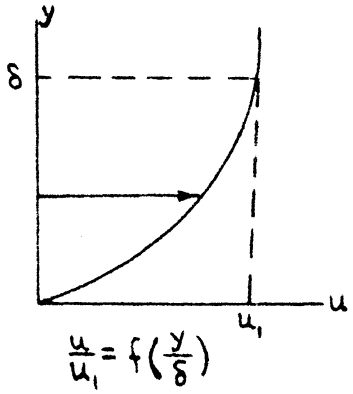


Subscript $(\ )_1$ indicates free stream conditions outside of the boundary layer.

A = cross-sectional area of the nozzle

u = velocity, (ft/sec)

x = distance along wall, (ft.)

y = distance normal to wall, (ft.)

$p$ = pressure ($lb/ft^2$)

$\rho$ = mass density, ($slugs/ft^3$)

$\tau_o$ = skin friction stress at wall, ($lb/ft^2$)

$cf$ = friction coefficient = $\dfrac{2\tau_o}{\rho_1 u_1^2}$

$\delta$ = total boundary layer thickness, $\dfrac{u}{u_1} \approx 1$ at $y = \delta$

$*$ = displacement thickness of boundary layer = $\displaystyle\int_o^{\delta} \left(1 - \frac{\rho u}{\rho_1 u_1}\right) dy$

$\theta = \displaystyle\int_o^{\delta} \frac{\rho u}{\rho_1 u_1} \left(1 - \frac{u}{u_1}\right) dy$

$T$ = absolute temperature, degrees Rankine,
$C_v$, $C_p$, $R$; gas constants, ft-lb/$^oR$

$\gamma = C_v/C_p$

$M$ = Mach number

$R_e$ = Reynolds number

2. Assumptions

Three approximating assumptions are made in the development of this method.

A. $\dfrac{\partial p}{\partial y} = 0$ through the boundary layer.

B. The velocity profile of the boundary layer,

$\dfrac{u}{u_1} = \left(\dfrac{y}{\delta}\right)^{1/7}$, is invariant with $M_1$ and $R_e$.

C. The value for skin friction coefficient is given by

$$\frac{1}{2} c_f = \frac{\tau_o}{\rho_1 u_1^2} = \frac{0.0225}{\left(\dfrac{u_1 \delta}{\nu_1}\right)^{1/4}}$$

The first assumption is undoubtedly a very good one since it is an experimental fact that wall pressure measurements and actual free stream pressures in nozzles are practically identical in expansive flow which is free of shocks. This can also be shown by an order of magnitude analysis of the pressures through a boundary layer.

Assumption (B) is a less satisfactory one. Since no measurements of velocities in a supersonic boundary layer are available, one can only guess the profile and hope the results are not seriously affected by a different profile. If new information on velocity profiles becomes available it can be incorporated into the general procedure outlined below. At this time, with no suitable data giving Reynolds number and Mach number effects, the profile $(u/u_1) = (y/\delta)^{1/7}$ is believed to be a reasonable candidate. This profile is an excellent choice for a turbulent boundary layer of an incompressible fluid.

Assumption (C) is also taken from the semi-empirical theory of incompressible fluid boundary layers. The value used for $c_f$ is the one which is associated with the 1/7 power boundary layer.*

## 3. Derivation of Evaluation for $\delta^*$

The momentum equation of the boundary layer is integrated to obtain an expression for $\delta^*$. When the momentun equation is derived the following form is obtained:

$$\tau_o = \frac{d}{dx}(\rho_1 u_1^2 \theta) + \rho_1 u_1 \delta^* \frac{du_1}{dx} \qquad (1)$$

All these quantities are assumed to vary with x. For each given nozzle $M_1$ can be found as a function of x. This can best be calculated by the one-dimensional equation relating $M_1$ and area ratio of the nozzle. This approximation is

*S. Goldstein, "Modern Developments in Fluid Mechanics" P. 361

sufficiently accurate in view of assumptions (B) and (C). Therefore the following functions are known:

$$M_1 = M_1 (x) \tag{2}$$

$$dx = \frac{dM_1}{dM_1/dx} \tag{3}$$

Equation (1) may be expanded to obtain -

$$\frac{d\theta}{dx} + \frac{\theta}{\rho_1}\frac{d\rho_1}{dx} + (2\theta + \delta^*)\frac{1}{u_1}\frac{du_1}{dx} = \frac{\tau_o}{\rho_1 u_1^2} \tag{4}$$

The quantities $\rho_1$ and $u_1$ are the values of density and velocity outside the boundary layer and are therefore related to $M_1$ by isentropic equations.

$$\frac{\rho_1}{\rho_o} = \left(1 + \frac{\gamma - 1}{2} M_1^2\right)^{-1/(\gamma - 1)}$$

$$\log \rho_1 - \log \rho_o = \frac{-1}{\gamma - 1} \log \left(1 + \frac{\gamma - 1}{2} M_1^2\right)$$

$$\frac{d\rho_1}{\rho_1} = - \frac{M_1 dM_1}{1 + \frac{\gamma - 1}{2} M_1^2}$$

Hence

$$\frac{\theta}{\rho_1}\frac{d\rho_1}{dx_1} = - \frac{\theta M_1}{1 + \frac{\gamma - 1}{2} M_1^2}\frac{dM_1}{dx} \tag{5}$$

Also

$$u_1 = a_1 M_1 = \frac{a_o M_1}{\left(1 + \frac{\gamma - 1}{2} M_1^2\right)^{1/2}}$$

$$\log u_1 = \log a_o + \log M_1 - \frac{1}{2} \log \left(1 + \frac{\gamma - 1}{2} M_1^2\right)$$

$$\frac{du_1}{u_1} = \frac{dM_1}{M_1} - \frac{\gamma - 1}{2} \frac{M_1 dM_1}{\left(1 + \frac{\gamma - 1}{2} M_1^2\right)}$$

$$= \frac{dM_1}{M_1 \left(1 + \frac{\gamma - 1}{2} M_1^2\right)}$$

Hence $$(2\theta + \delta^*)\frac{1}{u_1}\frac{du_1}{dx} = \frac{2\theta + \delta^*}{M_1\left(1 + \frac{\gamma - 1}{2} M_1^2\right)}\frac{dM_1}{dx} \qquad (6)$$

When equations (5) and (6) are substituted in equation (4) one obtains

$$\frac{d\theta}{dx} + \frac{(2 - M_1^2)\,\theta + \delta^*}{M_1\left(1 + \frac{\gamma - 1}{2} M_1^2\right)}\frac{dM_1}{dx} = \frac{\tau_o}{\rho_1 u_1^2} \qquad (7)$$

Substituting the identity

$$\frac{d\theta}{dx} = \frac{d\left(\delta^* \theta/\delta^*\right)}{dx} = \frac{\theta}{\delta^*}\frac{d\delta^*}{dx} + \delta^* \frac{d\left(\theta/\delta^*\right)}{dx}$$

and rearranging terms, (7) becomes

$$\frac{d\delta^*}{dx} + \delta^*\left\{\frac{\delta^*}{\theta}\frac{d(\theta/\delta^*)}{dx} + \frac{(2 - M^2 + \delta^*/\theta)\, dM_1/dx}{M_1\left(1 + \frac{\gamma - 1}{2} M_1^2\right)}\right\} = \frac{\tau_o}{\rho_1 u_1^2}\frac{\delta^*}{\theta} \qquad (8)$$

This equation should be thought of as a first order linear differential equation of the type -

$$\frac{d\delta^*}{dx} + P(x)\,\delta^* = Q(x) \qquad (9)$$

The quantity $M_1$ which appears in the P (x) term is a known function of x given by equation (2).

Under assumptions A and B it will now be shown that $\theta/\delta^*$ is also a known function of x. The quantities of $\delta^*$ and $\theta$ are defined:

$$\delta^* = \int_o^\delta \left(1 - \frac{\rho u}{\rho_1 u_1}\right) dy = \delta \int_o^1 \left(1 - \frac{\rho u}{\rho_1 u_1}\right) d\left(\frac{y}{\delta}\right) \qquad (10)$$

$$\theta = \delta \int_0^1 \frac{\rho u}{\rho_1 u_1} \left(1 - \frac{u}{u_1}\right) d\left(\frac{y}{\delta}\right) \tag{11}$$

Hence, $\theta/\delta^*$ is a dimensionless number independent of $\delta$. $u/u_1$ is a known function of $y/\delta$ under assumption (B).

$$\frac{u}{u_1} = \left(\frac{y}{\delta}\right)^{1/7} \tag{12}$$

Under assumption (A), p = const., through the boundary layer, the equation of state for a gas becomes

$$\frac{\rho_1}{\rho} = \frac{T}{T_1} \tag{13}$$

It can be shown that the energy equation, which holds through a boundary layer, may be put in the form

$$\frac{T}{T_1} = 1 + \frac{\gamma - 1}{2} M_1^2 \left(1 - \frac{u^2}{u_1^2}\right) \tag{14}$$

The integrals (10) and (11) can now be evaluated using relations (12), (13), and (14). $M_1$ is constant for this integration. The results are -

$$\delta^* = \delta \left\{ 1 - \frac{7}{(\gamma - 1) M_1^2} \left[ b^6 \log \frac{b^2}{b^2 - 1} - \left(b^4 + \frac{b^2}{2} + \frac{1}{3}\right) \right] \right\} \tag{15}$$

$$\theta = 7(b^2 - 1) \left[ \frac{b^6}{2} \log \frac{b^2}{b^2 - 1} - \frac{b^7}{2} \log \frac{b + 1}{b - 1} + b^6 - \frac{b^4}{6} - \frac{b^2}{20} - \frac{1}{42} \right] \tag{16}$$

Where

$$b^2 = \frac{1 + \frac{\gamma - 1}{2} M_1^2}{\frac{\gamma - 1}{2} M_1^2}$$

Curves for $\delta^*/\delta$, $\theta/\delta$ and $\delta^*/\theta$ as functions of $M_1$ are given in Figure III-5.

Therefore P in equation (9) is a known function of x.

The quantity $\frac{\tau_o}{\rho_1 u_1^2} = \frac{0.0225}{\left(\frac{u_1 \delta}{\nu_1}\right)^{1/4}}$ which appears in Q must be found by a step-by-step process. $u_1/\nu_1$ is Reynold's number per foot and is given in Figure III-7 as a function of $M_1$ for an expansion from a reservoir at atmospheric conditions.

Equation (9) when integrated becomes -

$$\delta^*(x) = \left\{ \int (Qe^{\int Pdx})\, dx + \text{const} \right\} e^{-\int Pdx}$$

If the integration is performed between limits,

$$\delta^*(x) = \left\{ \int_o^x (Qe^{\int_x Pdx})\, dx + \text{const.} \right\} e^{-\int_x Pdx}$$

Substituting x = 0, $\delta^*(0) = \delta^*_o = (\text{const})\, e^{-\int_x Pdx}$

$$\text{const.} = \delta^*_o\, e^{\int_x Pdx}$$

$$\delta^*(x) - \delta^*_o = \left\{ \int_o^x (Qe^{\int_x Pdx})\, dx \right\} e^{-\int_x Pdx} \qquad (17)$$

This result is not affected by choice of lower limit in the expression $\int_x Pdx$. Equation (17) is a general result being independent of assumptions (A), (B) and (C).

Simplification of Integrals

$$e^{\int_x Pdx} = \exp\left\{ \int_o^x \left[ \frac{\delta^*}{\theta} \frac{d(\theta/\delta^*)}{dx} + \frac{2 - M_1^2 + \delta^*/\theta}{M_1\left(1 + \frac{\gamma - 1}{2} M_1^2\right)} \frac{dM_1}{dx} \right] dx \right\}$$

$$= \exp\left\{ \log \frac{\theta}{\delta^*} \Big]_o^x + \int_o^x \left[ \frac{2 - M_1^2 + \delta^*/\theta}{M_1\left(1 + \frac{\gamma - 1}{2} M_1^2\right)} \frac{dM_1}{dx} \right] dx \right\}$$

$$= \left[\frac{\theta/\delta^*}{(\theta/\delta^*)_{x=o}}\right] \exp\left\{\int_{M_1(o)}^{M_1(x)} \frac{2 - M_1^2 + \delta^*/\theta}{M_1\left(1 + \frac{\gamma - 1}{2} M_1^2\right)} dM\right\}$$

by equation (3).

By definition, $g(M_1) = e^{\int_o^x P dx}$. With the aid of Figure III-5 the function $g(M_1)$ was calculated by numerical integration. Figure III-6 has a plot of this function. Therefore, from equation (17)

$$\delta^*(x) - \delta^*_o = \frac{1}{g} \int_o^x \left[\left(\frac{\tau_o}{\rho_1 u_1^2}\right)\left(\frac{\delta^*}{\theta}\right) g\right] dx \qquad (18)$$

since $$Q = \left(\frac{\tau_o}{\rho_1 u_1^2}\right)\frac{\delta^*}{\theta}$$

The usual assumption made at this point is that the thickness of the boundary layer is zero at the sonic throat. Assuming this and taking x = o at the throat one gets the following equation.

$$\delta^*(x) = \frac{1}{g} \int_o^x \left[\left(\frac{\tau_o}{\rho_1 u_1^2}\right)\left(\frac{\delta^*}{\theta}\right) g\right] dx \qquad (19)$$

4. Application to a Nozzle

Equation (19) may be conveniently solved by an iteration process. The nozzle axis should be divided into a suitable number of intervals. Then since Mach number is known at every station, g and $(\delta^*/\theta)g$ can be found from Figure III-6. The quantity $\tau_o/\rho_1 u_1^2 = 0.0225/(u_1 \delta / \nu_1)^{1/4}$ may be found from Figure III-7 which gives $u_1/\nu_1$ (Reynolds number per foot) as a function of Mach number, and from the value of $\delta$ calculated in the previous step. A sample calculation for a Mach number 2 nozzle is given in the following table.

## SAMPLE CALCULATION OF BOUNDARY LAYER THICKNESS

M = 2 Nozzle

$$\delta^* = \frac{1}{g}\int_0^x \left(\frac{\tau_0}{\rho_1 u_1^2}\right)\left(\frac{\delta^*}{\theta}\right) g \, dx$$

$$\frac{\tau_0}{\rho_1 u_1^2} = \frac{0.0255}{\left(\frac{u_1 \delta}{\nu_1}\right)^{1/4}} \quad , x \neq 0$$

$$= 0.0225 \quad , x = 0$$

| (1) | (2) | (3) | (4) | (5) | (6) | (7) | (8) | (9) | (10) | | | |
|---|---|---|---|---|---|---|---|---|---|---|---|---|
| x " | $M_1$ | $\frac{\delta^*}{\theta} g$ | $\frac{\delta^*}{\theta} g \frac{\tau_0}{\rho_1 u_1^2}$ | $\sum(4)$ | g | $\delta^*$ (in.) | $\frac{\delta^*}{\delta}$ | $\delta$ (ft.) | $\frac{u_1}{\nu_1} \times 10^{-6}$ | $\frac{u_1}{\nu_1}\delta$ | $\left(\frac{u_1}{\nu_1}\delta\right)^{1/4}$ | $\frac{\tau_0}{\rho_1 u_1^2}$ |
| 0 | 1 | 1.733 | - | 0 | 1 | 0 | - | - | - | - | - | .0025 |
| 5 | 1.25 | 2.77 | .0216 | .0216 | 1.386 | .0156 | .175 | .0074 | 4.85 | 36,100 | 13.78 | .001633 |
| 10 | 1.55 | 3.86 | .0226 | .0442 | 1.650 | .0268 | .198 | .0113 | 4.50 | 50,700 | 15.00 | .001500 |
| 15 | 1.76 | 4.52 | .0290 | .0732 | 1.695 | .0432 | .216 | .0166 | 4.20 | 70,000 | 16.26 | .001384 |
| 20 | 1.89 | 4.84 | .0313 | .1045 | 1.679 | .0623 | .226 | .0229 | 3.99 | 91,500 | 17.39 | .001295 |
| 25 | 1.97 | 4.97 | .0313 | .1358 | 1.645 | .0825 | .234 | .0294 | 3.84 | 115,900 | 18.45 | .001220 |
| 30 | 2.00 | 5.01 | .0303 | .1661 | 1.631 | .1019 | .236 | .0360 | 3.80 | 129,500 | 18.96 | .001187 |
| 33.5 | 2.00 | 5.01 | .0199 | .1860 | 1.631 | .1140 | - | - | - | - | - | - |

# APPENDIX IV

## CALCULATIONS OF THE TIME REQUIRED TO BRING BALLAST TANK TO SAME PRESSURE AS THAT OF TEST SECTION, UTILIZING VENT NOZZLES

### Nomenclature

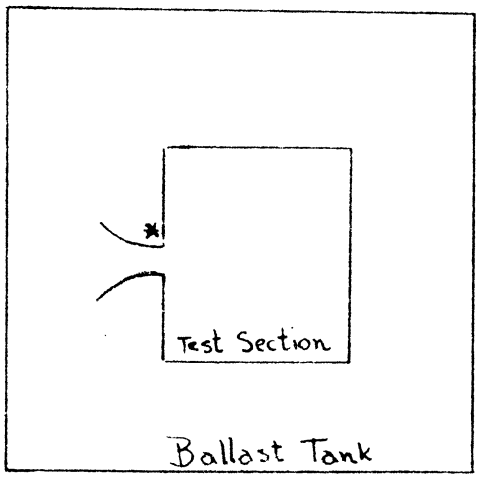


$P_o$, $\rho_o$, $T_o$: Tank conditions at t = o

$P$, $\rho$, $T$: Tank conditions at t = t

$P_1$, $\rho_1$, $T_1$: Tank conditions at $t = t_1$ when $P_e/P = .527$

$P_e$, $\rho_e$, $T_e$: Test section conditions and conditions within tank at final $t = t_e$

$P^*$, $\rho^*$, $A^*$: Vent nozzle throat conditions

where:

$P$ = pressure in lbs/sq.ft.

$\rho$ = slugs/ft$^3$ (lb. sec$^2$/ft$^4$)

$T$ = temperature in °F abs.

$A^*$ = throat area in sq. ft.

$V$ = volume of ballast tank (cu. ft.)

$R$ = gas constant 1715 ft$^2$/sec$^2$ °F

$u,a$ = velocities in ft/sec.

$M$ = slugs (lb. sec$^2$/ft.)

$m$ = mass flow, slugs/sec. (lb. sec/ft.)

The problem is considered in two parts:

I. Calculation of time required to diffuse supersonically, $t_o$ to $t_1$.

That is, for $\frac{P_e}{P_o} \leq \frac{P_e}{P} \leq .527$

II. Calculation of time required to diffuse subsonically, $t_1$ to $t_e$.

That is, for $1 \geqq \frac{P_e}{P} \geqq .527$

I. Calculation of the Time Required to Diffuse Supersonically

The mass flow per second at the vent nozzle is equal to the mass discharge of the tank per second:

$$\rho^* A^* a^* = -V \frac{d\rho}{dt} \tag{1}$$

Assuming an adiabatic expansion,

$$\rho = \frac{\rho_o}{P_o^{1/\gamma}} P^{1/\gamma} \tag{2}$$

and

$$d\rho = \frac{1}{\gamma} \frac{\rho_o}{P^{1/\gamma}} P^{\frac{1-\gamma}{\gamma}} dP \tag{3}$$

also,

$$\rho^* = \rho_o \left(\frac{P}{P_o}\right)^{1/\gamma} \left(\frac{2}{\gamma+1}\right)^{\frac{1}{\gamma-1}} \tag{4}$$

and $a^*$ can be reduced to

$$a^* = \left(\frac{2}{\gamma+1}\right) \left(\frac{1}{\rho_o} P_o^{1/\gamma} P^{\frac{\gamma-1}{\gamma}}\right)^{1/2} \tag{5}$$

Substituting (3), (4) and (5) into equation (1), and simplifying yields the following:

$$\frac{dP}{dt} = C_1 P^{\frac{3\gamma-1}{2\gamma}} \tag{6}$$

where

$$C_1 = -\frac{A^*}{V} \gamma^{3/2} \left(\frac{2}{\gamma+1}\right)^{\frac{\gamma+1}{2(\gamma-1)}} \left(\frac{1}{\rho_o}\right)^{1/2} P_o^{\frac{1}{2\gamma}} \tag{7}$$

By integrating equation (6),

$$t \Big]_{t_2}^{t_1} = C_2 P^{\frac{1-\gamma}{2\gamma}} \Big]_{P_o}^{P_1} \tag{8}$$

where

$$C_2 = \left[ \frac{A^*}{V} \gamma^{1/2} \left(\frac{\gamma - 1}{2}\right) \left(\frac{2}{\gamma + 1}\right)^{\frac{\gamma + 1}{2(\gamma-1)}} \left(\frac{1}{\rho_o}\right)^{1/2} P_o^{\frac{1}{2\gamma}} \right]^{-1} \tag{9}$$

Setting $t_o = 0$, equation (8) becomes

$$t_1 = C_2 \left(P_1^{\frac{1-\gamma}{2\gamma}} - P_o^{\frac{1-\gamma}{2\gamma}}\right) \tag{10}$$

for

$$P = 1.4$$

$$P_o = 2116 \text{ lb/sq.ft.}$$

$$\rho_o = .002378 \text{ slugs per cu.ft.}$$

$$V = 50 \text{ cu. ft.}$$

$$P_e = 2116\ (.00653) = 13.9 \text{ lb/sq.ft. (Mach 4 case)}$$

$$P_1 = \frac{13.9}{.527} = 26.4 \text{ lbs/sq.ft.}$$

equation (10) becomes

$$t_1 = \frac{.339}{A^*} \tag{11}$$

## II. Calculation of the Time Required to Diffuse Subsonically

It can be shown that

$$-V \frac{d\rho}{dt} = A^* \sqrt{\frac{2\gamma}{\gamma - 1} P\rho \left(\frac{P_e}{P}\right)^{\frac{2}{\gamma}} \left[1 - \left(\frac{P_e}{P}\right)^{\frac{\gamma-1}{2\gamma}}\right]} \tag{12}$$

which can be reduced to

$$dt = C_3 \left[1 - b^2 P^{2a}\right]^{-\frac{1}{2}} P^{3a}\, dP \tag{13}$$

where

$$C_3 = -\frac{V}{A^*} \left(\frac{\gamma - 1}{2\gamma^3}\right)^{1/2} \rho_o^{1/2} \left(\frac{1}{P_o}\right)^{\frac{1}{2\gamma}} \left(\frac{1}{P_e}\right)^{\frac{1}{\gamma}} \tag{14}$$

$$b = \left(\frac{1}{P_e}\right)^{\frac{1-\gamma}{2\gamma}} \tag{15}$$

$$a = \frac{1}{2}\left(\frac{1-\gamma}{\gamma}\right) \tag{16}$$

Setting

$$P = \left[\frac{1}{b}\sin\alpha\right]^{\frac{1}{a}} \tag{17}$$

and substituting in equation (13) and integrating,

$$t\Big]_{t_1}^{t_e} = \frac{C_3}{ab^{\left(\frac{3a+1}{a}\right)}}\int_{\alpha_1}^{\alpha_e}\sin^{\left(\frac{2a+1}{a}\right)}\alpha\, d\alpha \tag{18}$$

If $\frac{2a+1}{a}$ is an integer number, which it is for $\gamma = 1.4$, equation (18) can be conveniently solved. For $\gamma = 1.4$, $\frac{2a+1}{a} = -5$ and (18) can be rewritten as

$$t\Big]_{t_1}^{t_e} = \frac{C_3}{ab^{\left(\frac{3a+1}{a}\right)}}\int_{\alpha_1}^{\alpha_e}\frac{d\alpha}{\sin^5\alpha} \tag{19}$$

The solution of this equation yields

$$t\Big]_{t_1}^{t_e} = \frac{C_3}{ab^{\left(\frac{3a+1}{a}\right)}}\left[-\frac{1}{4}\frac{\cos\alpha}{\sin^4\alpha} - \frac{3}{8}\frac{\cos\alpha}{\sin^2\alpha} + \frac{3}{8}\log\tan\frac{\alpha}{2}\right]_{\alpha_1}^{\alpha_e} \tag{20}$$

For the values of $\gamma$, $P_o$, $\rho_o$, V, $P_1$, and $P_e$ given previously, equation (20) becomes

$$t_e - t_1 = \frac{.1013}{A^*} \tag{21}$$

Substituting this in equation (11), an expression for the total time can be obtained

$$t_e = \frac{.440}{A^*} \qquad \text{(Mach 4 case)} \tag{22}$$

Equation (22) gives the time required to equalize ballast tank and test section pressures when the tunnel is operated at Mach 4. When the tunnel is operated at Mach 2, $P_e = 2116\ (.1278) = 270$ lb/sq.ft. and $P_1 = \frac{270}{.572} = 472$ lbs/sq.ft. The equation for $t_e$ then becomes,

Since one of the factors which often serves to introduce errors into experimental work involving measurements with wire strain gages is temperature effect on the electrical zero of the equipment, a preliminary investigation was undertaken to determine the magnitude of this effect. It was found that, during the warm-up period of the power supply and amplifier units, there is a definite drift of the zero caused by the temperature unbalance of that half of the bridge circuit which is internal to the recording equipment. However, as shown in Figure V (3), for the amplifications which will ordinarily be used with the balance system (gains 6 to 18 which are lower amplifications than gain 3) a warm-up period of two hours will be ample to insure that this effect will be negligibly small for the time interval of a standard run (maximum of 20 seconds). Maximum amplification was used for this investigation.

The temperature effect on the external half of the bridge circuit, the two wire strain gages, and the leads connecting them to the amplifier, will be extremely small over the short duration of a standard run. The gages (standard Baldwin-Southwark Type SR-4 gages) are mounted immediately adjacent to each other and are outside of the walls of the tunnel channel, in a region which is not directly affected by the temperature variations within the channel. So long as any changes in temperature occur simultaneously in both gages, no zero shift will occur.

With the temperature effects accounted for, the calibration of the element itself was carried out. The wire gages mounted on opposite sides of the cantilever beam are inserted in opposite arms of the bridge circuit. With the beam in bending, that gage on the tension side increases the resistance in one arm of the bridge, the gage on the compression side decreases the resistance in the opposing arm, and the combination effectively doubles the strain-

sensitivity of the circuit. On the other hand, if the beam is put in pure compression (or pure tension), instead of bending, both gages decrease (or increase) the resistance of their respective bridge arms the same amount, and no change is recorded. Thus, this system actually records only bending strains. The first calibration tests revealed a large inconsistency in data in Ranges 2 and 3, but not in Range 1. A discontinuity in slope at the origin of the load-strain curves was observed in all ranges. This evidence indicated mechanical looseness in the assembly. The unit was modified to provide more secure clamping of the beams at the base, and the roller clutch mechanisms were selectively tightened to less than .0005-in. clearance. A second set of tests was then begun, and the data obtained were very consistent.

Results of these tests are shown in Figures V (4) to V (9). For Range 1, Figures V (4) and V (5), the load-strain (load-current or load-oscillograph scale reading) relation was consistently linear from zero to one pound regardless of whether the beam was loaded progressively from zero to full-scale or unloaded from full-scale to zero. The Range 2 calibration was comparable for one direction of loading only. When the load was applied as shown in Figure V (7), the results were linear and repeatable. When the beam was inverted and thereby loaded in the opposite direction, an offset in the data appeared between 6.0 and 7.0 lbs., as shown in Figure V (6). The results were consistent, however. Range 3 data for the same direction of loading showed the same characteristic at the identical load point (see Figure V (8). In addition to the offset region, the Range 3 data indicated sensitivity of the unit to loading technique. If the loads were progressively increased and decreased in 50-lb. ranges, two loops were formed as shown in Figures V (8) and (9). Since steps were taken to eliminate effects of static friction during the runs, it was

concluded that the hysteresis loops, as well as the offset characteristic, were the result of interplay among the beams and clutch assembly.

The calibration data indicated that ±3 per cent accuracy (based on full-scale readings) was the best obtainable for Range 3, although ±1 per cent accuracy was available from Ranges 1 and 2. In order to improve the over-all accuracy of the unit, it was concluded that it would be necessary to eliminate the clutch mechanism. It was also desirable to reduce the deflection of the gage units under load in order to reduce mechanical tares (see Appendix VI). A modified design has been developed featuring an individual beam for each range.

The existing gage units are sufficiently accurate for use in preliminary calibration and testing with the assembled balance system until the redesigned units are available.

# APPENDIX VI

## Damping System

Preliminary tests made on the balance system with the beam gages in position indicate the desirability of having damping in the system to decrease the relaxation time of the oscillations induced by the dynamic application of the air loads to the model. There are, however, certain qualifications imposed on the damping to assure satisfactory balance operation, viz -

1. The damping must be non-frictional -- any type of hydraulic viscous or electrical eddy current dampers satisfy this requirement.

2. Relatively high damping at the beginning of the run. This is desirable to absorb the initial shock and to reduce vibration amplitude rapidly.

3. Relatively low damping during final portion of run. This is desirable to minimize the effect of the damper on the system and to eliminate the effect of any friction in the balance system or gases on the readings.

The damping system used consists of two dampers mounted on the vertical plane centerline to dampen lift and pitch oscillations, and two dampers mounted close to the horizontal plane of the center of gravity to dampen drag and yaw oscillations. Actually to keep the vibration energy at a minimum, the drag dampers should be mounted in the plane of the dynamic center (center of percussion), however, it is felt that satisfactory vibratory control can be maintained through a wide range of locations.

The analysis is based upon the following assumptions:

1. The frictional damping, inherent in any practical system, is small enough to be negligible.

2. The dampers used are purely viscous.

The differential equation of motion for free vibration with viscous damping has the form

$$m\ddot{x} + c\dot{x} + kx = 0 \qquad (1:0)$$

where m is the mass of the system

c is the damping coefficient

k is the spring constant

x is the displacement at any time, t

which has the general solution

$$x = e^{-(c/2m)t}\left[c_1 (\cos qt + j\sin qt) + c_2 (\cos qt - j\sin qt)\right. \qquad (2:0)$$

where $q = \left(\frac{k}{m} - \frac{c^2}{4m^2}\right)^{1/2}$

For simplicity this can be rewritten thus

$$x = e^{-(c/2m)t}\,(c_1' \cos qt + c_2' \sin qt) \qquad (2:1)$$

Referring to figure (a) the following conditions can be set up

At $t = o$

$x = x_o$

$\dot{x} = o$

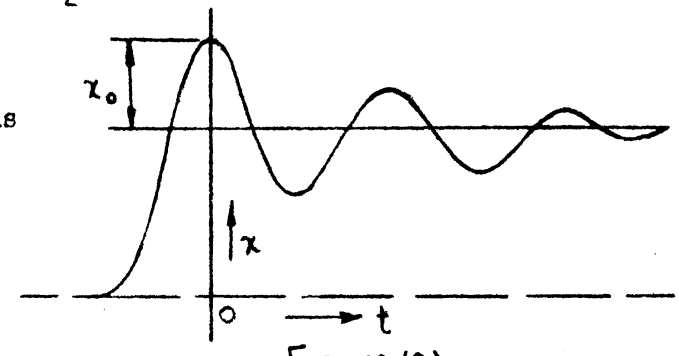

Figure (a)

Using these conditions to evaluate the arbitrary constants $c_1'$ and $c_2'$ we obtain from $x = x_o$, $t = t_o$

$$x_o = 1\,(c_1' \times 1 + c_2' \times o) \qquad \text{or } c_1' = x_o$$

and from $\dot{x} = o$ at $t = o$

$$\dot{x} = -\frac{c}{2m}e^{-\frac{c}{2m}} - \frac{c}{2m}\,t\,(c_1' \cos qt + c_2' \sin qt) + \left\{e^{\left(\frac{-c}{2m}\right)t}\right\}(-c_1' q \sin qt + c_2' q \cos qt)$$

$$o = -\frac{c}{2m}(c_1' \times 1 + c_2' \times o) + 1\,(-c_1' q \times o + c_2' q \times 1)$$

$$o = -\frac{c}{2m}c_1' + c_2' q$$

or

$$c_2' = -\frac{cx_o}{2mq}$$

Substituting back in equation 2:1

$$x = x_o e^{-(c/2m)t}\left(\cos qt + \frac{c}{2mq}\sin qt\right) \qquad (3{:}0)$$

It will be noted that the portion $x = x_o e^{-(c/2m)t}$ is actually the equation of the envelope of the successive maximums of oscillations.

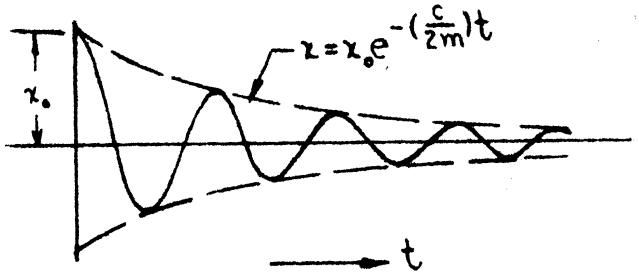


It is possible to determine the amount of damping required to relax the system to any desired percentage in time, t, thus -

$$x = x_o e^{(-c/2m)t} \qquad \frac{c}{2m}t = \ln\frac{x_o}{x}$$

$$\frac{x_o}{x} = e^{(c/2m)t} \qquad c = \frac{2m}{t}\ln\frac{x_o}{x}$$

Hence, if in time, t we want the amplitude to be 1 per cent of the original amplitude,

$$\frac{x_o}{x} = 100, \text{ and } c = \frac{9.71\ m}{t} \qquad (4:0)$$

Vertical Oscillations

Due to the method of subspending the box (shown at right) the motion is defined by the differential equation

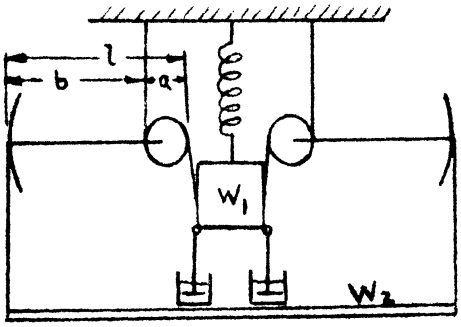


$$I\ddot{\Phi} + c^+\dot{\Phi} + k^+\Phi = o$$

where I = Moment of inertia - lb in sec$^2$
$c^+$ = Damping coefficient - lb in sec
$k^+$ = Spring constant - lb in
$\Phi$ = Angular displacement - Rad.

The constants can be evaluated and equation 4:0 transformed to equation 1:0 thus -

$x = \Phi a;\quad \dot{x} = \dot{\Phi} a;\quad \ddot{x} = \ddot{\Phi} a$ see figure above

whence

$$\frac{I}{a}\ddot{x} + \frac{c^+\dot{x}}{a} + \frac{k^+}{a}x = o$$

Note that:

1.A. x is the displacement at the floating box $w_1$

B. Unit deflection, $\Phi = 1$, produces a torque from the spring of $k^+ = kax$ but at $\Phi = 1$, $x = a$
or $k^+ = ka^2$

2.A. $\dot{x}$ is the velocity of the box and the relative velocity of the piston with respect to the dash pot is $b + a = l$ times as great

B. The torque produced by the damper is $c^+ = c(a + b) = cl$

Substituting back in equation 5:0

$$\frac{I}{a}\ddot{x} + \frac{cl^2}{a}\dot{x} - \frac{ka^2}{a}x = o$$ in torque units or

$\frac{I}{a^2}\ddot{x} + \frac{cl^2}{a^2}\dot{x} + kx = o$ (7:0) in the same units as equation 1:0

Hence if

$$m = \frac{I}{a^2} \; ; \quad c = \frac{cl^2}{a^2}$$

equation 6:0 is identical with equation 1:0 and the constants can now be evaluated

$$m = \frac{I}{a^2} = \frac{w_1 a^2 + w_2 b^2}{a^2} = w_1 + w_2 \left(\frac{b}{a}\right)^2$$

where $w_1 = 300$ lbs

$w_2 = 75$ lbs

$b/a = 4$

$$m = \frac{300 + 75 \times 4^2}{386} = 3.88 \text{ lb sec}^2/\text{in}$$

If the dampers are used as shown then the total damping coefficient will be

$c_{tot} = 2\frac{c' l^2}{a^2}$ where $\frac{l}{a} = 5$ $c_{tot} = 50c'$

from equation 4:0

$$c_{tot} = \frac{9.21\ m}{t} = 50c' \qquad c' = \frac{9.21\ m}{50\ t}$$

if the relaxation time to 1 per cent is assumed 5 sec

$$c' = \frac{9.21 \times 3.88}{50 \times 5} \qquad c' = 0.143$$

Vibration data taken from tests of the undamped box indicate damping exists ranging from about c = .11 in range 1 to about .21 in range 3. This is equivalent to 1/50 x .11 = .0022 and 1/50 x .21 = .0042 at the dash pots and is considered negligible.

For dash pots having the configuration shown at right the damping coefficient is

$c = 6\pi\mu l \frac{R^3}{h^3}$ where l, R, and h are the dimensions shown on the figure and $\mu$ is the fluid viscosity.

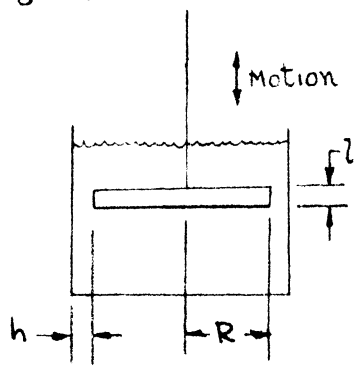


This value is for the piston well centered and drops to 0.4c for piston touching side.

Using SAE 10 oil and l = 0.200, R and h become $\frac{R}{h} = \left(\frac{c}{6\pi\mu l}\right)^{1/3}$

$$= \left(\frac{0.143}{6\pi \times 1.45 \times 10^{-5} \times 0.200}\right)^{1/3} = (2620)^{1/3} = 14.8$$

using 6.0" od x .06 wall tube for the dash pot

h = 2.937 - 14.8 h
h = 2.937/15.8 = 0.1858
R = 2.937 - 0.186 = 2.751

## Horizontal Oscillations

Using an analogy similar to the vertical problem the horizontal differential equation of motion becomes

$$m\ddot{x} + c\frac{l^2}{a^2} + kx = o$$

in which

$$m = (300 + 24)/386 = 0.840 \text{ lb sec}^2/\text{in}$$

$$c_{tot} = 2c'\left(\frac{l}{a}\right)^2 \quad \text{where} \quad \frac{l}{a} = \frac{4}{1.5} = 2.667$$

$$c_{tot} = 14.22\, c'$$

whence from equation 4:0

$$c_{tot} = \frac{9.21\ m}{t} = 14.22\ c' \qquad c' = \frac{9.21\ m}{14.22\ t}$$

again if the relaxation time to 1 per cent is assumed 5 seconds

$$c' = \frac{9.21 \times 0.840}{14.22 \times 5} \qquad c' = 0.1089$$

using similar type dash pots

$$\frac{R}{h} = \left(\frac{0.1089}{6\pi \times 1.45 \times 10^{-5} \times 0.2}\right)^{1/3} = (1990)^{1/3} = 12.55$$

using 4.0" od x .06 wall tube for dash pot $h = 1.937 - R$

Solving for h

$h = 1.937 - 12.55h$
$h = 1.937/13.55 = 0.143$
$R = 1.937 - 0.143 = 1.794$

With the simple type dash pot as used thus far it is not possible to obtain the variable damping necessary for the simultaneous satisfaction of requirements 2 and 3. A cross-sectional view of the modification employed in the balance system dampers is shown in figure below. Under suddenly applied load or in cases where high velocity exists, the floating discs are forced against the piston which then acts as in the simple dash pot with solid piston. When the oscillation velocity decreases (toward the end of the run) the discs are forced away from the piston by spring and gravitational force allowing the fluid to flow through the holes in

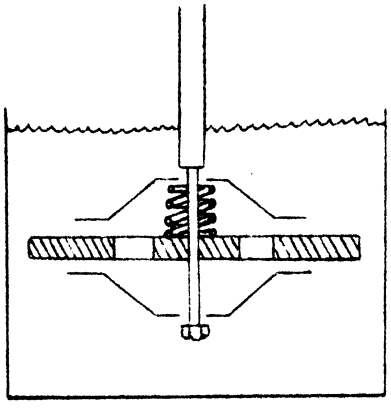

the piston as well as though the annular orifice, resulting in a lower ultimate damping coefficient.

This type of dash pot design lends itself very readily to modification which is considered important in that it is difficult to predict theoretically exactly the optimum damping desired. To change the characteristics of the dash pot it is only necessary to remove the piston assembly from the oil and then remove the nut on the bottom of the shaft. Following are the methods of modifying the load record curve obtained in the oscillograph.

1. To change the load record shown at right above to that shown below either (a) decrease the viscosity of the fluid or (b) turn down the diameter of the piston (increasing the width of the annular orifice).

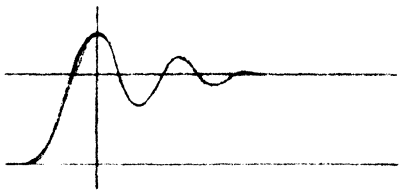

2. To change the load record shown at right above to that shown below (a) increase the number and size of holes in piston under discs (b) increase distance between discs and piston or (c) cut down the length of flat on the discs.

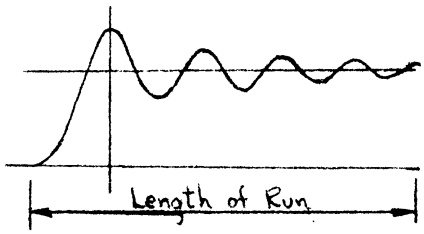


With the present dash pots it is possible to obtain damping coefficients any where from 0 to critical.

## Wind Tunnel Balance System Vibration Frequency Data

1. Weights

Floating box weight = 300 lbs (actual weight)
Counter balance weight = 75 lbs (center balance arm ratio 4:1)
Center balance arm weight = 24 lbs (estimated)

2. Spring Constants - lbs/in

| Range | Lift (1) | Drag upper (3) | Drag Lower (2) |
|---|---|---|---|
| 1 0-1 | 11.0 | 10.4 | 10.0 |
| 2 0-10 | 104.7 | 97.3 | 100.0 |
| 3 0-100 | 789.3 | 811.5 | 774.0 |
| Suspension | Negligible | | 10 (estimated) |

Vertical Vibrations - m = 3.88

| Beam gage range | 1 | 2 | 3 |
|---|---|---|---|
| Total spring constant k - lb/in | 11.0 | 104.7 | 789.3 |
| Frequency $F = \frac{1}{2\pi}\sqrt{\frac{k}{m}}$ cps | 0.268 | 0.826 | 2.26 |
| Critical damping constant $C_c = 2\sqrt{mk}$ | 13.06 | 40.3 | 110.5 |

Horizontal Vibrations - m = 0.840

| Beam gage range | 1 | 2 | 3 |
|---|---|---|---|
| Total spring constant k - lb/in | 30.4 | 207.3 | 1595 |
| Frequency $F = \frac{1}{2\pi}\sqrt{\frac{k}{m}}$ cps | 0.958 | 2.49 | 6.93 |
| Critical damping constant $C_c = 2\sqrt{mk}$ | 10.01 | 26.4 | 73.1 |

Conclusions

Deflection (proportional to load) vs. time curves indicative of action of the present vertical dampers, and for comparison the undamped curves for ranges 1 and 2 are presented in this report. The oscillations from the original shock are in all cases damped out in about 7 seconds. The method of modifying these curves has been discussed in a previous section, however, it is recommended that prior to further modification, observations be made under actual tunnel operating conditions to ascertain the exact nature of the desired change. It should be noted that the width of the annular orifice has already been increased from the theoretical value given in the text to 0.250 in. because it was felt that the damping was too great.

Of interest is the higher frequency ripple (about 15 cps) particularly noticeable in the higher load ranges 2 and 3. This is introduced through the base of the beam gage from the supporting structure and as such is not damped by the dash pots. The significance of this, of course, is that unless suitable precautions are taken, exciting oscillations from outside sources, motors, vacuum pumps,et cetera, will probably cause objectionable ripples in the recorded data. It is recommended that the pressure box encasing the balance system and all other supports be mounted on "isomode" pads or some similar absorber, and if possible all sources of vibrations mounted in like manner.

A check of the oil in a vacuum indicates that once the entrained air is removed from the oil no more "boiling" occurs. This can be done mechanically or very simply by placing the oil in a vacuum for a minute, or

two. No noticeable evaportion was observed. Further tests will be run to determine the effect of moving the piston in the oil, under low pressure.

Preliminary investigations of eddy current type dampers indicate the feasibility of their use in this application. Because of their greater damping control and other advantages it is recommended that this type be given serious consideration for any future design.

# APPENDIX VII

## EXPERIMENTAL WORK

### Results of Some Preliminary Pressure Measurements in the Supersonic Wind Tunnel

The data presented here were taken during the initial operation of the wind tunnel when all its components were in their first stage of development. It should, therefore, not be regarded as final calibration data from which one might draw conclusions regarding the flow characteristics of the supersonic wind tunnel. It was found that deflections existed in the nozzle section due to the loads experienced during operation. It was also found that air leakage to the interior of the tunnel was present at the nozzle section. A new nozzle section is now being installed due to these considerations and also to simplify the job of replacing nozzle blocks. Since this is a considerable change in the physical set-up, the measurements will have to be repeated and one would expect the results to change accordingly. Nevertheless, the work discussed here was necessary and valuable since the tunnel crew and data reduction group learned in the only way possible the techniques associated with this sort of research work.

Included is a description of the technique of pressure measurement utilizing a manometer. Wall pressure measurements at the test section are exhibited and the results of flow inclination measurements and total head measurements are shown.

### Pressure Measurement Techniques

The pressure measurements are taken from a multiple mercury manometer board consisting of 50 tubes manifolded to a common reservoir. Two of

these are always left open to the atmosphere in order that a reference value may be obtained.

Some difficulty was experienced in connection with oscillations of the mercury level. When a run is made with all the mercury levels initially at a common elevation, the level of the tubes must in general rise a distance which is of the order of 25 inches in the course of a run. Since the damping is less than critical, the levels always overshoot the equilibrium position and continue to oscillate about it until the motion is dissipated. The normal length of run of this tunnel is limited to 15 seconds which is so short that it is questionable if equilibrium is reached. It has been possible to minimize this difficulty by using a device for clamping off the rubber tubing which connects the tunnel orifices with the manometer board. A short "pre-run" of 4 to 5 seconds duration is made which brings the levels into rough equilibrium. The clamp is applied immediately before the pre-run ceases and holds the measurements until the vacuum tanks are exhausted for the actual run. As soon as the actual run has begun, the clamp is released, exposing the manometer once more to the pressures being measured. This run continues for approximately 15 seconds when a photograph of the manometer board is taken. In this way, the pressures are recorded while the manometer tubes are exposed to the pressures being measured. Hence, it is not necessary to rely upon the clamping device to function perfectly as would be the case if the data were read off the board after the run is completed.

The camera used for these pictures was a 4 x 5 inch speed graphic with an f 4/5, 6-3/8" focal length lens. The pictures were taken at f/22, 1/10 second. Figure VII (1) is an example of the pictures from which the measurements of pressure are obtained. The smallest divisions of the scale

used are 0.05 inch. It has been found that, when two people read the same picture independently, the differences are usually 0 or 0.01 inch and are never greater than 0.02 inch. This accuracy is considered more than adequate. A reading glass is sometimes used to facilitate taking the data from the pictures.

Wall Pressure Measurements

A wall plate which may be inserted in place of any of the six windows of the Mach number 1.9 (M = 1.9) wind tunnel furnishes most of the wall pressures measured. Pressure taps with a spacing of 1 inch cover the whole plate. With a given hook-up of the pressure plate to the manometer board, one can therefore survey pressures over six areas of the wind tunnel with a minimum amount of set-up time. A double row of pressure taps is also available on the top wall of the testing section. The isentropic formula relating pressure with Mach number makes it possible to calculate Mach number from these measurements. Mach number at the test section walls is plotted in Figure VII (2). Figure VII (3) is another set of the same type of data presented in a different fashion.

Accuracy of Pressure Measurement

The data presented in Figure VII (2) and Figure VII (3) show what is believed to be large and undesirable variations of Mach number in the test section. Therefore, 3 runs were made in order to find out if the errors associated with the methods of pressure measurement were great enough to account for these variations.

Runs (a), (b), and (c) were made in this connection:

(a) Pressure plate hook-up shown in Figure VII (3), pressure plate in the test section.

(b) Same as (a) but plate rotated in its plane through an angle of 180°.

(c) A repeat run of (a).

When runs (a) and (c) are compared, one gets a measure of reproducibility of pressure measurements for identical configurations. When runs (a) and (b) are compared, one gets a measure of the effect of different orifices measuring the same pressure as well as reproducibility of runs. This is due to the fact that, when the pressure plate is rotated, different orifices are brought into the same original positions on the test-section wall.

At corresponding positions, the difference between each measurement included in (a) and (c) was found. The absolute values of these differences were then averaged over the 45 points of the pressure plate and found to be 0.033 inch of mercury. At M = 1.9, such a difference in wall pressure corresponds to a difference in Mach number of 0.005. The three greatest individual discrepancies were 0.11, 0.09 and 0.08 inch of mercury or 0.017, 0.014 and 0.012 in the Mach number. Following the same procedure, the average change between (a) and (b) was also found to be 0.033 inch of mercury or 0.005 in the Mach number. The greatest individual discrepancies between (a) and (b) were 0.270, 0.121 and 0.071 inch of mercury or 0.040, 0.018 and 0.011 in the Mach number.

One would expect that the average <u>random</u> error of measurement would be somewhat smaller than this since items of <u>constant</u> error, such as inaccurate reading of reference pressures and barometric pressures, were not separated from the overall error. Therefore, considering the small size of

these errors, it seems apparent that the major trends shown in Figure VII (2) and Figure VII (3) are legitimate phenomena actually characteristic of the flow.

Pressure Measurements in the Interior of the Tunnel

A double wedge section, Figure (a) below, was used for these measurements. The double wedge spans the tunnel in a horizontal position, and surface pressure taps are located on the upstream surfaces, top and bottom. Since a shock wave exists at the leading edge of this airfoil, it is necessary to make use of oblique shock wave tables in the reduction of the data. When this is done, one obtains a curve of the Mach number in front of the nose shock as a function of the measured pressures. The only assumption involved is that of isentropic flow upstream of the nose shock. If the inclination of the flow relative to the chord line of the double wedge is no greater than 2 degrees, it has been found exceedingly accurate to use the mean pressure between the upper and lower surfaces at a given station for the purpose of calculating the Mach number. It is also possible to calculate the inclination of the flow in the plane normal to the span of the double wedge by using the difference in pressures at a given spanwise station in connection with the oblique shock wave tables.

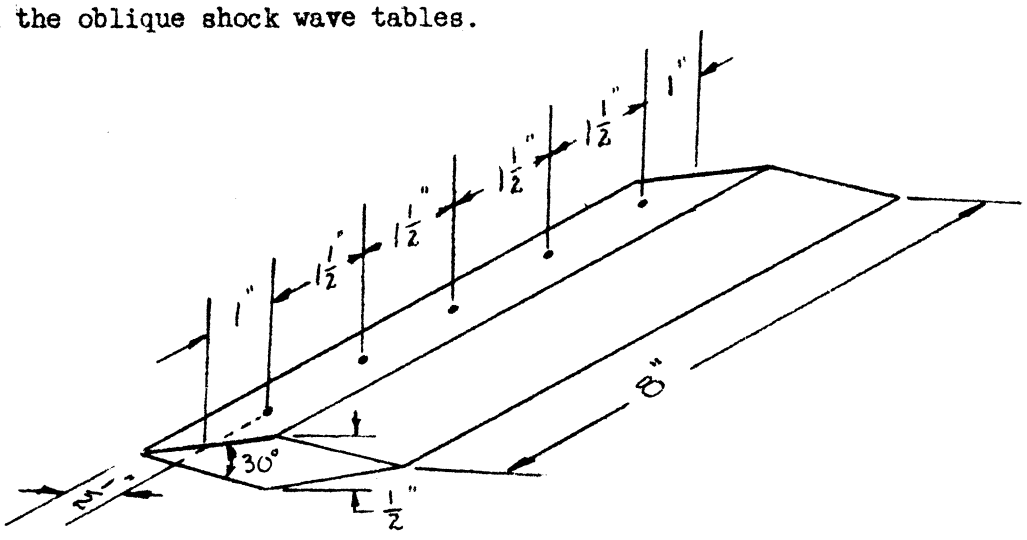


Figure (a). Double Wedge Pressure Section

Measurements of the total heat pressure were also made with a second double wedge section. The spanwise stations of this device were the same as for the surface pressure measurements, but the total head tubes extended 1/4 inch in front of the leading edge. Application of the formula for the change in reservoir pressure across a normal shock* makes it possible to calculate the Mach number of the stream where the total head tube is placed. The validity of this calculation depends upon the flow being isentropic upstream of the nose shock which stands in front of the total head tube.

Figure VII (4) exhibits a few of these measurements. An interesting feature of these data is the relatively good agreement between the Mach numbers found in the two different ways at stations near the center of the wind tunnel and the poor agreement at the stations 1 inch from the wall. It has been suggested that the discrepancy is due to the fact that this station is inside the boundary layer of the wind tunnel wall. If this is true, then the equations used in the data reduction were not applicable near the wind tunnel wall and poor agreement should not be surprising.

Measurements of total head pressure are plotted in Figure VII (5). These plots are relatively uniform over the tunnel interior and show no consistent change at the stations nearest the walls as one would expect if the measurements were taken in a boundary layer. It is believed that these data do not rule out the possibility of a thick boundary layer since there are two

---

* $$f(M) = \left(\frac{2\gamma}{\gamma+1} M^2 - \frac{\gamma-1}{\gamma+1}\right)^{\frac{1}{\gamma-1}} \left(\frac{\frac{\gamma+1}{2} M^2}{1+\frac{\gamma-1}{2} M^2}\right)^{\frac{\gamma}{\gamma-1}} = \frac{p_o'}{p_o}$$

effects which may cancel each other out to a large extent. The quantity $p_o'/p_o$ which is plotted is essentially a measure only of $p_o'$ since $p_o$ is the constant value of barometric pressure. $p_o'$ is given by an equation of the form $p_o' = p_s^f(M)$ where $p_s$ is the local stagnation pressure in a supersonic boundary layer. But $p_s = p_o$, the value of stagnation pressure in the free stream. In a boundary layer M, the local Mach number is smaller than in the free stream which leads to a larger value of f(M) since the shock losses are not as great for lower Mach numbers. Therefore,. in a boundary layer, it is possible that $p_o'$ may be left essentially constant as was shown in Figure VII (5). This discussion is, of course, an unsatisfactory substitute for more complete measurements. Unfortunately, Schlieren data cannot be taken at these walls.

If this explanation is correct, the boundary layer must be an abnormally thick one, since its effect is not small at a distance 1 inch from the wall. Air leakage to the interior of the wind tunnel has been suggested as an explanation for such a thick boundary layer.

Wing Tunnel Choking

Some information regarding the choking characteristics of the tunnel has been obtained and is presented here. It is believed that the forward projected area of obstructions placed in the wind stream is the most important consideration related to wind tunnel choking, although for equal projected areas, bodies which are more slender or sharpnosed are considered less likely to cause choking. The following configurations, Figures (b) and (c) below, have been placed in the test section. The first configuration resulted in satisfactory flow while the second choked the tunnel. These tests were made at a Mach number of 1.95. Observation of the choking was made with the Schlieren equipment.

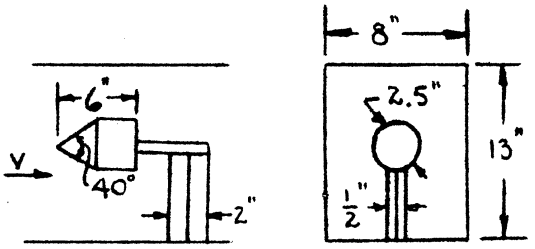


Projected Area – 8.5 m²

Figure (b)

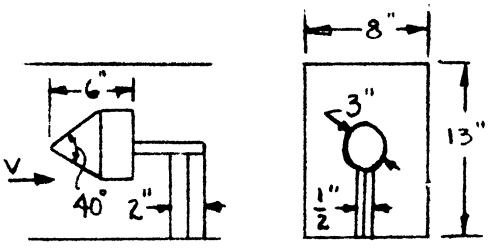


Projected Area – 9.6 in²

Figure (c)

There was considerable air leakage into the wind stream when these tests were made. It is possible that the results may change significantly when this difficulty has been eliminated.

Choking phenomena may be explained after a fashion by the one-dimensional channel flow theory. It is assumed that, when the flow is being established in the wind tunnel, a normal shock exists at the test section in front of the obstruction as shown in Figure (d).

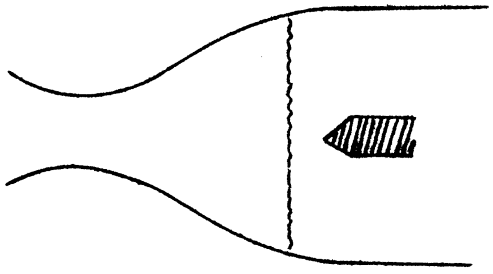

Figure (d)

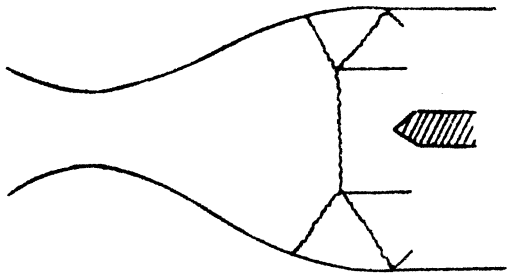

Figure (e)

For the case of the normal shock, one can calculate the new throat area at the station where the sonic speed is reached. If the projected area is large enough so that the area of the passage at this station is less than the area one calculates, the tunnel must remain choked. If the projected

area of the obstruction is smaller than this critical number, the normal shock will be drawn downstream eliminating the choked condition. In this way, one can calculate the permissible blocking of the tunnel for any Mach number.

It is known, however, that this theory is inadequate. In the choked condition, one often sees the shock configuration sketched in Figure (e) with oblique shocks and flow separation present and non-uniform flow in the test channel. The one-dimensional theory cannot describe such things, and one actually finds that much less blocking will be sufficient to choke the channel. One cannot even be sure that the situation will improve at higher Mach numbers as is indicated on the curve. Test results at a Mach number of 4 will be made available in the near future.

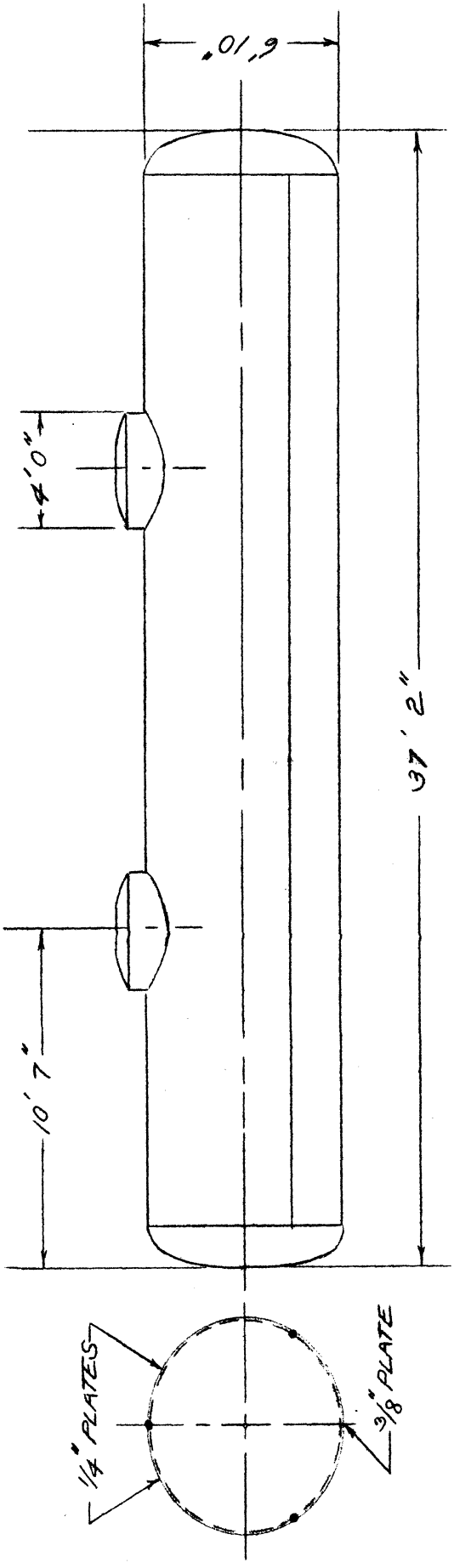


FIGURE 4.
DIMENSIONS OF TYPICAL VACUUM TANK

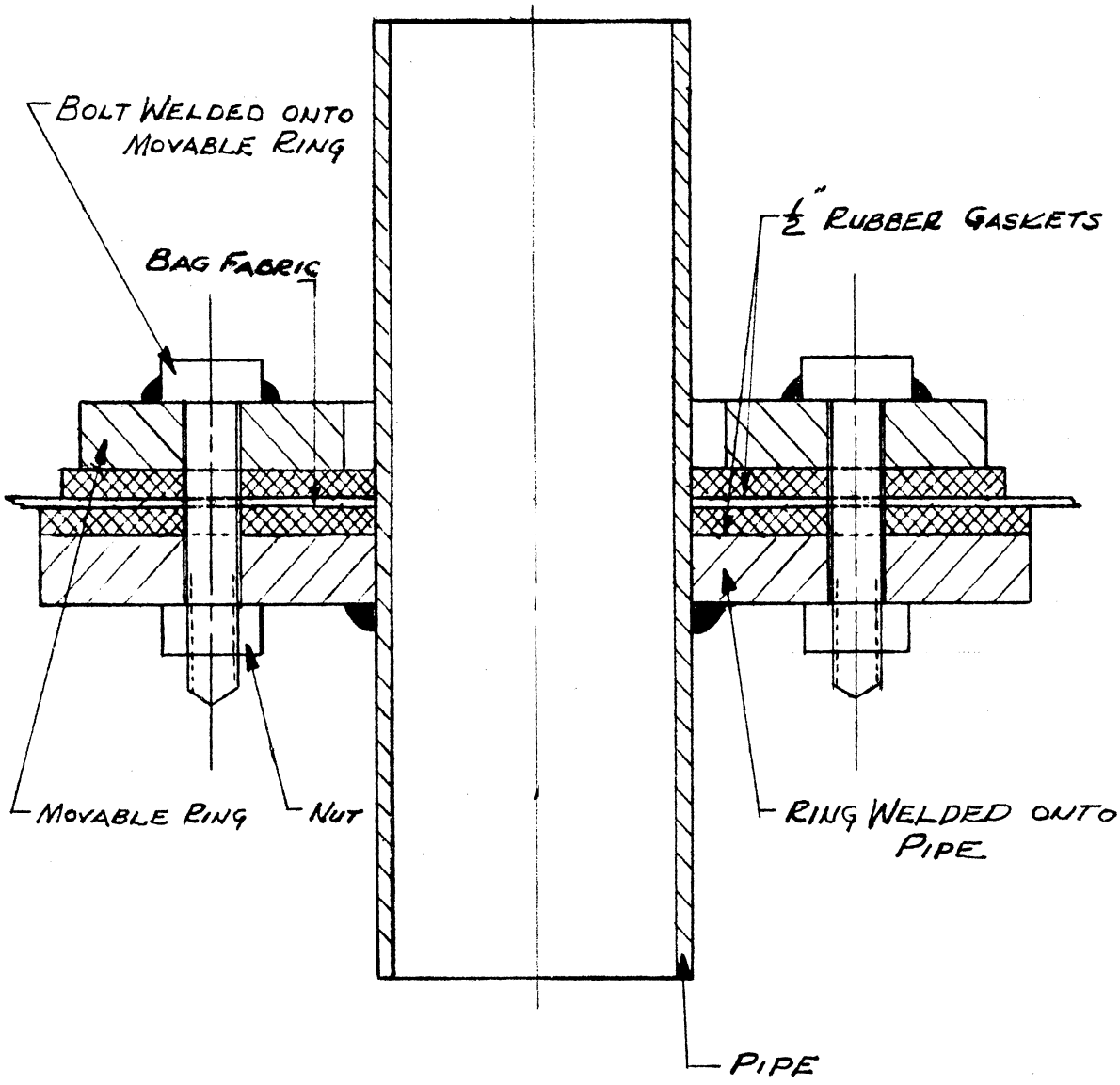


FIGURE 12.

TYPICAL OPENING INTO BAG

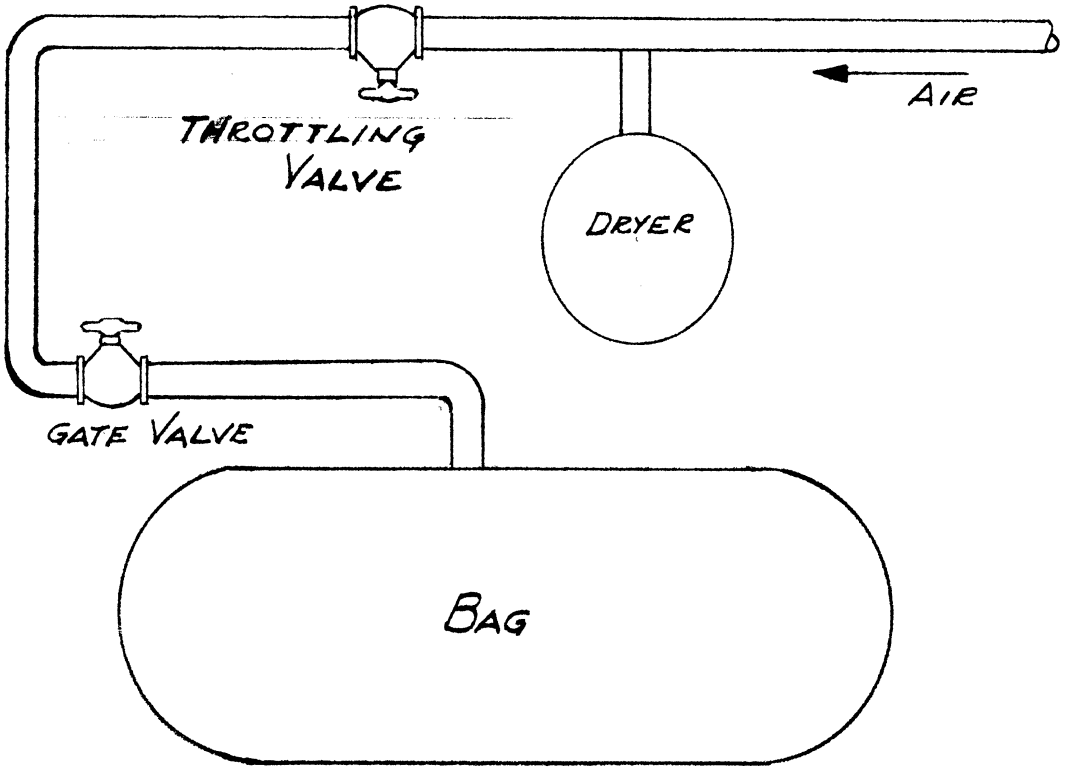


FIGURE 16 a.
ORIGINAL DRYING SHUNT

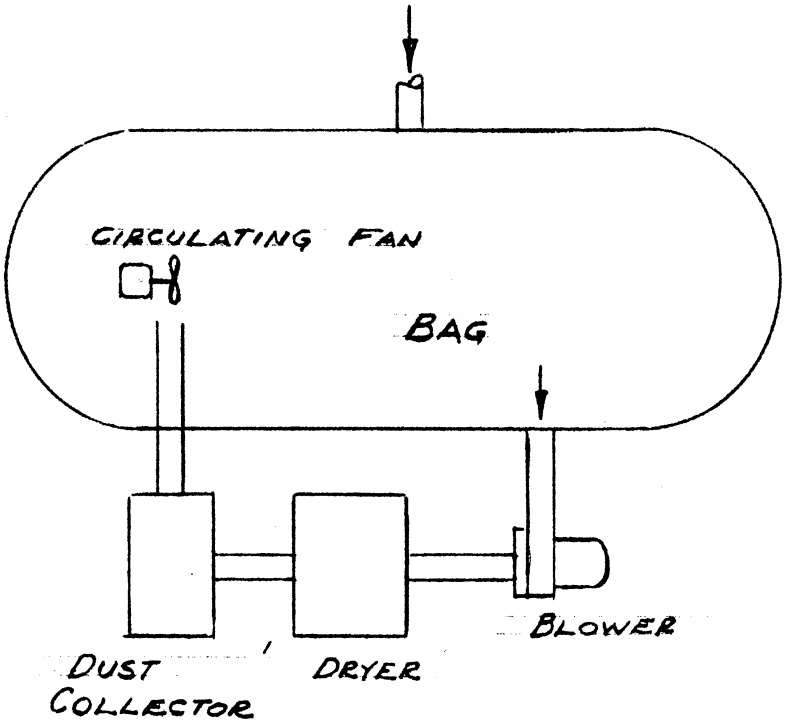


FIGURE 16 b.
FINAL DRYING CIRCUIT

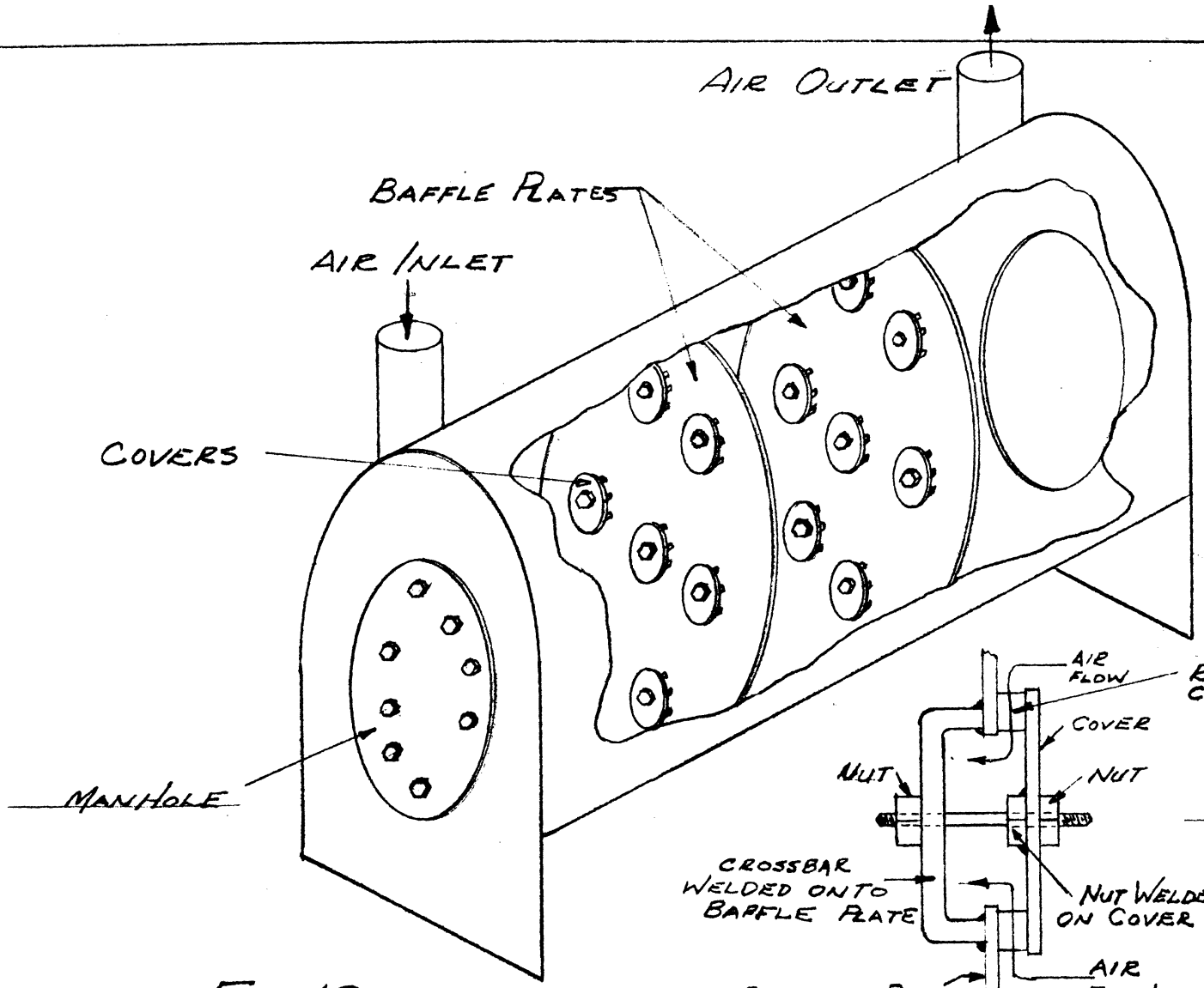


FIG. 18

SKETCH OF SETTLING TANK




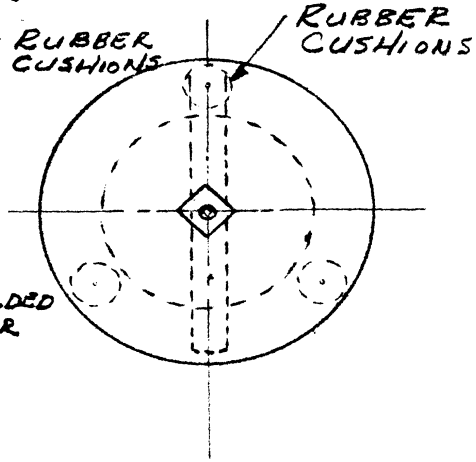


DETAIL OF COVERPLATES

Prepared by

Approved by

Date

DEPARTMENT OF ENGINEERING RESEARCH
UNIVERSITY OF MICHIGAN

Page

Project

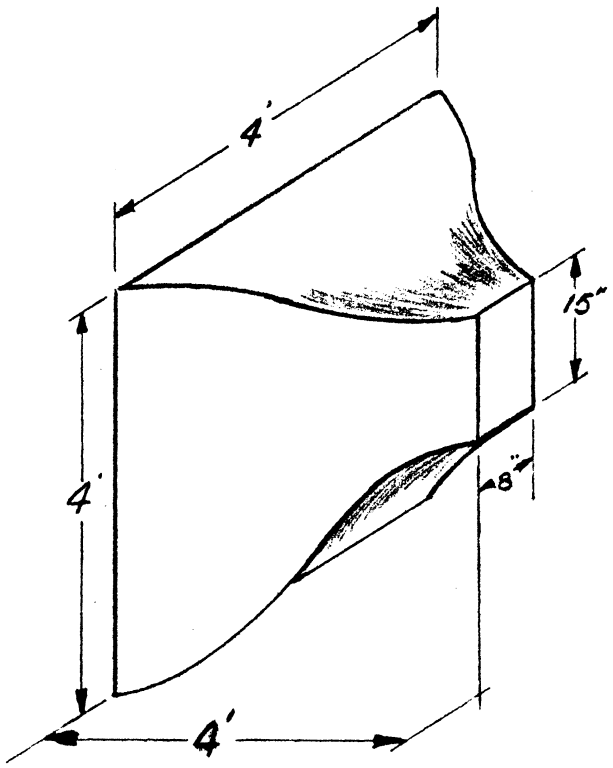


FIGURE 23

CONVERGING SECTION

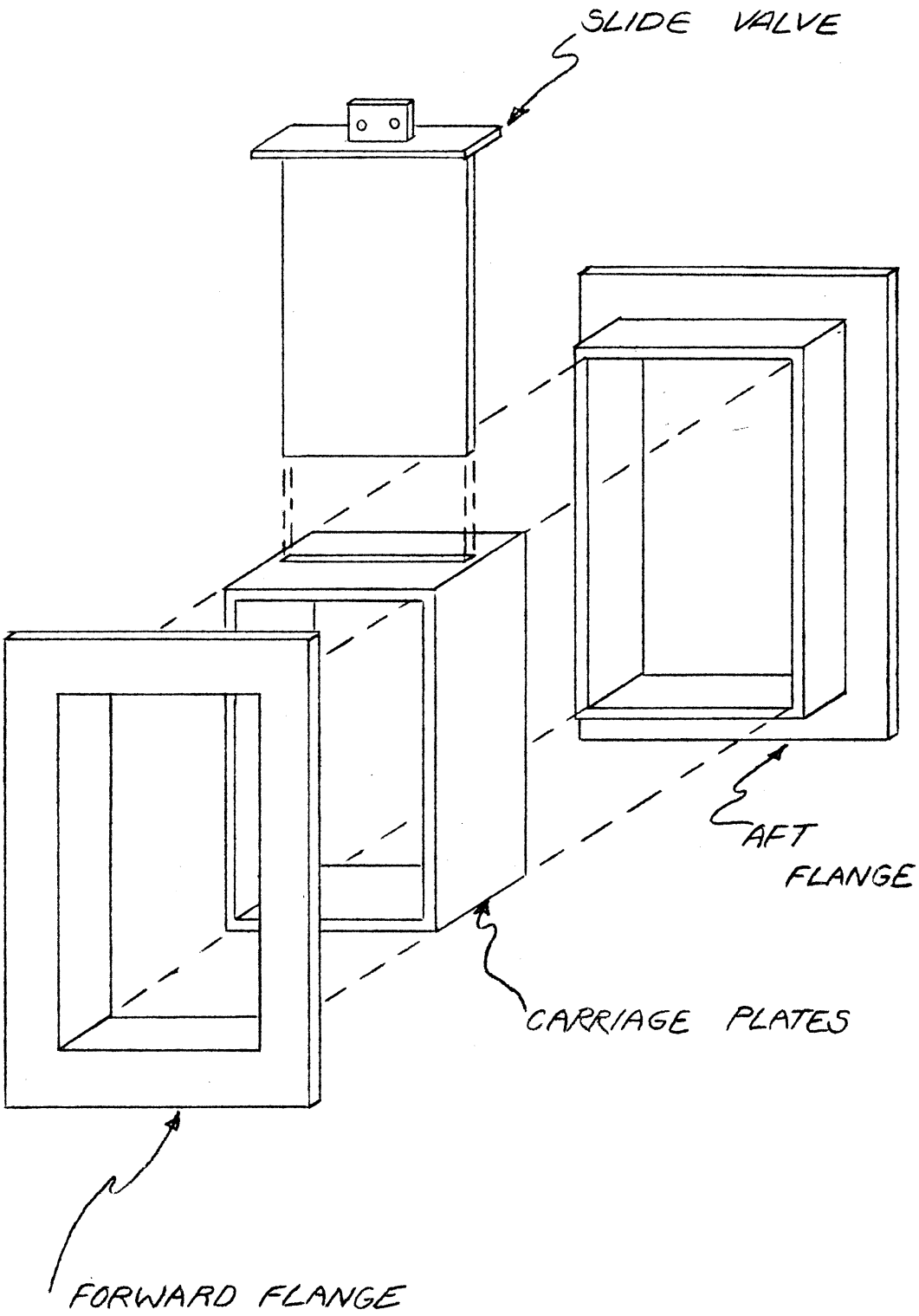


FIGURE 24.

SLIDE VALVE SECTION

| Prepared by | | Page |
|---|---|---|
| Approved by | | Project |
| Date | DEPARTMENT OF ENGINEERING RESEARCH<br>UNIVERSITY OF MICHIGAN | |

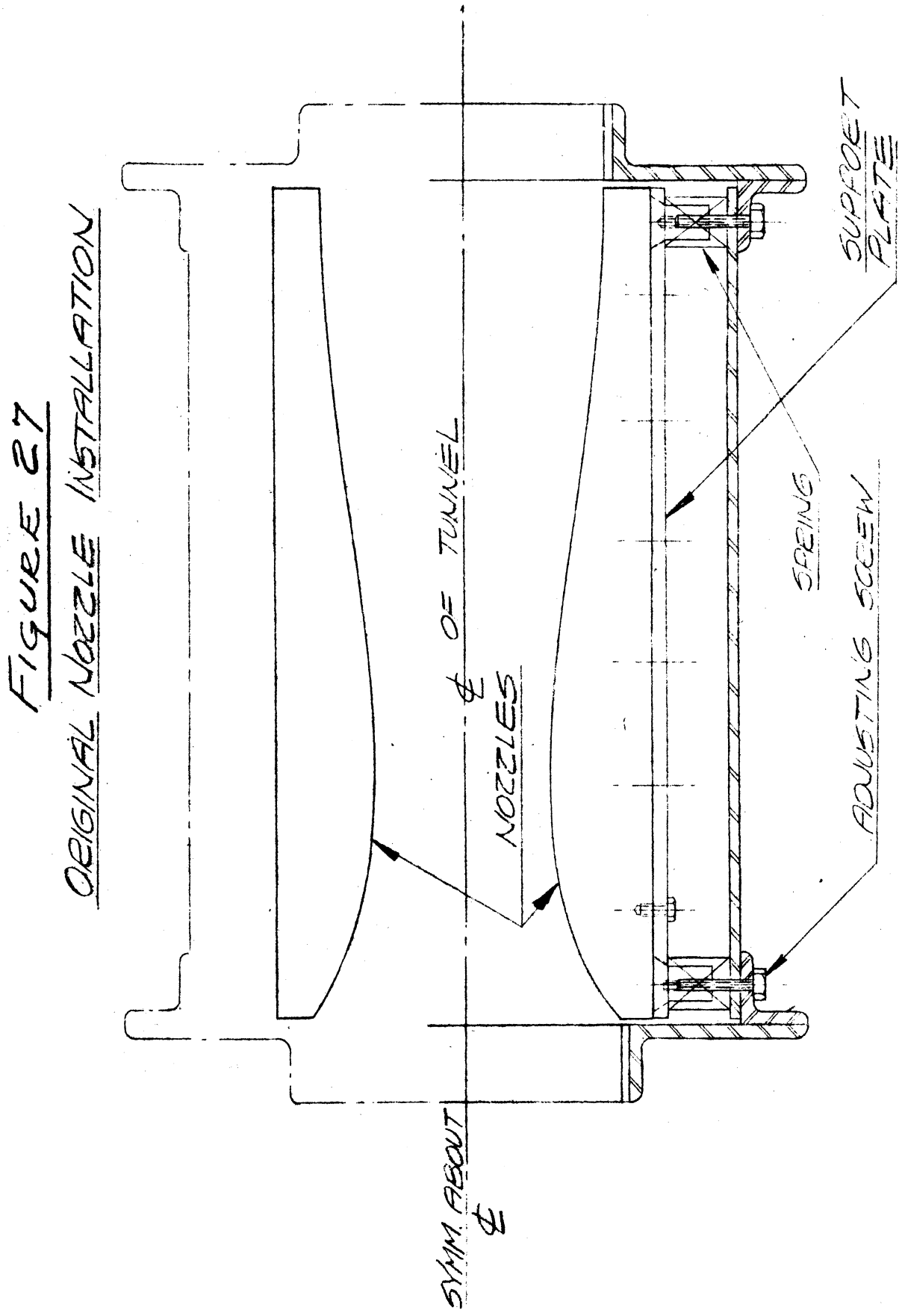


FIGURE 27
ORIGINAL NOZZLE INSTALLATION

| Prepared by | | Page |
|---|---|---|
| Approved by | | Project |
| Date | DEPARTMENT OF ENGINEERING RESEARCH<br>UNIVERSITY OF MICHIGAN | |

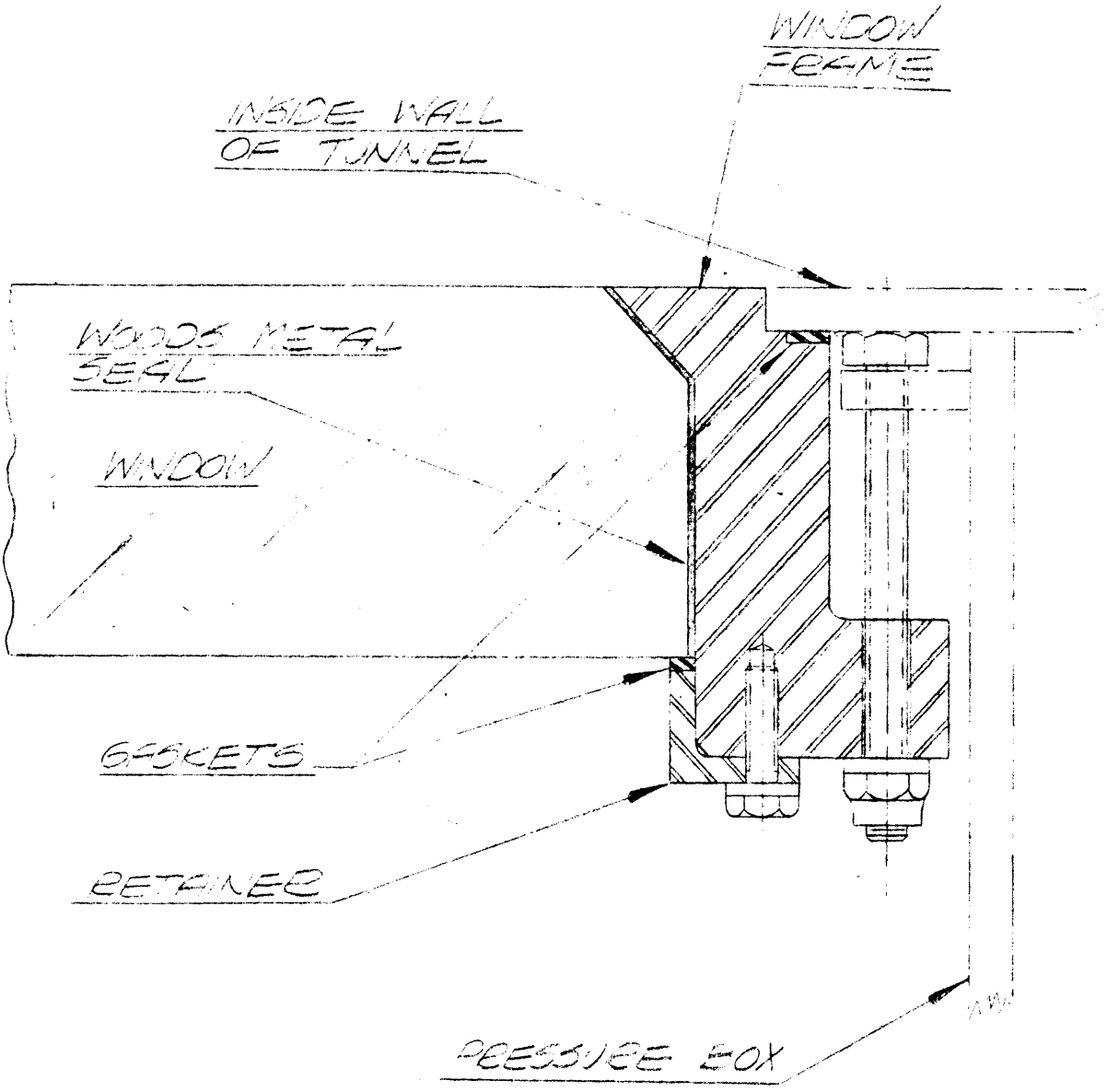


FIGURE 28.

DETAILS OF WINDOW MOUNTING

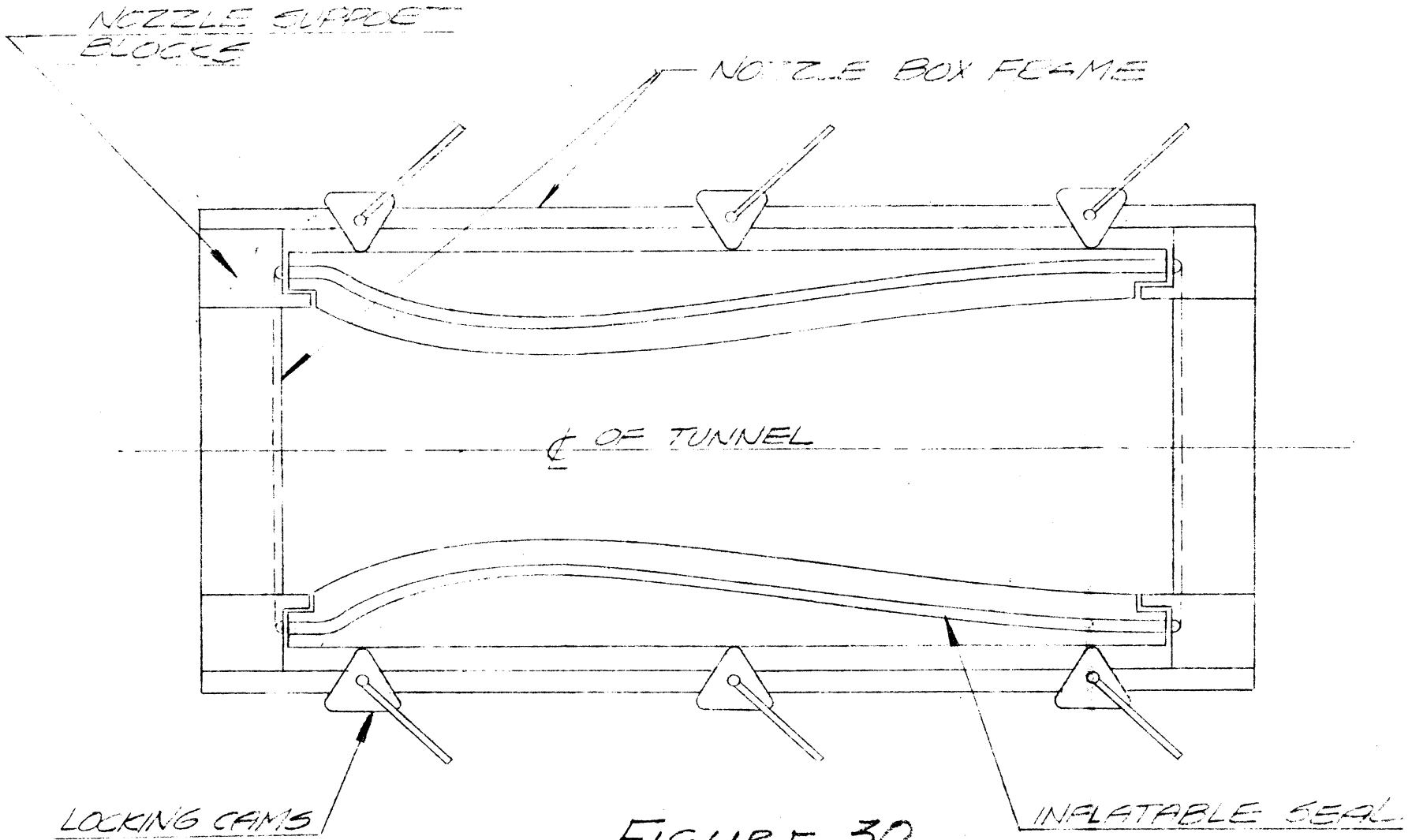


FIGURE 30.

PRESENT NOZZLE INSTALLATION

Prepared by

Approved by

Date

DEPARTMENT OF ENGINEERING RESEARCH
UNIVERSITY OF MICHIGAN

Project

Page

| Prepared by | | Page |
|---|---|---|
| Approved by | | Project |
| Date | DEPARTMENT OF ENGINEERING RESEARCH<br>UNIVERSITY OF MICHIGAN | |

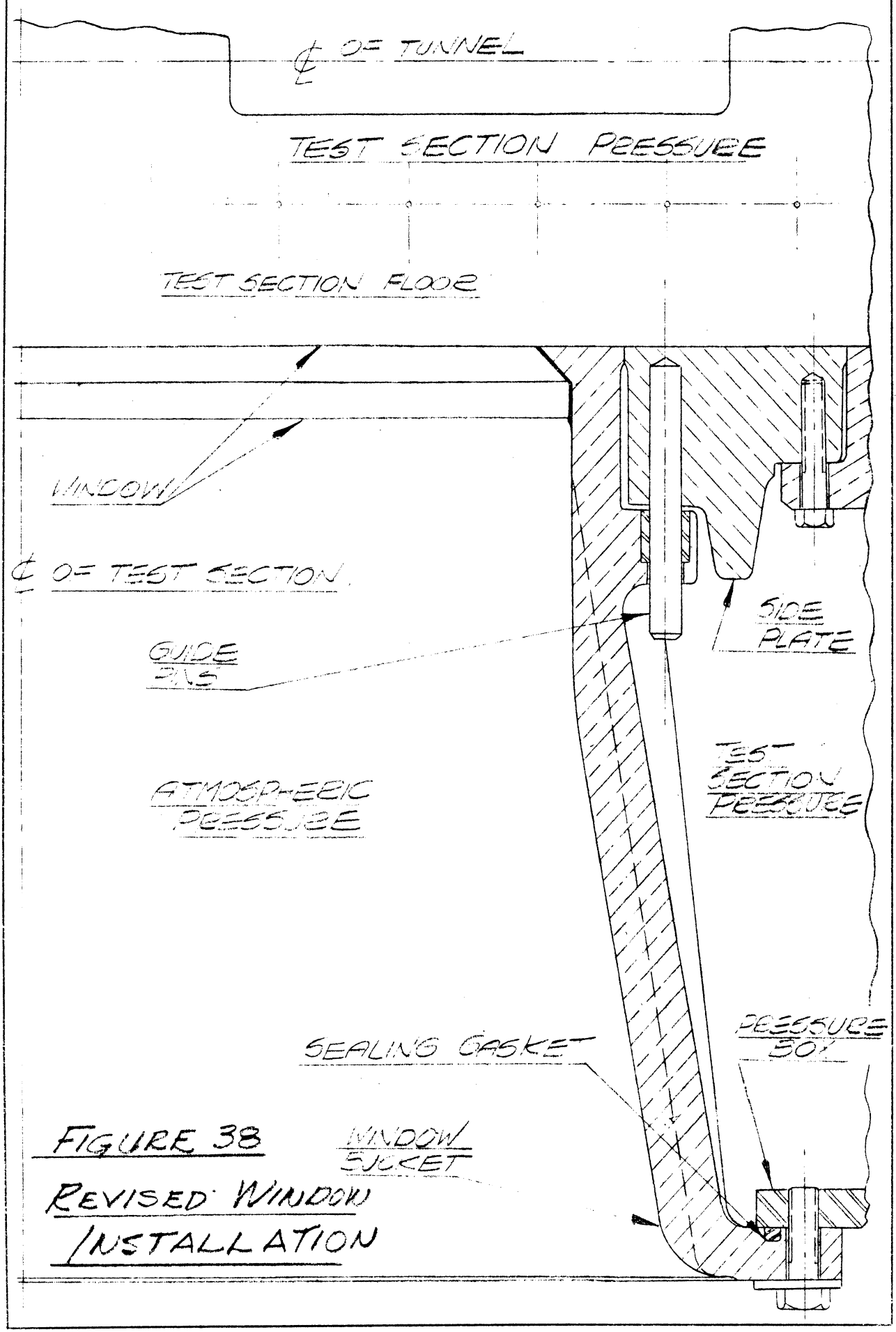


FIGURE 38

REVISED WINDOW INSTALLATION

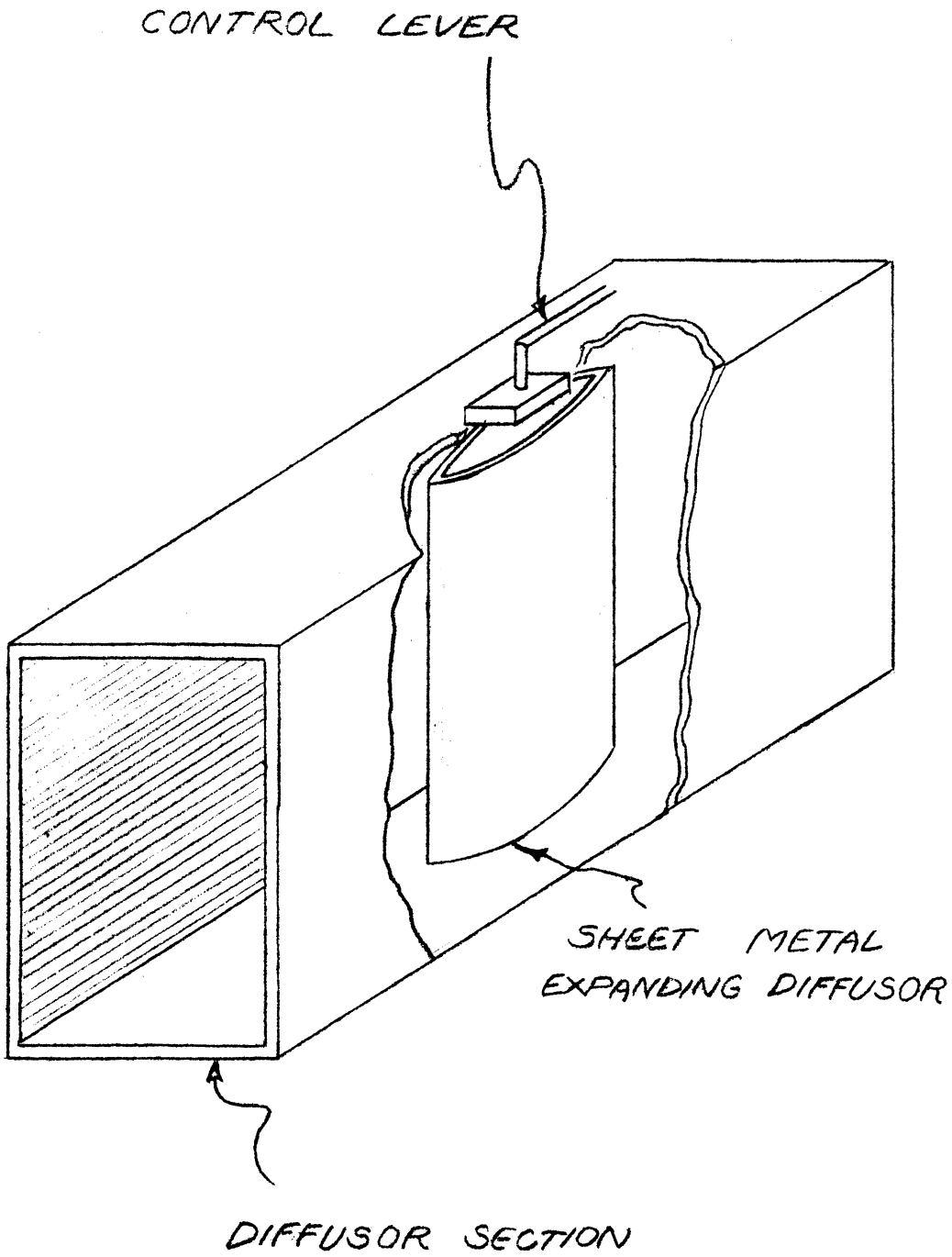


FIGURE 39
AIRFOIL DIFFUSOR ARRANGEMENT

# FIGURE 50.
## RECORDING OSCILLOGRAPH - CIRCUIT DIAGRAM

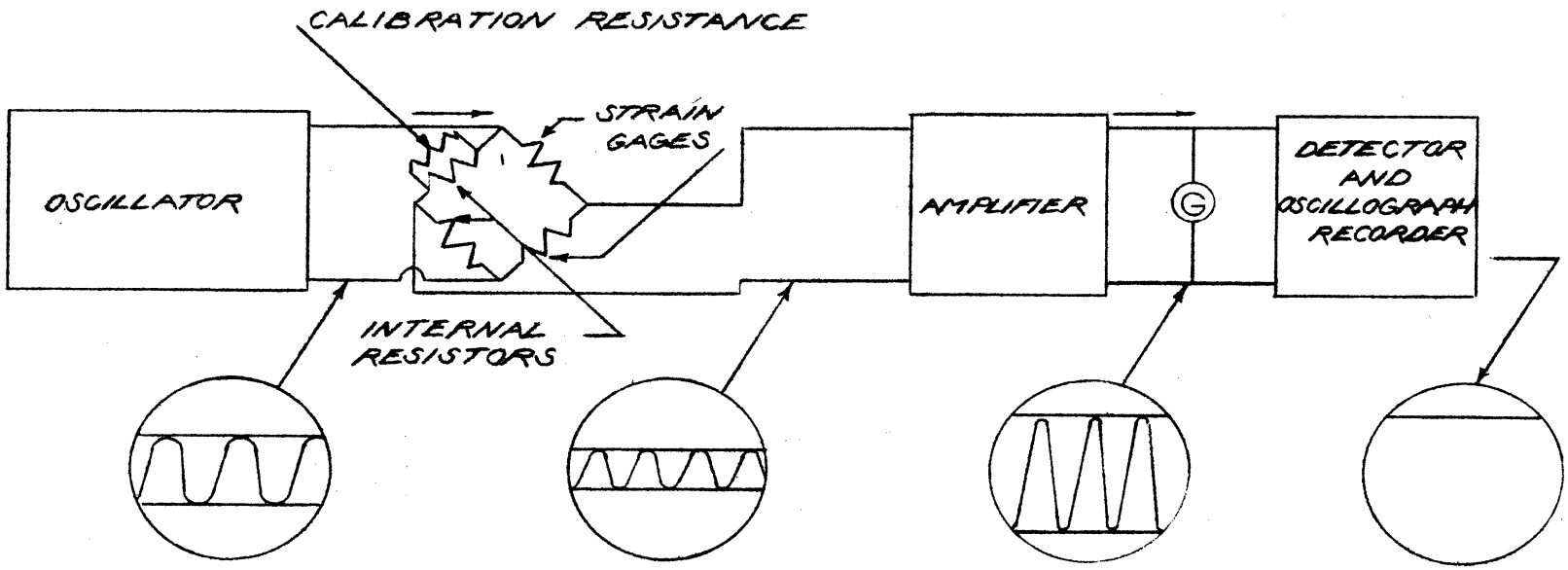


OSCILLATOR FEEDS CARRIER WAVE TO UNBALANCED BRIDGE

BRIDGE MODULATES HIGH FREQUENCY CARRIER WAVE FEEDS AMPLIFIER

AMPLIFIER INCREASES WAVE AMPLITUDE FEEDS OSCILLOGRAPH GALVANOMETER

FILM RECORDS BRIDGE MODULATION, ELIMINATES CARRIER WAVE

Prepared by

Approved by

Date

DEPARTMENT OF ENGINEERING RESEARCH
UNIVERSITY OF MICHIGAN

Project

Page

FIGURE I (1)

PRESSURE RATIO - SUPPLY TO DIFFUSER VS. TEST MACH NUMBER (ESTIMATE ACCORDING TO L. CROCCO)

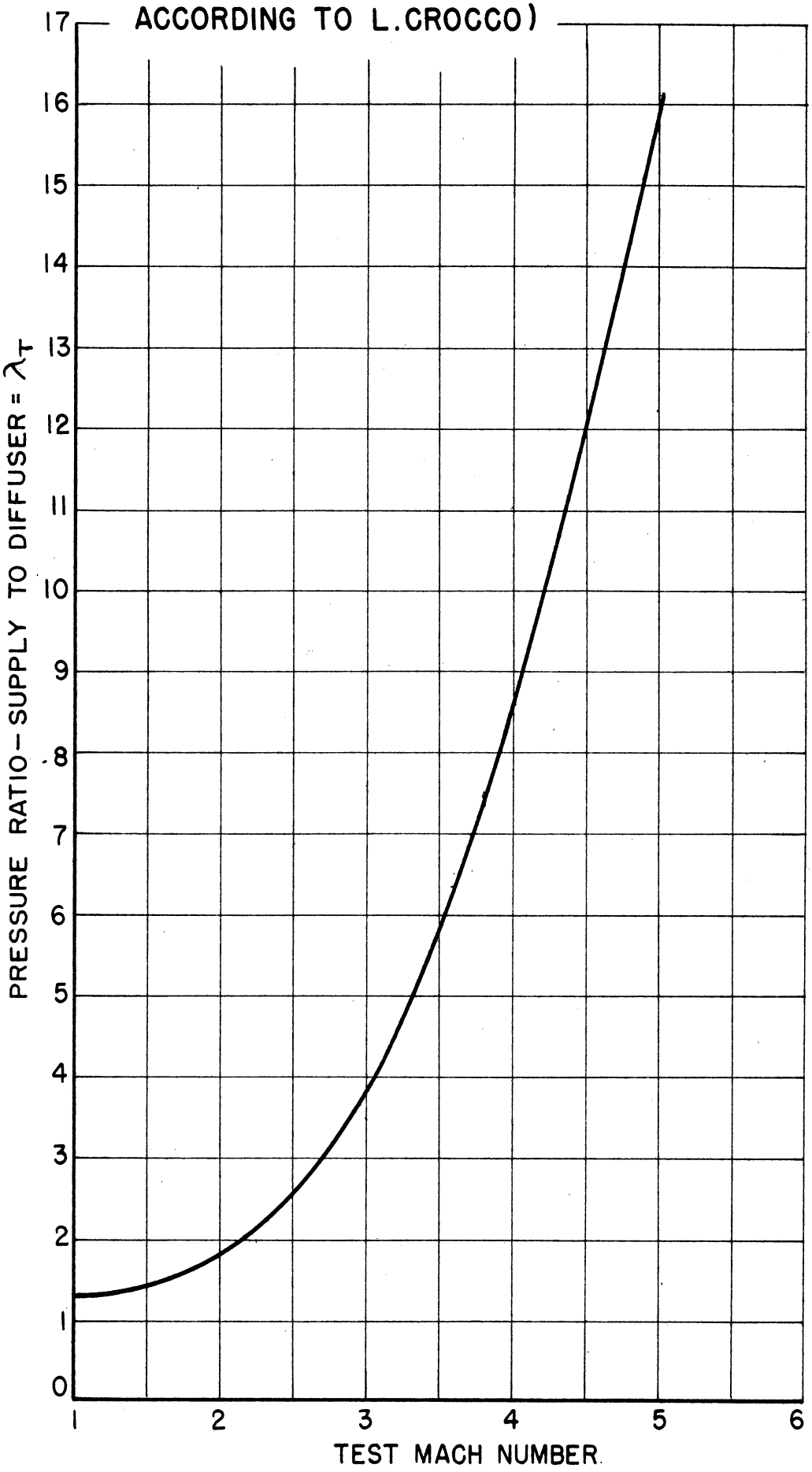

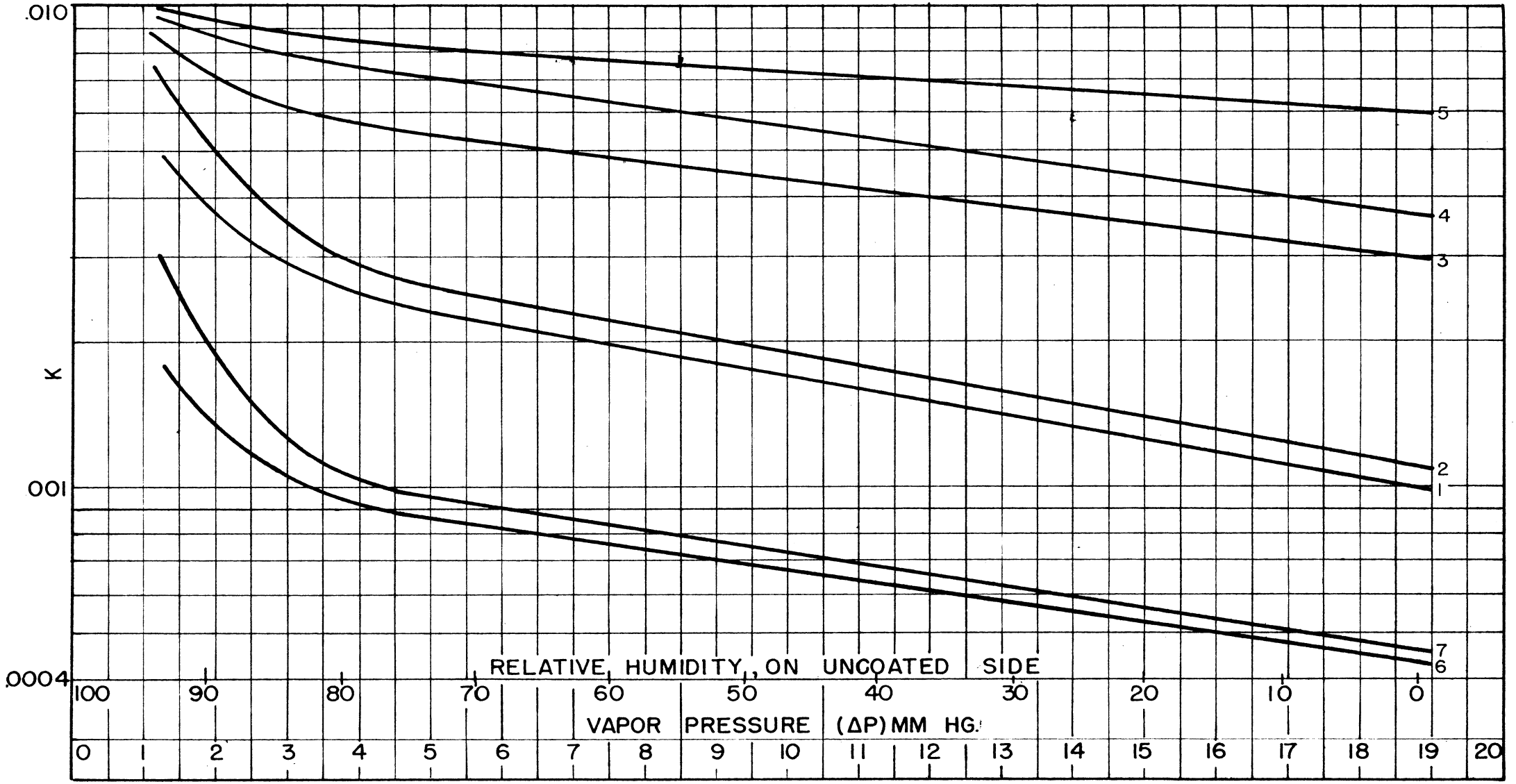


100% RH ON ONE SIDE (COATED SIDE)
ΔP = DIFFERENCE IN WATER VAPOR PRESSURE
K = PERMEABILITY FACTOR
$K = \frac{Mg\ H_2O}{(mm\ Hg)(cm^2)}$

CLOTH NUMBER
(SEE TABLE II-2)

FIG. II (1)

PERMEABILITY FACTORS FOR BALLON CLOTH TREATED WITH VARIOUS COATINGS AT 70°F

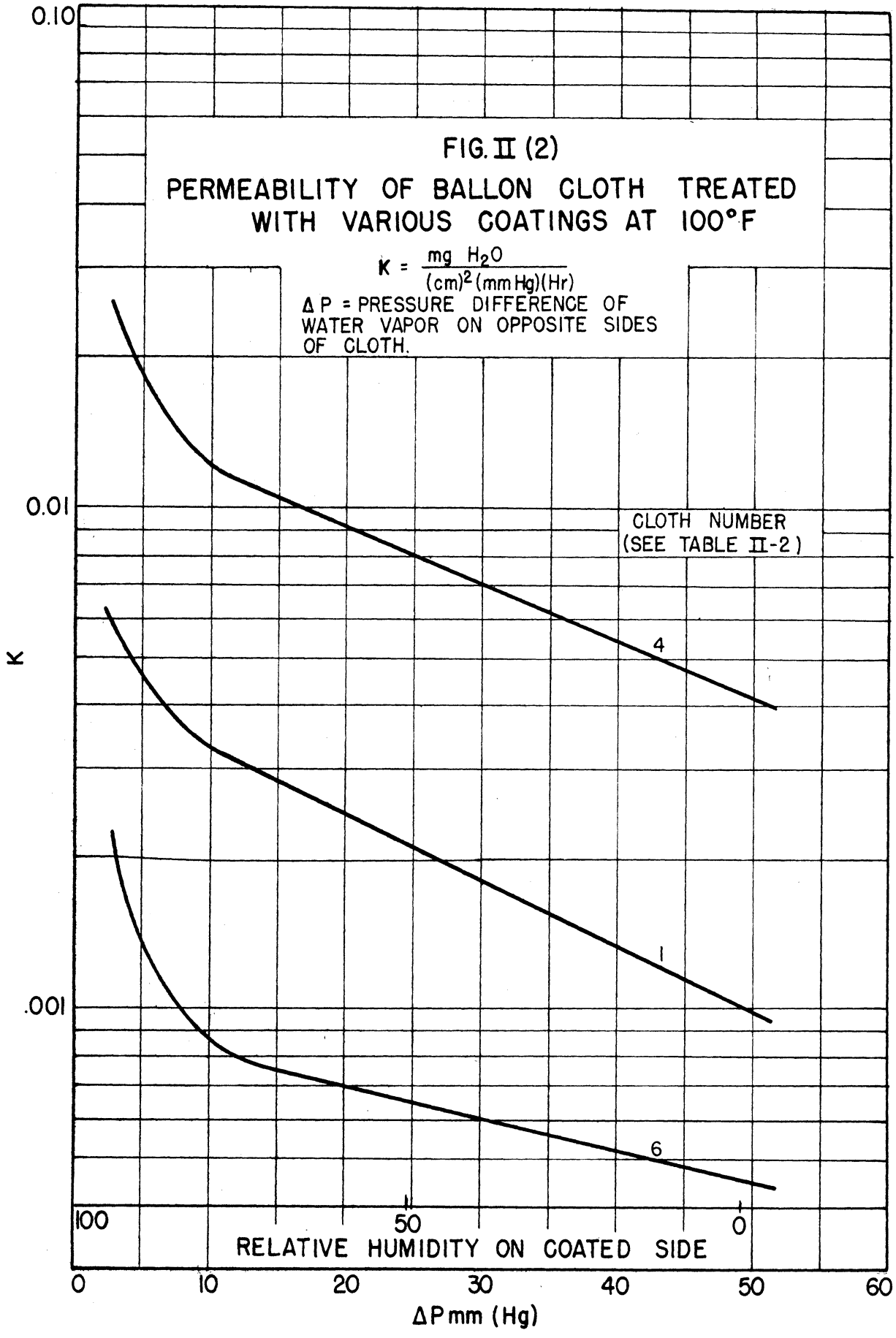
FIG. II (2)
PERMEABILITY OF BALLON CLOTH TREATED WITH VARIOUS COATINGS AT 100°F
K = mg H2O / (cm)2 (mm Hg)(Hr)
Δ P = PRESSURE DIFFERENCE OF WATER VAPOR ON OPPOSITE SIDES OF CLOTH.
CLOTH NUMBER (SEE TABLE II-2)
4
1
6
0.10
0.01
.001
K
100
50
0
RELATIVE HUMIDITY ON COATED SIDE
0
10
20
30
40
50
60
ΔP mm (Hg)

FIGURE II (3)

BAG DEW POINT VS. TIME
FOR CONTINUOUS CIRCULATION

CONDITIONS
ATMOS. TEMP. = 90° F
ATMOS. D.P. = 70° F
DRIER D.P. = − 40° F
K = 0.0214 x $10^{-9}$

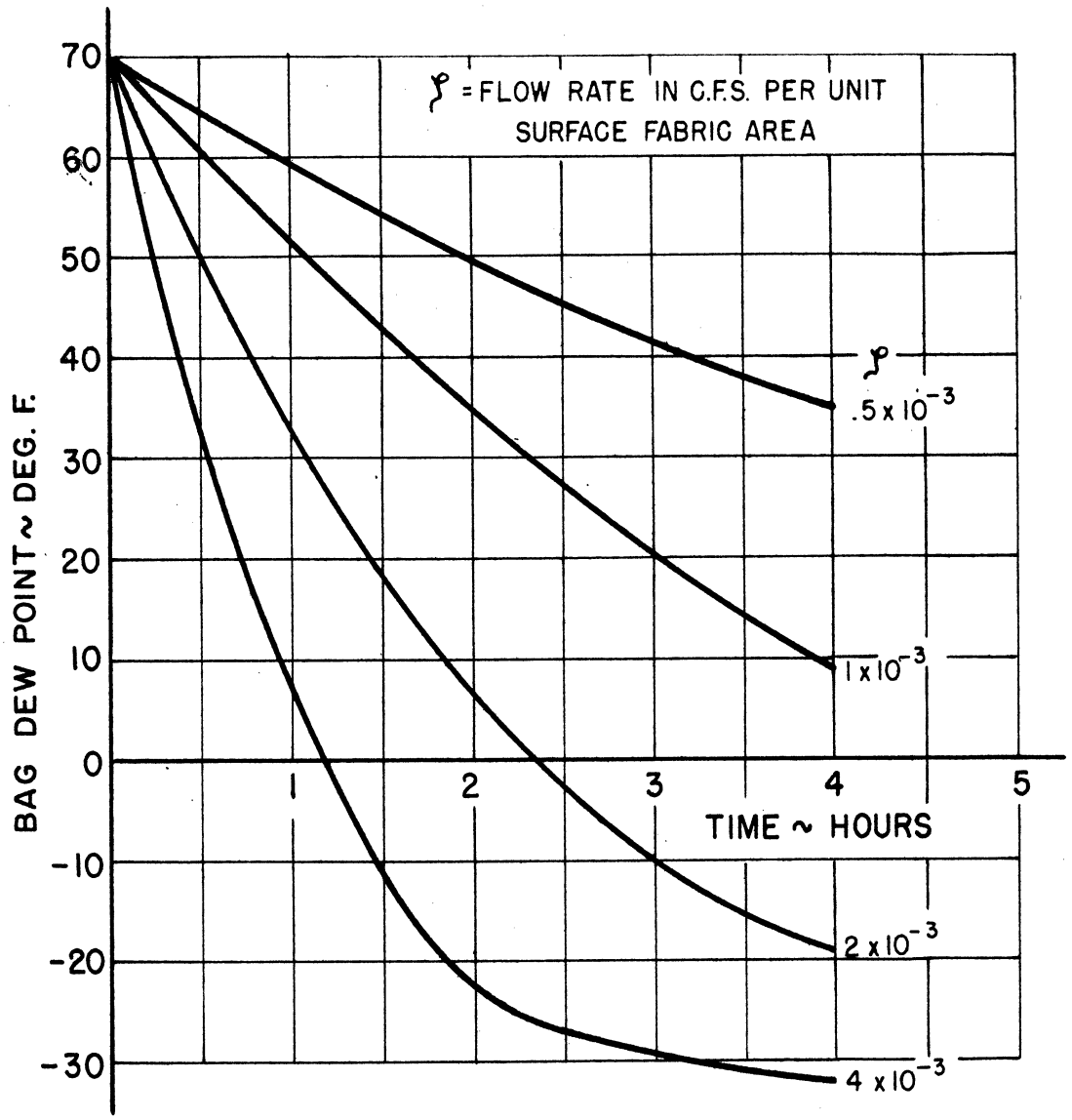

FIGURE II (4)

EFFECT OF K AND $\wp$ UPON LIMIT BAG DEWPOINT, $t = \infty$

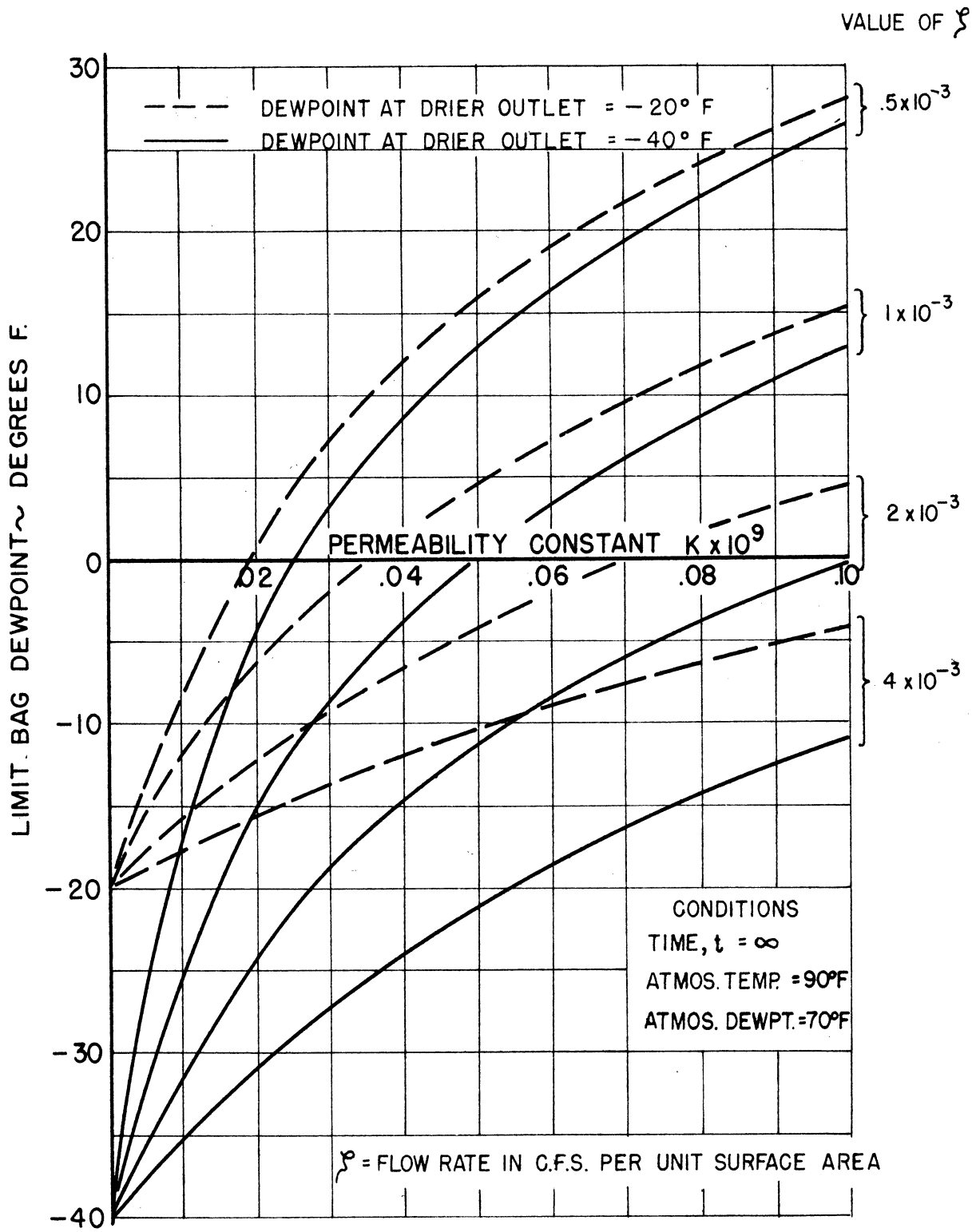

# FIGURE II (5)
# EFFECT OF ATMOSPHERIC DEW POINT UPON BAG DEW POINT

CONDITIONS:

$K = 0.01 \times 10^{-9}$

TIME = $\infty$

$\rho$ = DRIER FLOW RATE PER UNIT SURFACE AREA ~ C.F.S.

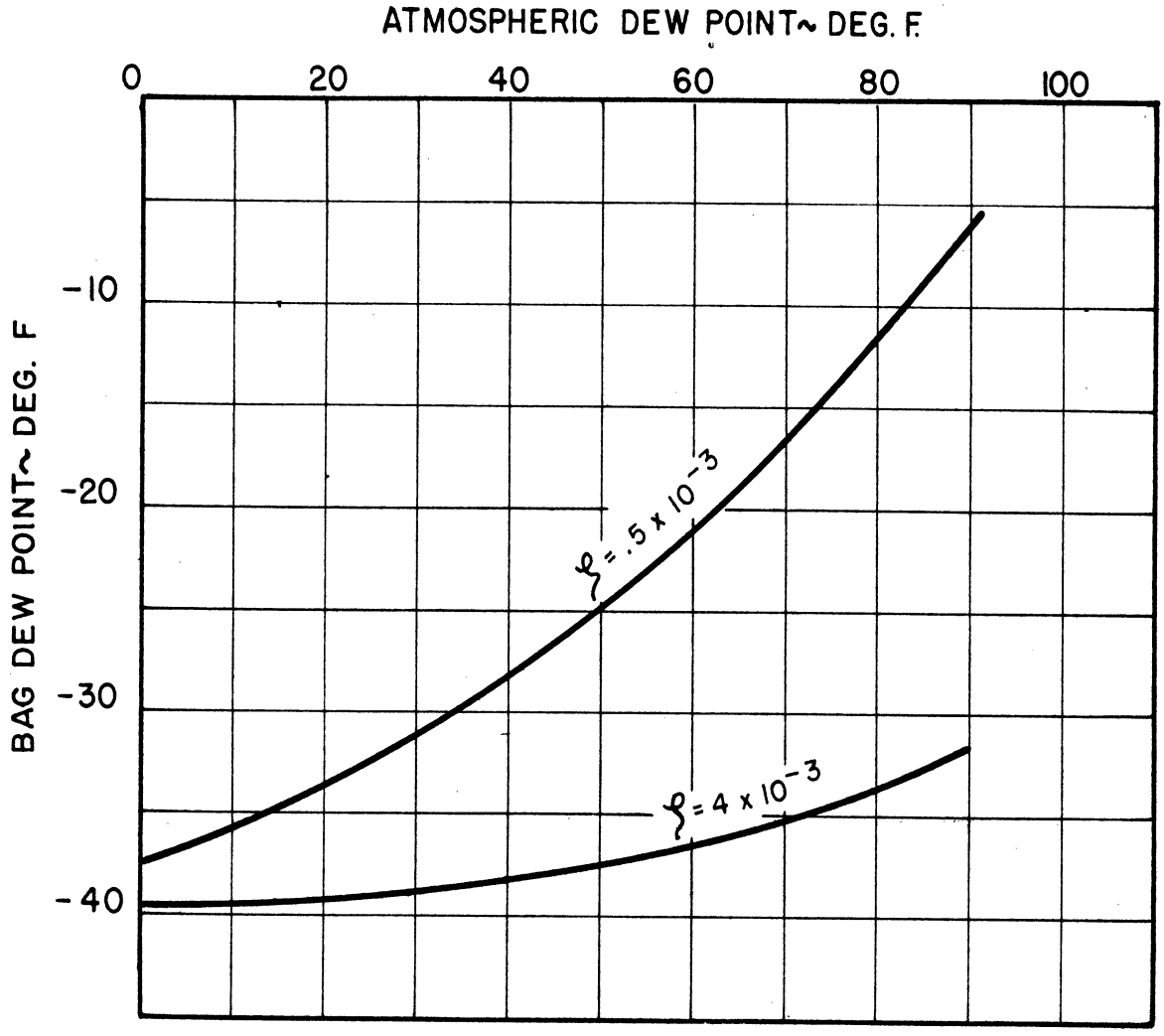

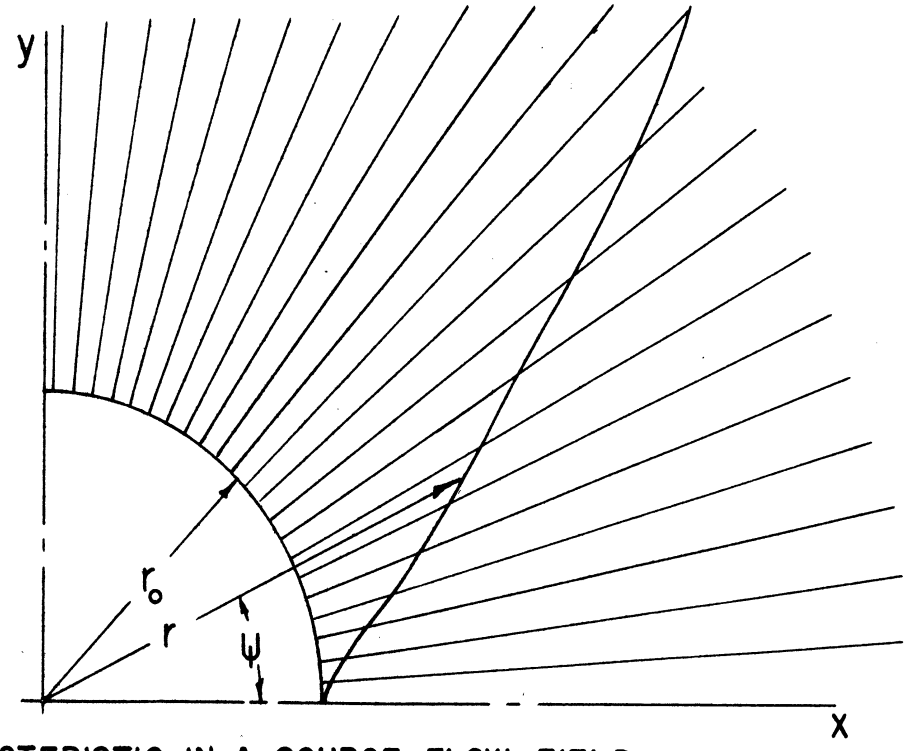


FIGURE III(1)

PLOT OF A CHARACTERISTIC IN A SOURCE FLOW FIELD

THE RADIAL LINES ARE STREAMLINES

r AND ψ ARE THE POLAR COORDINATES OF THE CHARACTERISTIC

$r_o$ IS THE RADIUS OF THE M=1 CIRCLE

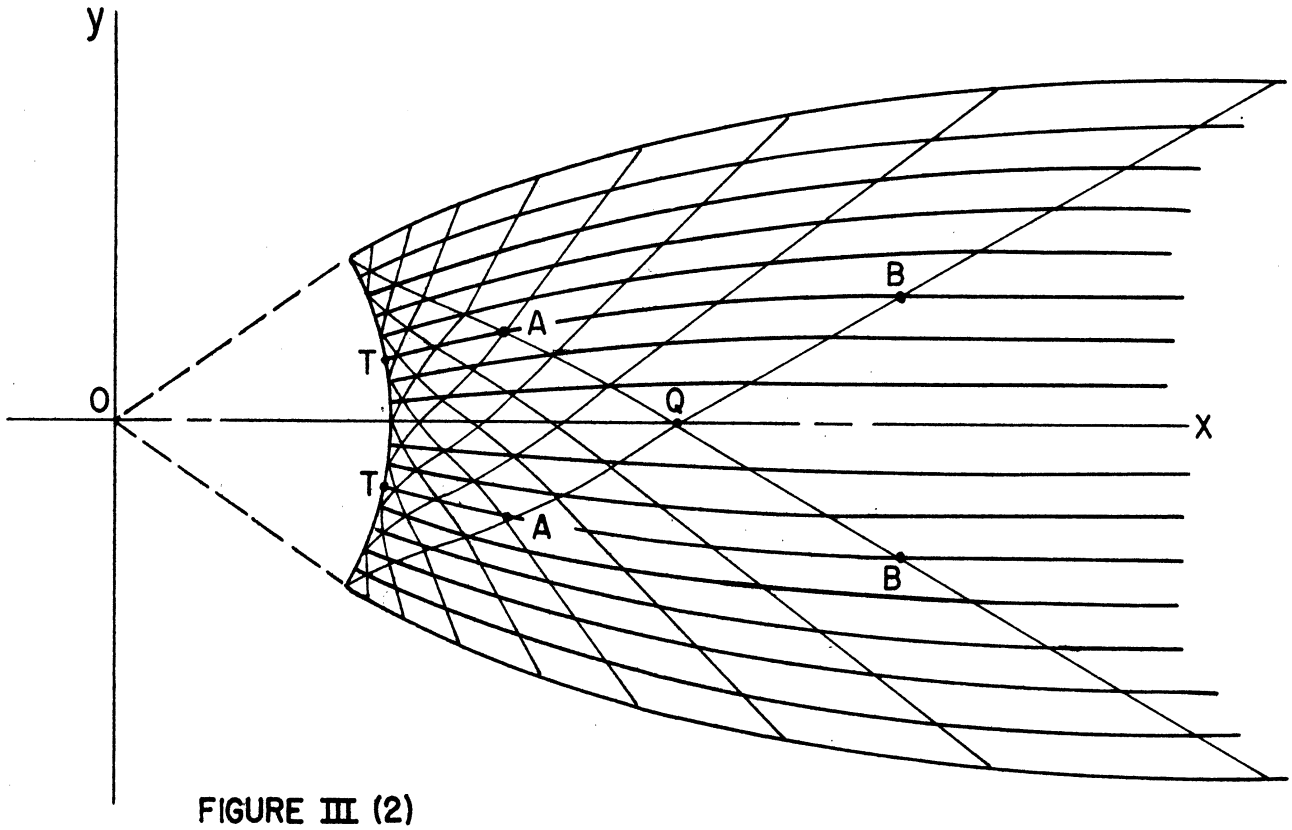


FIGURE III (2)

STREAMLINES AND CHARACTERISTIC LINES OF THE NOZZLE FLOW FIELD. TEXT GIVES DISCUSSION

FIGURE III (3)
SKETCH OF NOZZLE CONTOURS
ILLUSTRATING SOME OF THE PARAMETERS

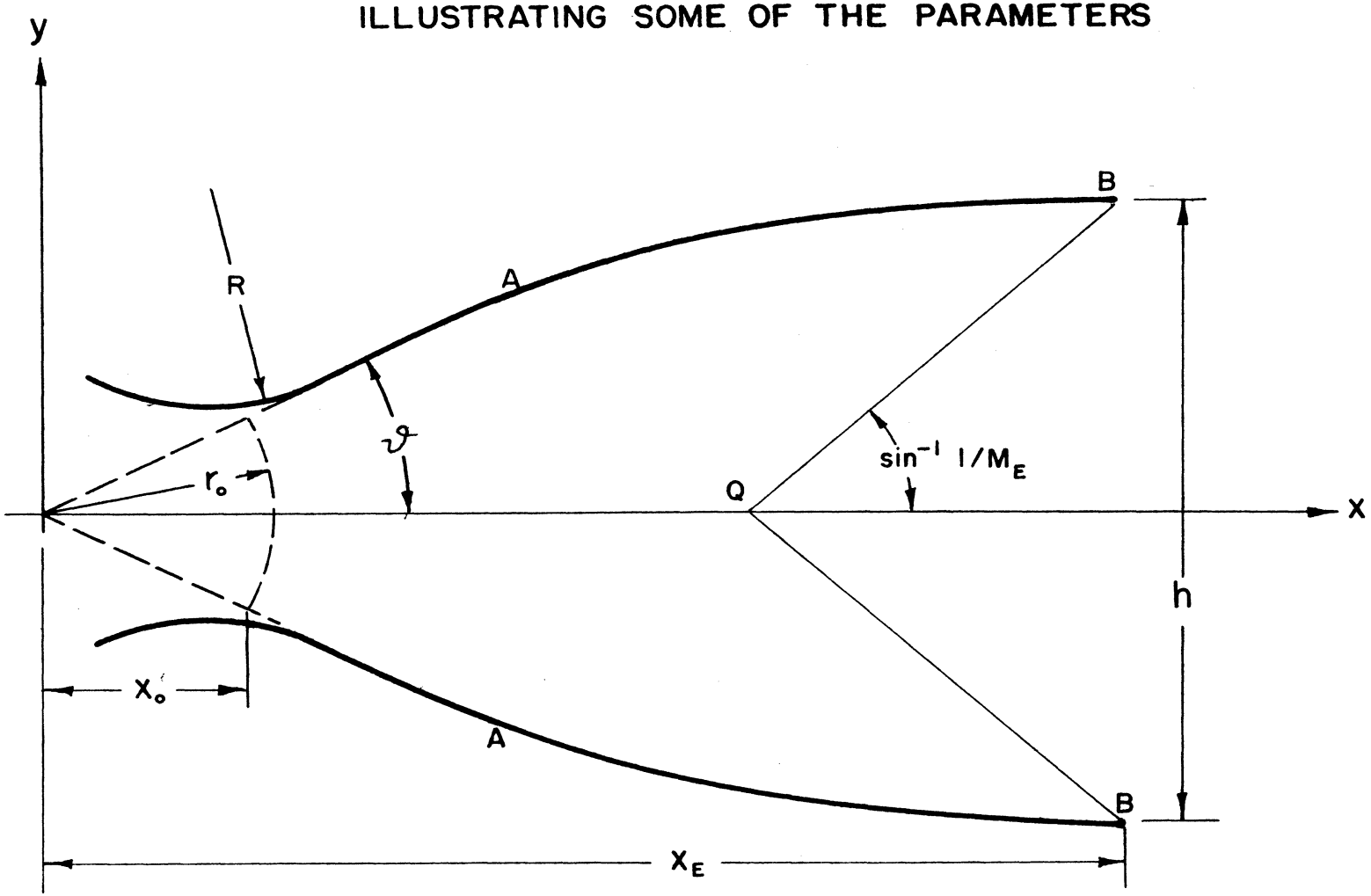

FIGURE V (7) RANGE II (DOWN)
SCALE READING VS. LOAD

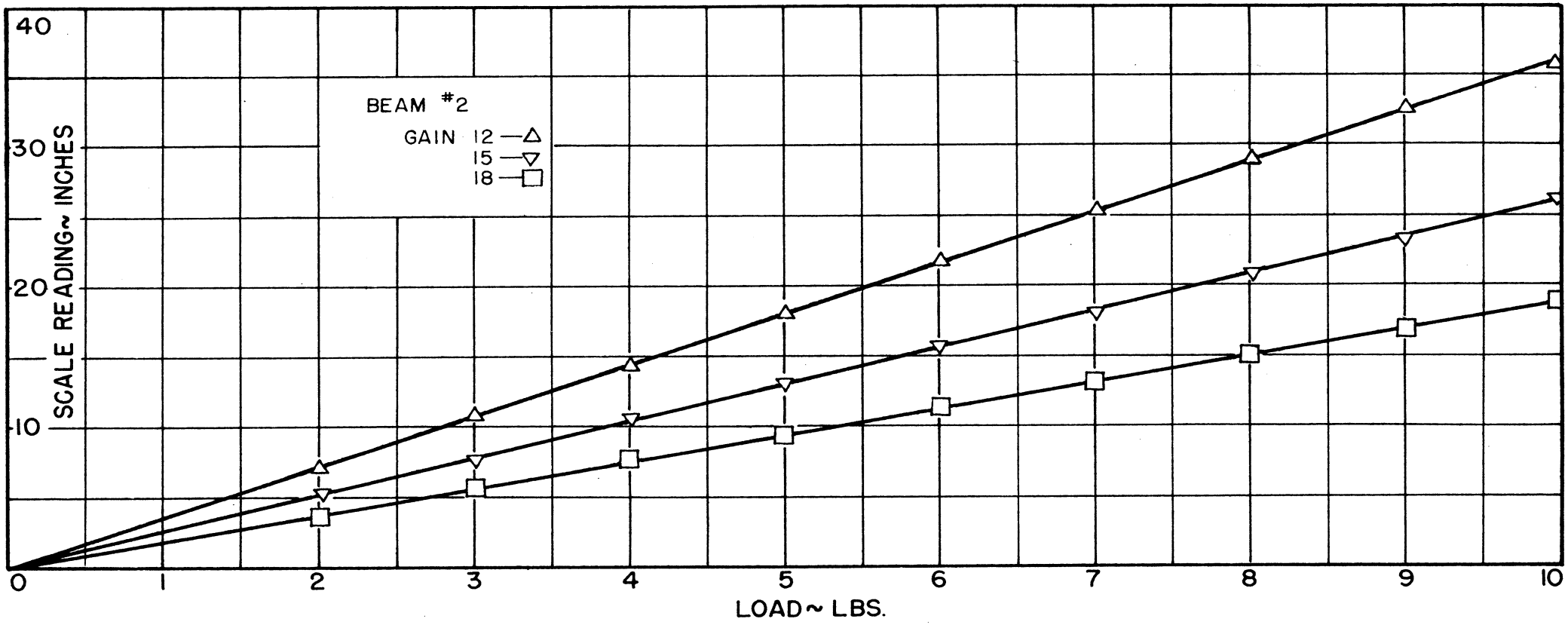

FIGURE V (8) RANGE III (UP)
SCALE READING VS. LOAD

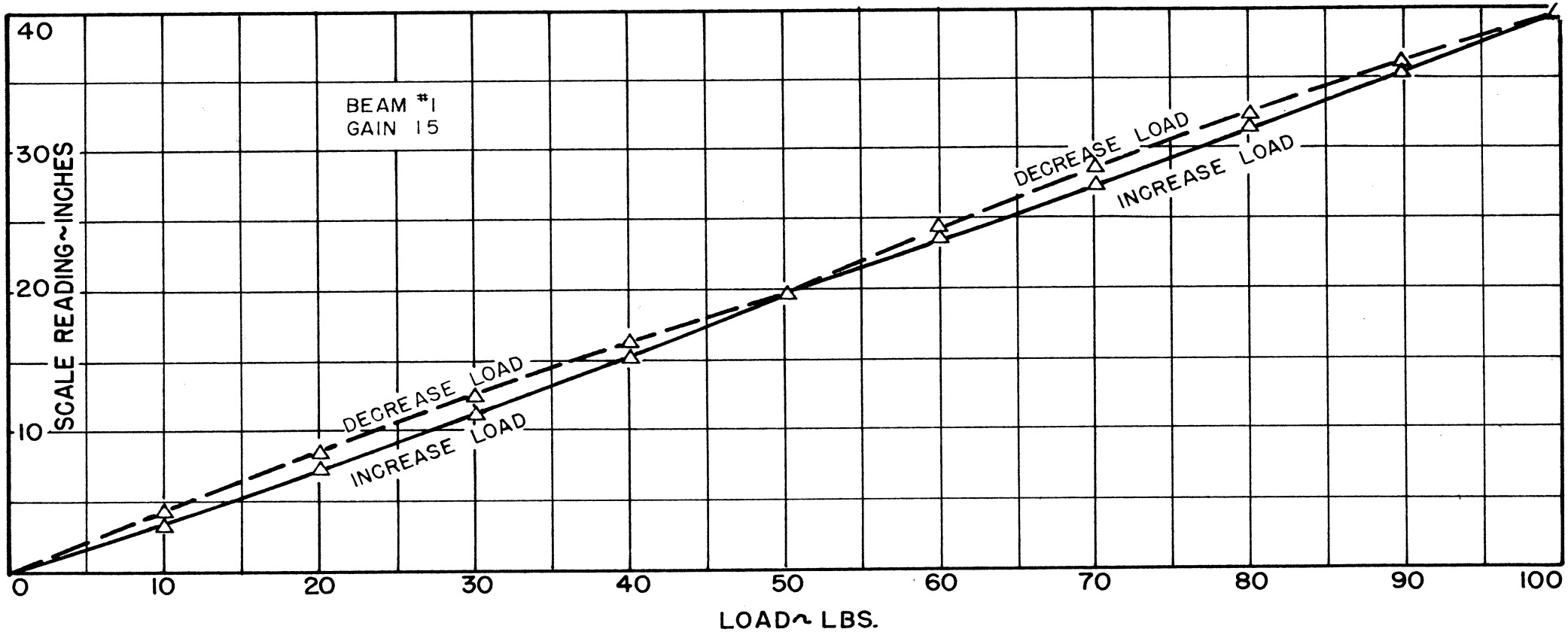

FIG. V (9)

RANGE III (DOWN)

SCALE .READING VS. LOAD

BEAM #
GAIN 15

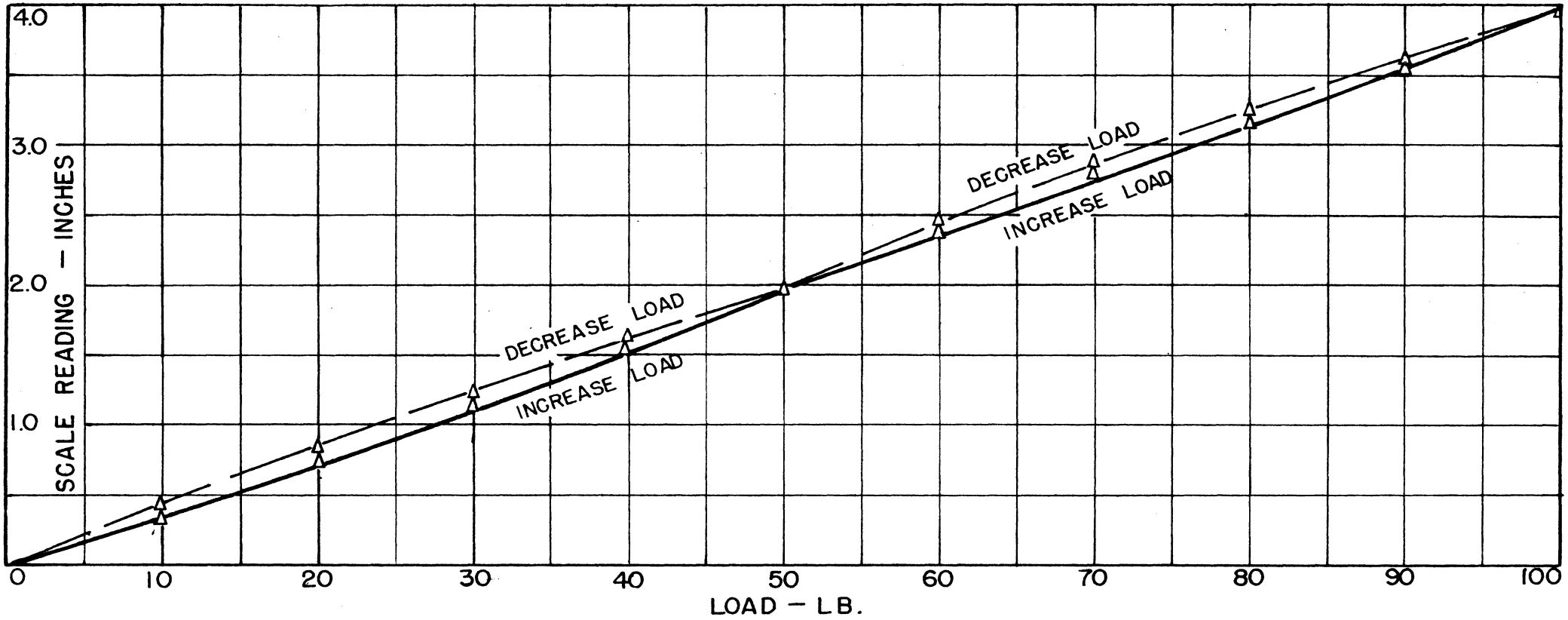

FIGURE V (3)
CHANGE IN CURRENT WITH WARM-UP TIME.

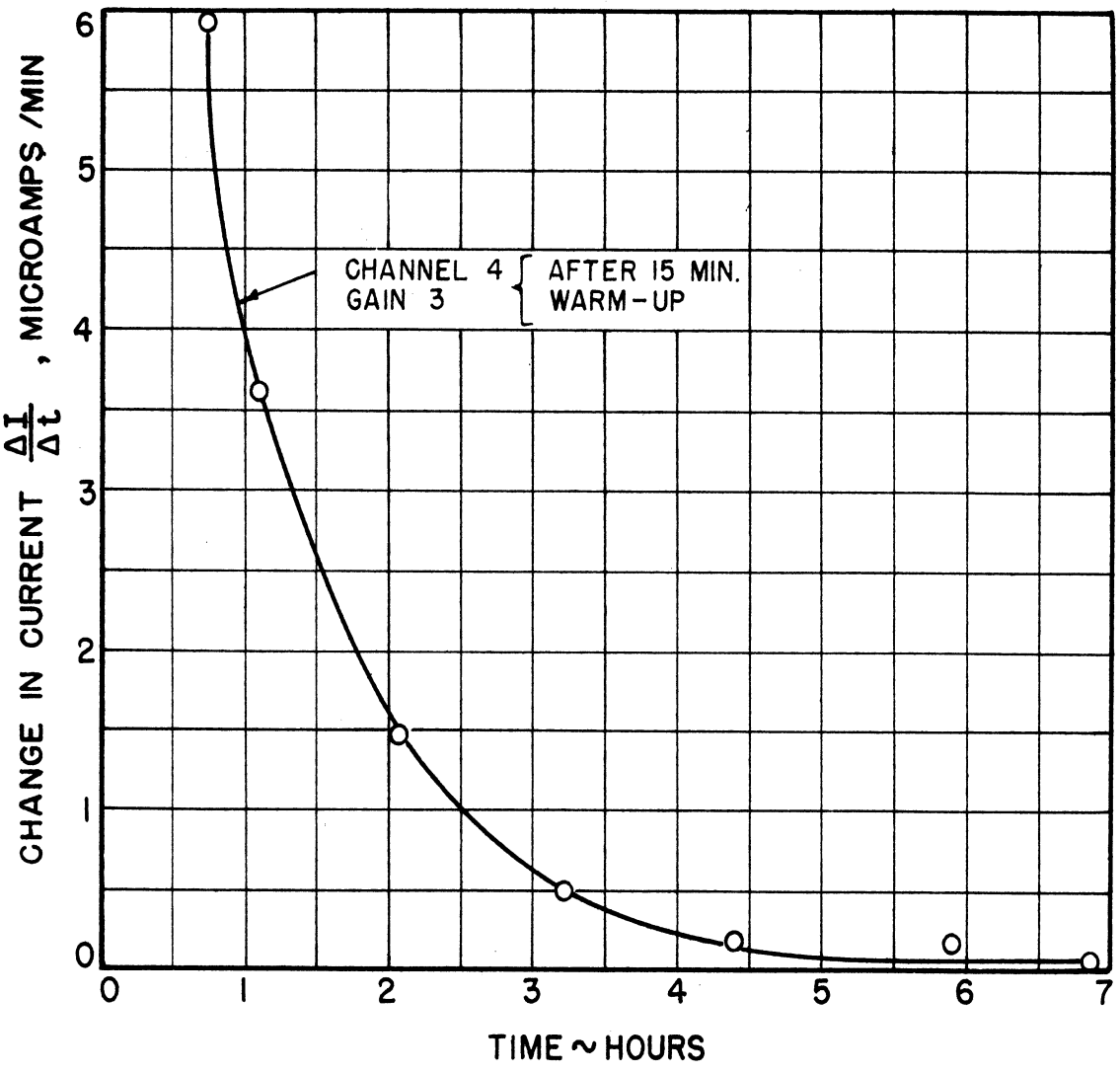

FIG VII (2)

# TEST SECTION MACH NUMBER FROM PRESSURE MEASUREMENTS HORIZONTAL TRAVERSES.

ooo LEFT HAND WALL
+++ RIGHT HAND WALL
(LOOKING UPSTREAM)

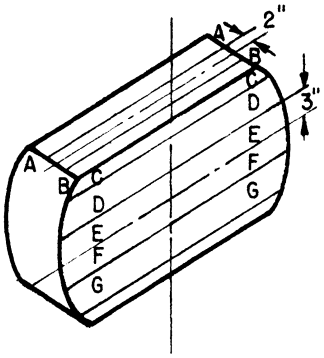


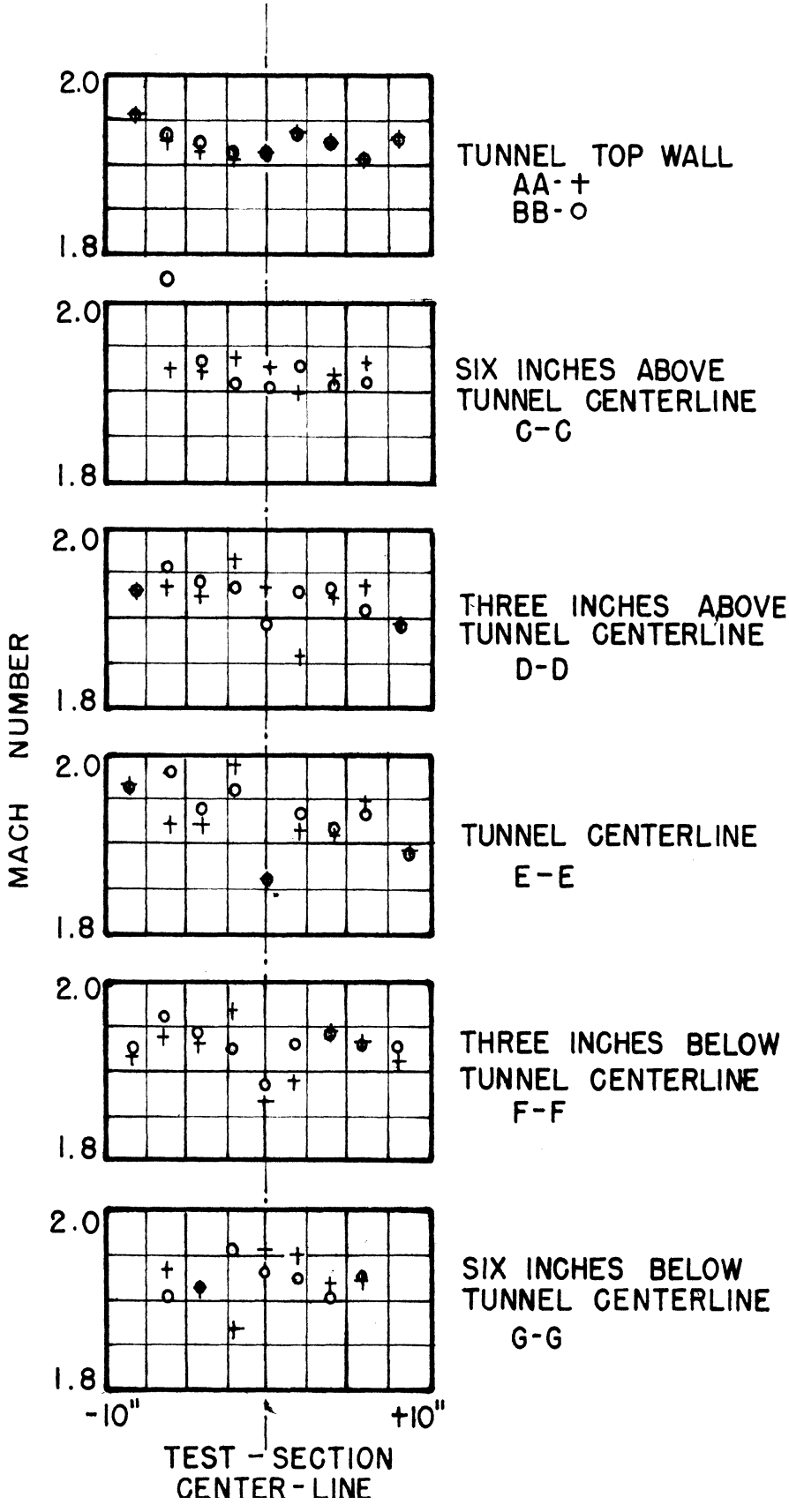

FIGURE VII (3)

MACH NUMBER FROM WALL PRESSURE MEASUREMENTS

TEST SECTION, (EMPTY), LEFT HAND WALL (LOOKING UPSTREAM)

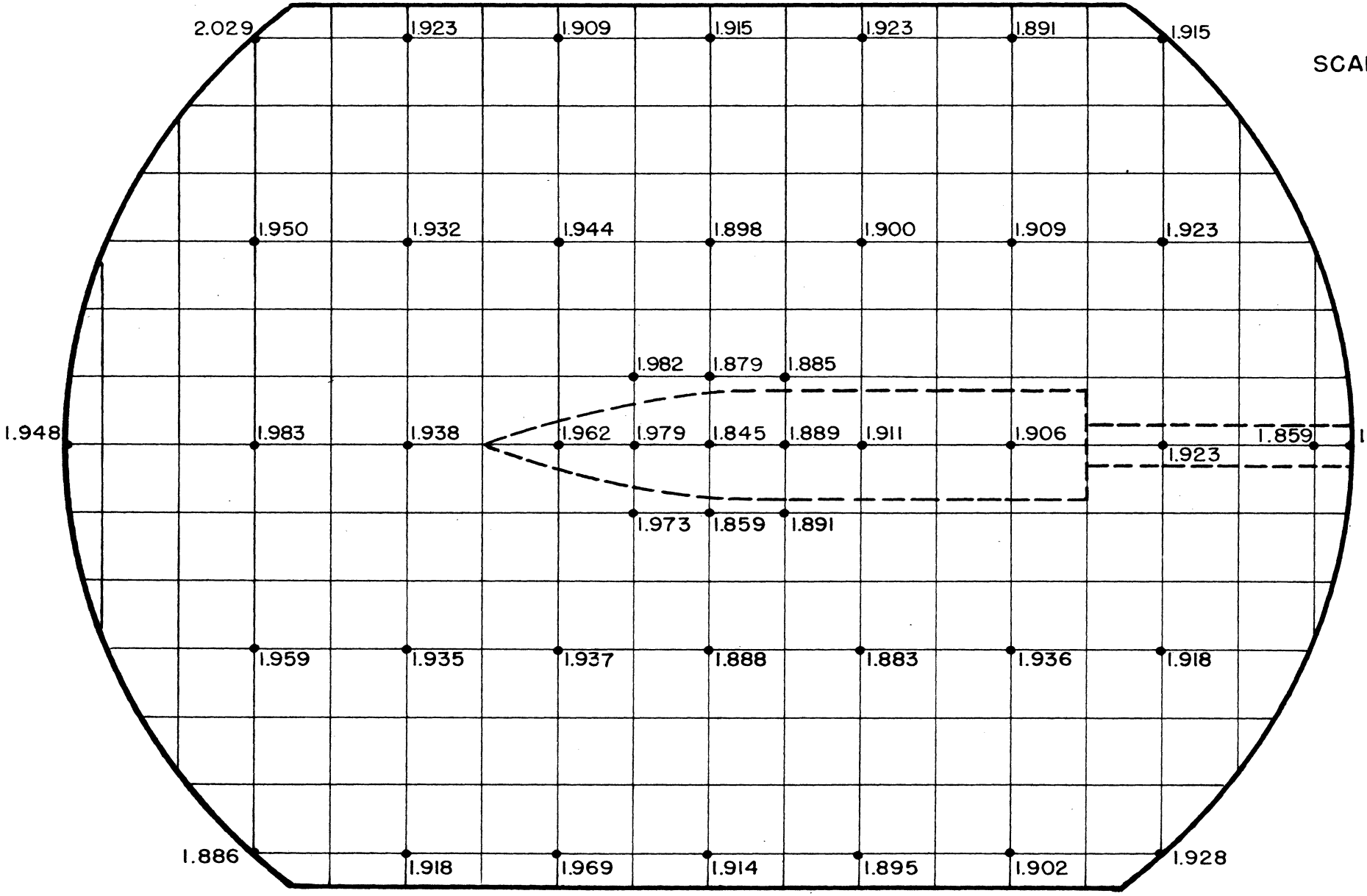

FIG. VII (4)

MACH NUMBER AND FLOW INCLINATION FROM PRESSURE MEASUREMENTS IN THE INTERIOR OF M=1.9 WIND TUNNEL.

FROM SURFACE PRESSURE MEASUREMENTS ooo
FROM TOTAL HEAD MEASUREMENTS +++

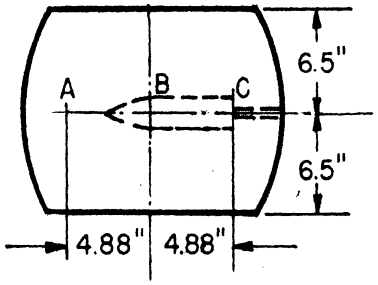


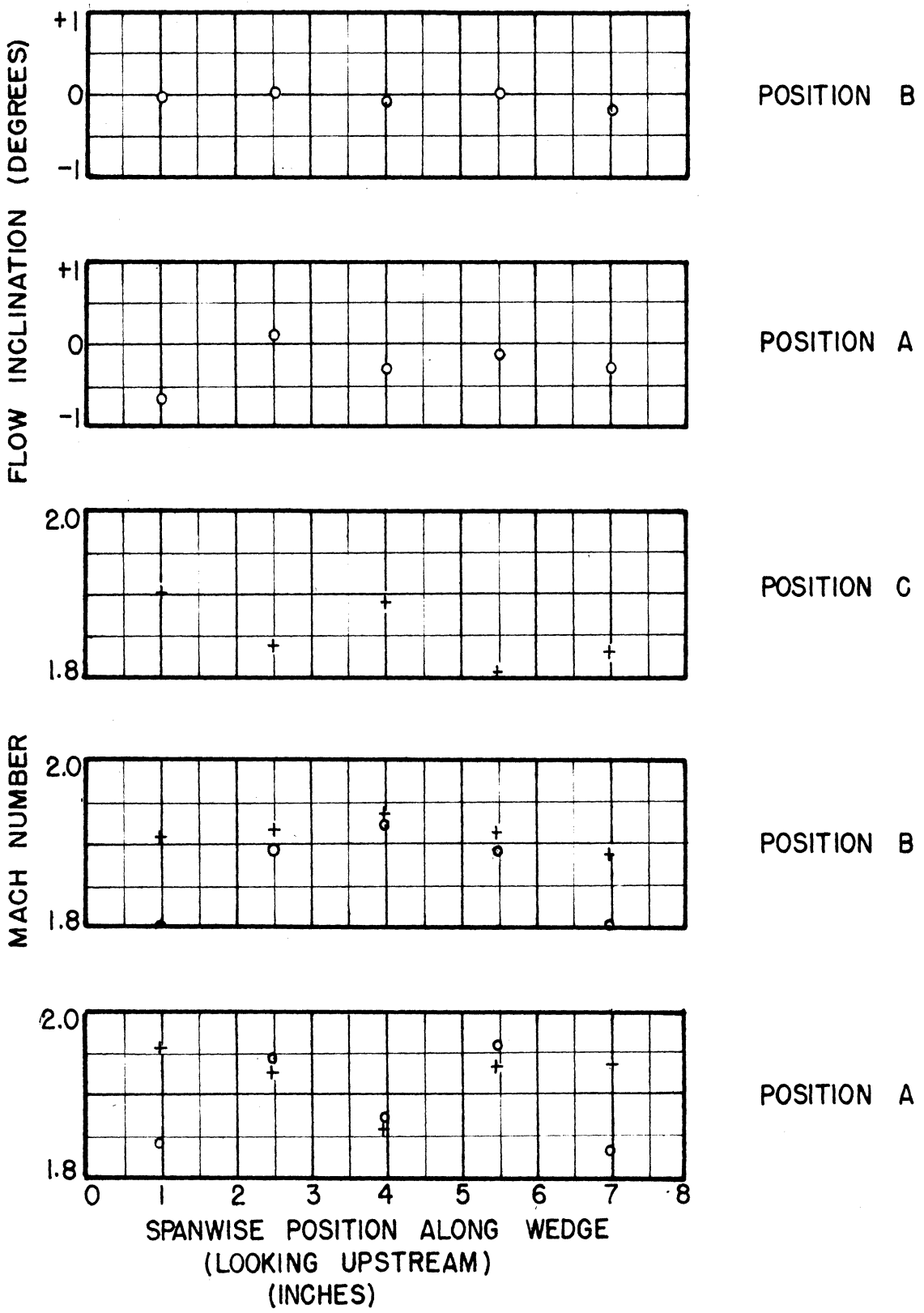

FIGURE VII (5)

TOTAL HEAD PRESSURE MEASUREMENTS IN THE INTERIOR OF M=1.9 WIND TUNNEL

$P_o'$ MEASURED STAGNATION PRESSURE

$P_o$ RESERVOIR STAGNATION PRESSURE

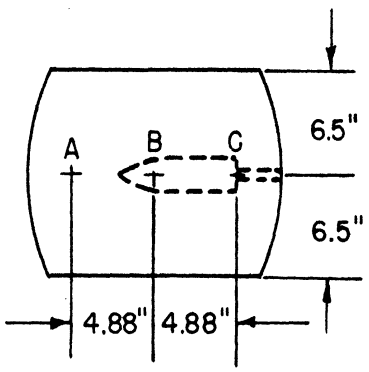


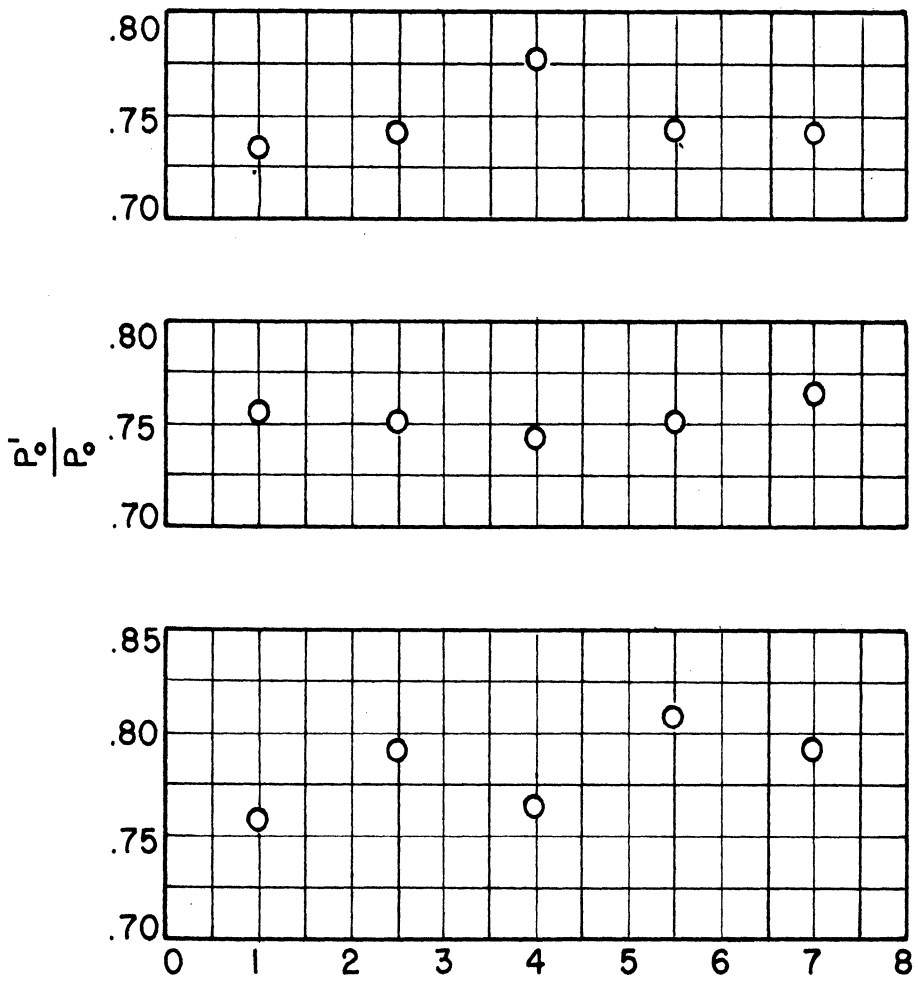

FIG. III (4)

LENGTH FROM THROAT TO EXIT OF NOZZLES DESIGNED AFTER THE METHOD OF NA-235-2

h = 13"

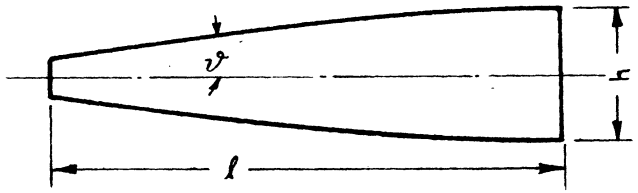


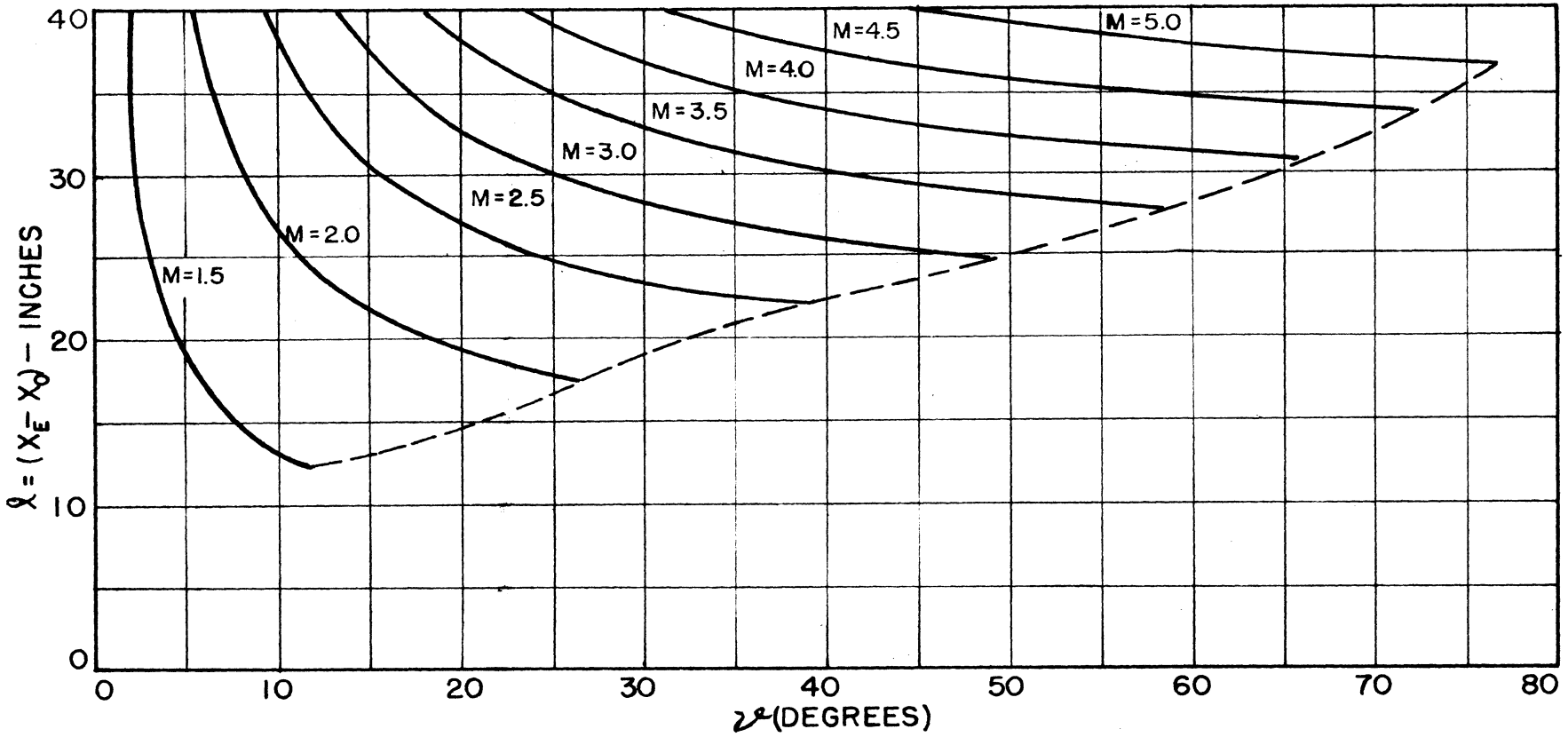

FIGURE III (5)

$\delta^*/\delta, \theta/\delta, \theta/\delta^*$ FOR THE BOUNDARY LAYER PROFILE $(U/U_1)_1 = (Y/S)^{1/7}$

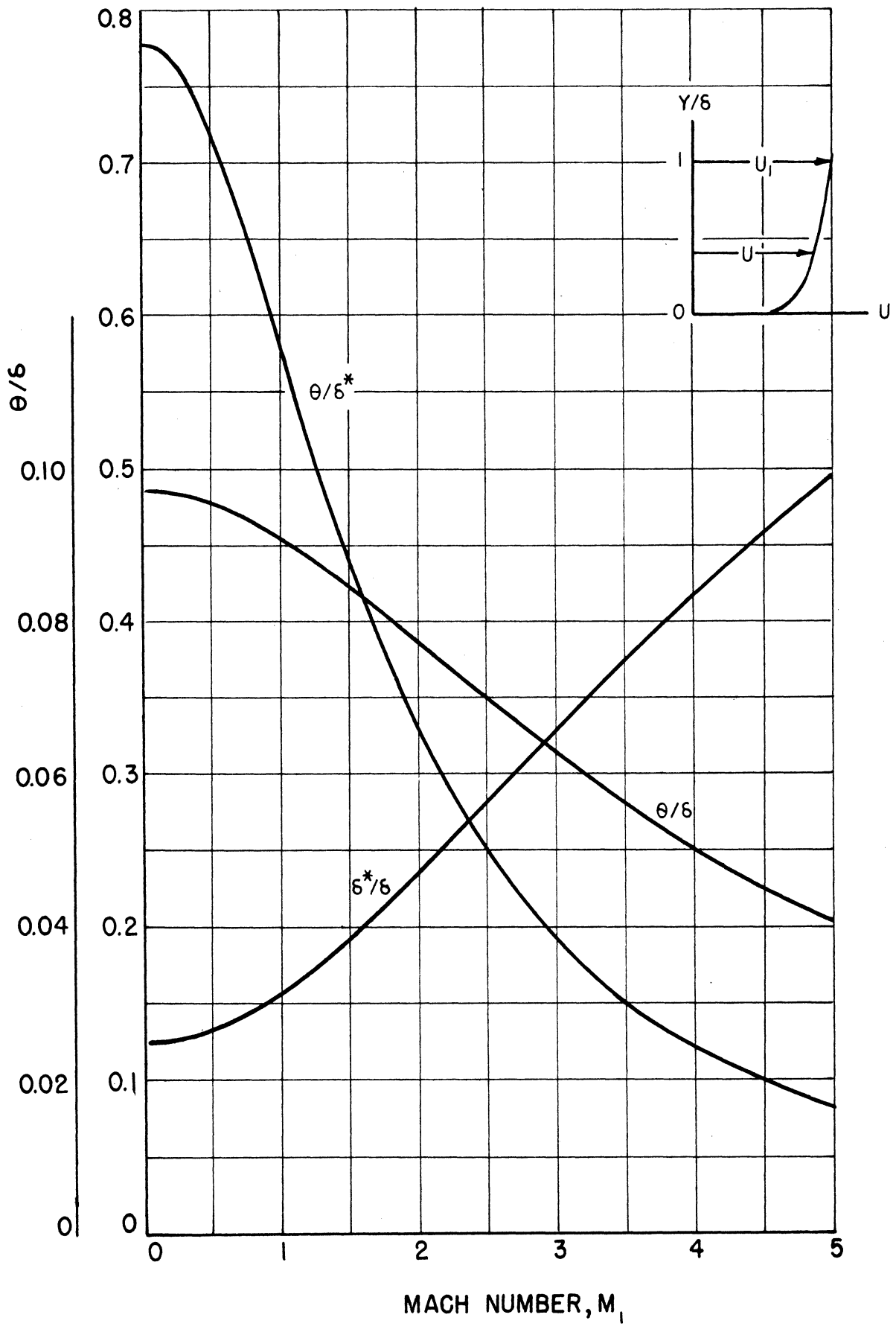

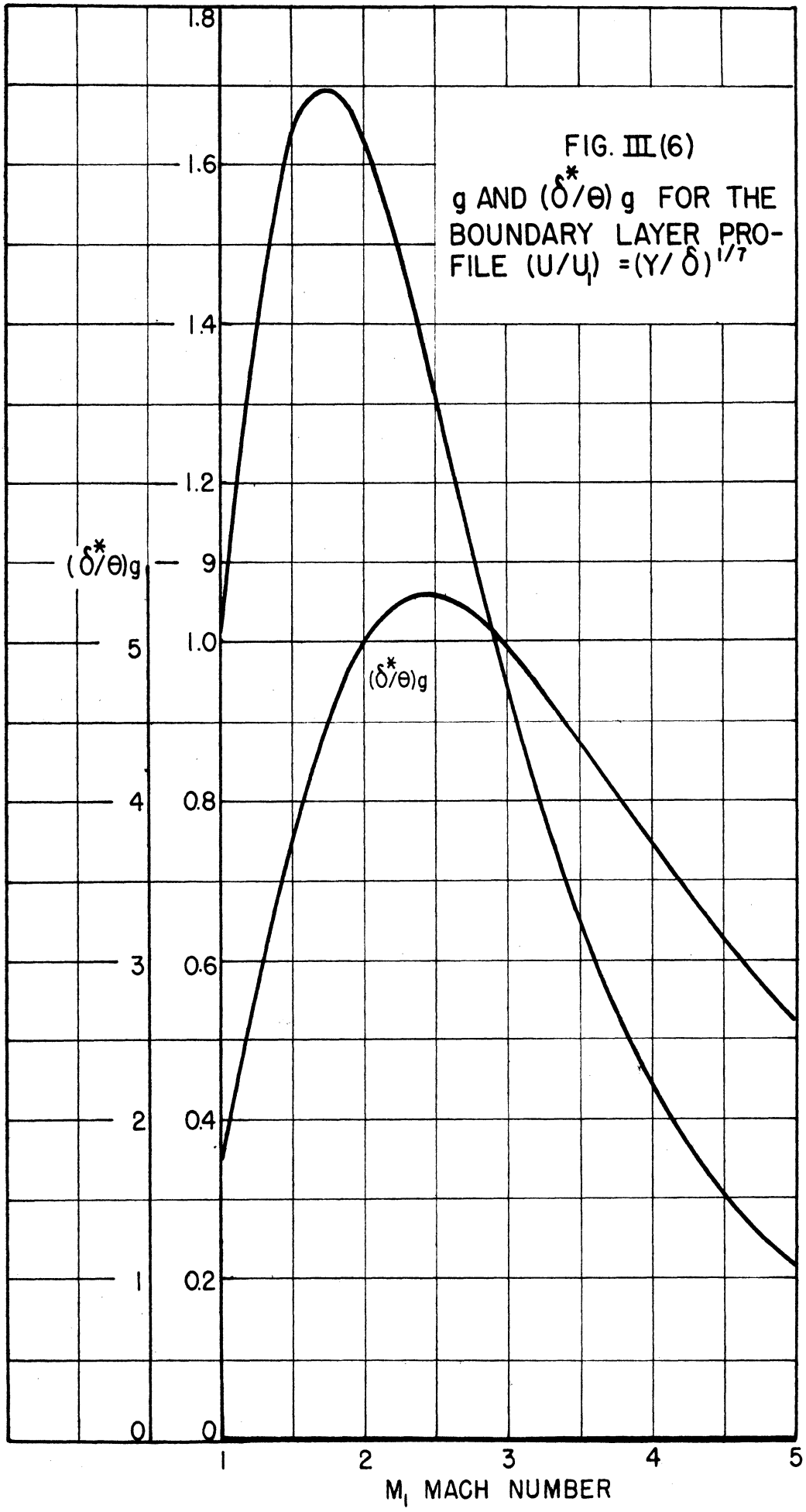


FIG. III.(6)

g AND $(\delta^*/\theta)g$ FOR THE BOUNDARY LAYER PROFILE $(U/U_1) = (Y/\delta)^{1/7}$

FIG. III (7)

REYNOLD'S NUMBER PER FOOT FOR AN EXPANSION FROM AN ATMOSPHERIC RESERVOIR.

$$R = \frac{7.02 \cdot 10^{-6} M_1}{(1+0.2\, M_1^2)^{2.232}}$$

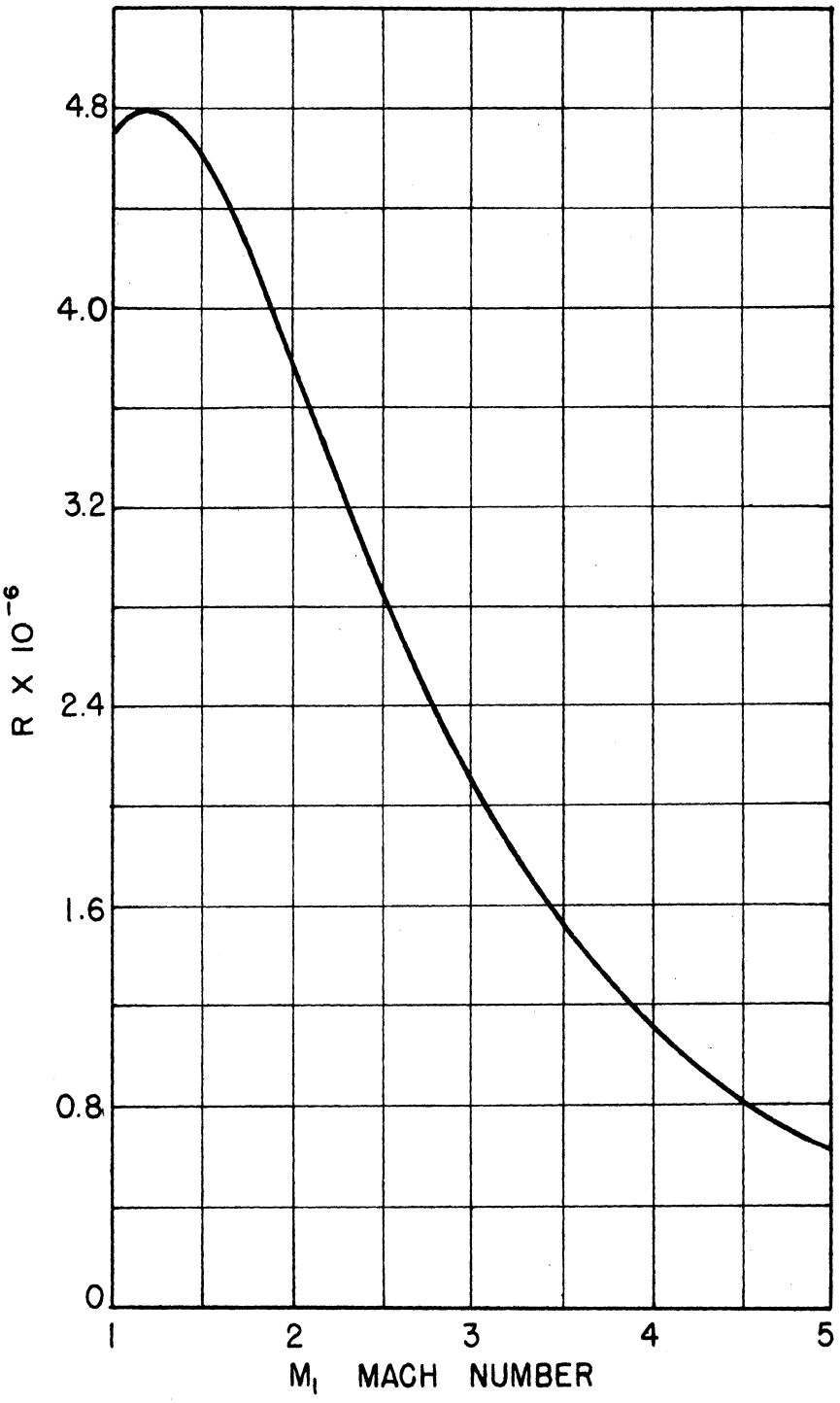

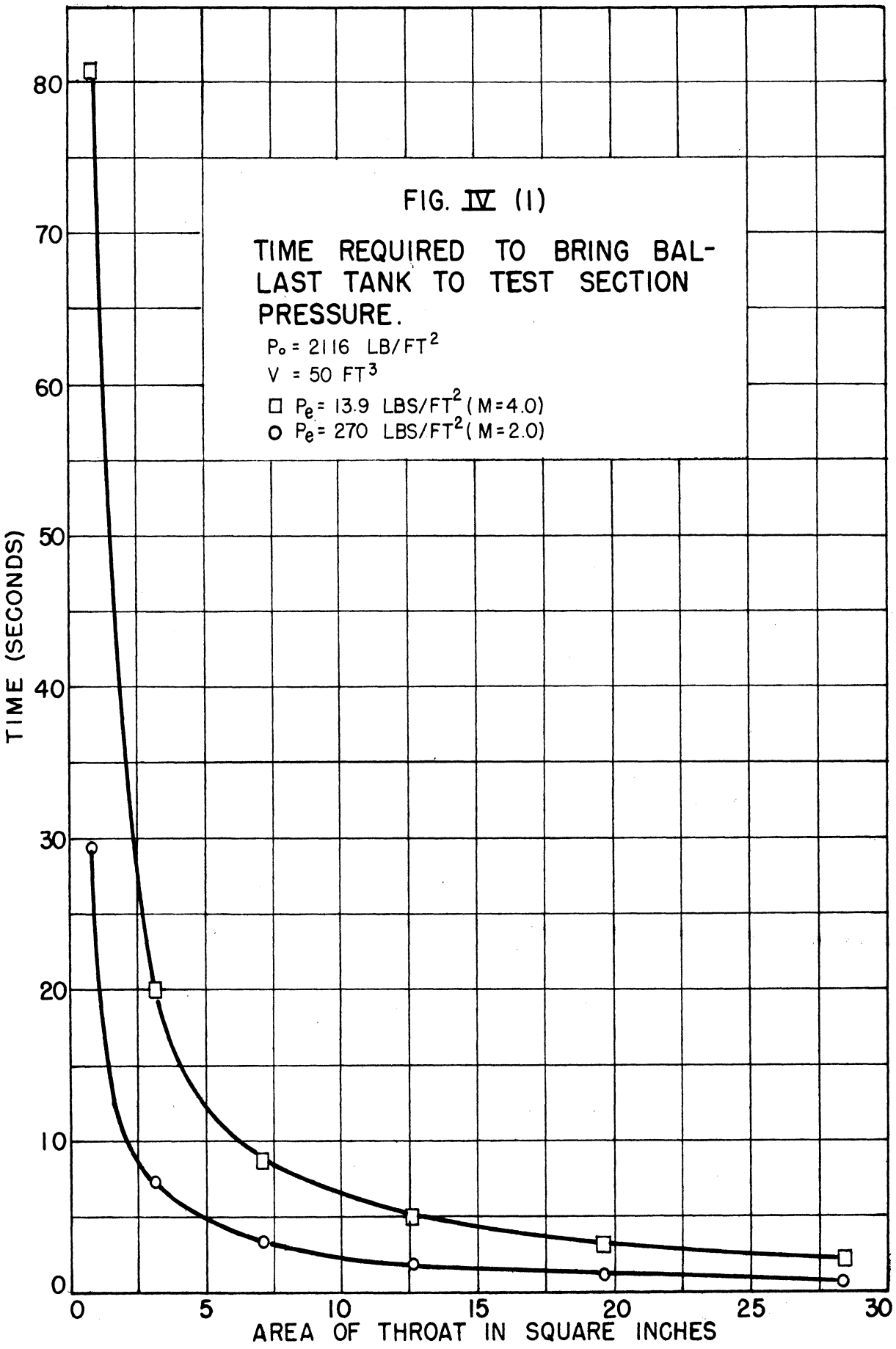
FIG. IV (1)
TIME REQUIRED TO BRING BALLAST TANK TO TEST SECTION PRESSURE.
$P_o$ = 2116 LB/FT$^2$
V = 50 FT$^3$
□ $P_e$ = 13.9 LBS/FT$^2$ (M=4.0)
○ $P_e$ = 270 LBS/FT$^2$ (M=2.0)
TIME (SECONDS)
0
10
20
30
40
50
60
70
80
0
5
10
15
20
25
30
AREA OF THROAT IN SQUARE INCHES

FIG. V (4)
RANGE I (UP)
LOAD VS. SCALE DEFLECTION

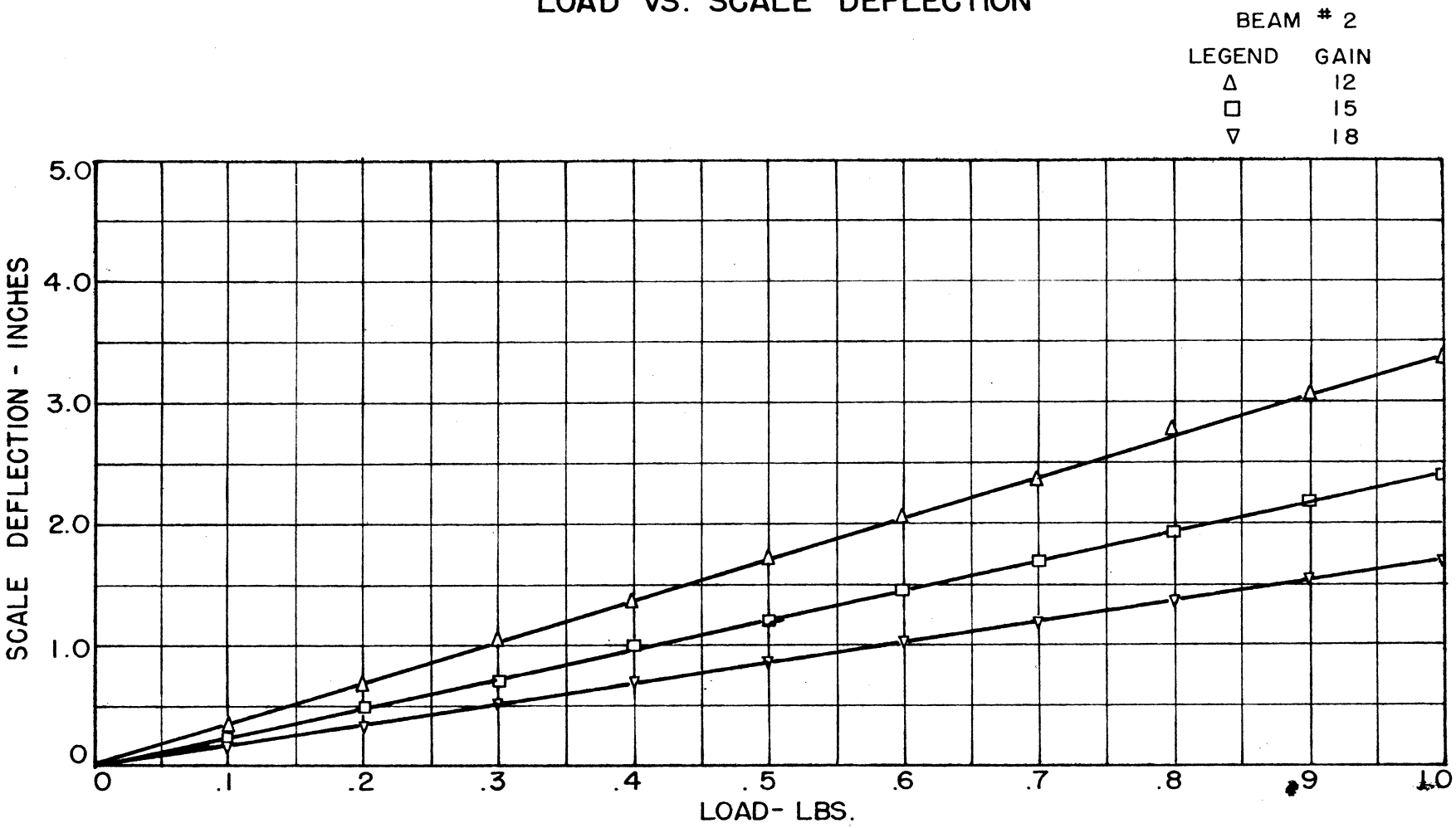

FIG. V (5)
RANGE I (DOWN)
LOAD VS. SCALE DEFLECTION

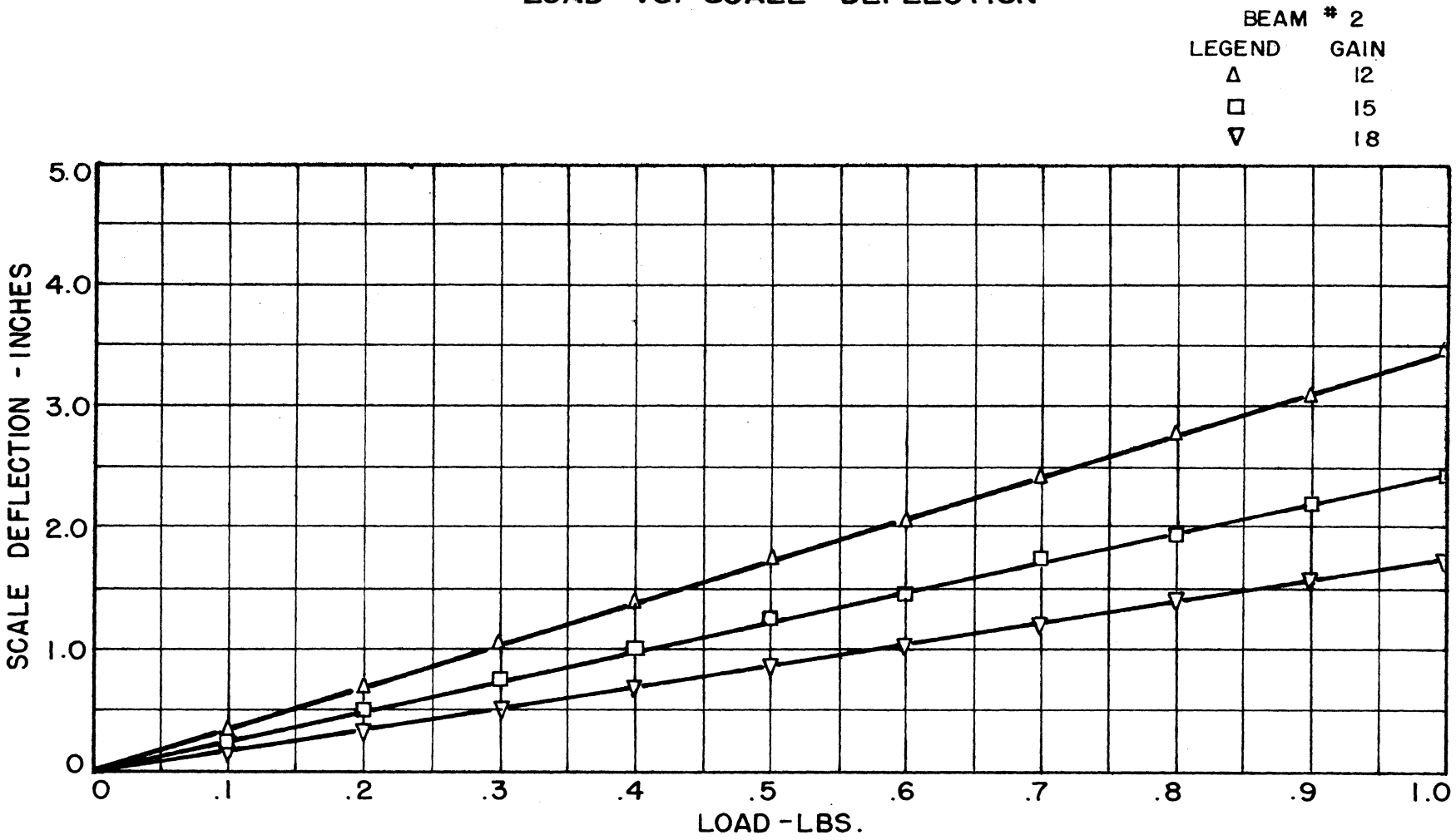

$$t_e = \frac{.160}{A^*} \qquad \text{(Mach 2 case)} \qquad (23)$$

Equations (22) and (23) are plotted in Figure IV (1). Time in seconds is given versus orifice area in square inches. A vent of 25 square inches area should be sufficient to equalize the ballast tank pressure in under 5 seconds of running time.

# APPENDIX V

## CALIBRATION WORK ON A STRAIN-SENSITIVE ELEMENT OF THE BALANCE SYSTEM

The sensitivity requirement, the need for three distinct force ranges with relatively high accuracy of measurement in each range, indicated the trend of the development work on the strain-sensitive unit. The multiple beam unit which was designed permits this type of sensitivity, and the roller clutch incorporated was to allow easy range selectivity from outside the tunnel.

The element, slightly larger than full size, is shown in Figure V(1). (A) is the base of the unit, supplying rigid support to the load-carrying cantilever beams. (B) is a wire strain gage. There are two of these, one on the top and one on the bottom of the center beam. (C) are the cantilever beams, which resist in bending the load to be measured. (D) is the roller clutch assembly, which permits resistance by the center beam alone, by the middle three beams, or by all five beams together, according to the position in which the clutch is placed. (E) is the terminal strip, joining the wire strain gage leads to the leads from the recording equipment, and (F) is the loading plate, transmitting the load from thin metal straps to the center beam.

For ease in discussion, the three force ranges of 0-1, 0-10, and 0-100 lbs., corresponding to resistance by the center beam alone, three beams or five beams have been termed Ranges 1, 2 and 3, respectively. The calibrations were carried out by applying dead weights to the loading plate through the same thin metal straps to be used in the balance assembly. The arrangement is shown in Figure V (2). The loads were reversed by inverting the strain unit.

FIG. V (6)
RANGE II (UP)
SCALE READING VS. LOAD